THE ROLE OF PALLADIN IN ACTIN ORGANIZATION: IMPLICATIONS FOR THE GLIAL SCAR

Daniel Kenneth Arneman

A dissertation submitted to the faculty of the University of North Carolina at Chapel Hill in partial fulfillment of the requirements for the degree of Doctor of Philosophy in the Department of Cell and Molecular Physiology.

Chapel Hill
2007

Approved by:

Eva Anton, PhD

Richard Cheney, PhD

Rick Meeker, PhD

Carol Otey, PhD

Juli Valtschanoff, MD

ABSTRACT

Reactive gliosis is the central nervous system's consistent response to injury. Activated astrocytes migrate to the wound periphery where they hypertrophy and deposit a dense extracellular matrix. Commonly, the glial scar that forms after physical trauma presents a barrier to neurite outgrowth and the functional recovery of severed axonal circuits. Previous reports from our lab demonstrated that immunoreactivity of the actin-associated phosphoprotein palladin rapidly increased in activated astrocytes both *in vitro* and *in vivo*, but further questions on the method of up-regulation and the functional significance of this change remained. In this work, we demonstrate that both 90 kDa and 140 kDa palladin are transcriptionally regulated after endothelin treatment in a cell culture model of gliosis. The consequence of this up-regulation in glial scar formation remains to be elucidated, but palladin appears to be critical for some types of three-dimensional motility, including dynamic actin-based ruffles and podosomes. Formation of these invasive structures is inhibited in paladin knockdown cells. On the molecular level, palladin may exert its influence on actin organization directly, as it was shown to bind and bundle actin filaments via its immunoglobulin-like domains. Taken together, palladin is shown to be an early marker of reactive astrocytes where it may play a role in cell migration and actin organization.

DEDICATION

I dedicate this dissertation to the memory
of Andrew S. Rachlin, whose exceptional intelligence,
creativity, and friendship still live in the memory of those who knew him.

ACKNOWLEDGEMENTS

This dissertation represents the efforts of countless collaborators, colleagues, supporters, family and friends, to whom I owe my gratitude.

TABLE OF CONTENTS

LIST OF TABLES

Table

LIST OF FIGURES

Figure

CHAPTER 1

INTRODUCTION AND BACKGROUND

1.1 Astrocyte form and function

For many years, scientists studying the central nervous system (CNS) focused almost exclusively on understanding the function of neurons, while astrocytes – the star shaped cells that outnumber neurons in the human CNS – were considered merely supporting players. Recently, however, new roles for astrocytes are being uncovered, including important contributions to the maintenance and modification of neuronal function. (Newman, 2003; Fields and Stevens-Graham, 2002)

Astrocytes have a round cell body and extend many thin processes that interact with neurons, endothelial cells, and other astrocytes (Vise et al., 1975; Ventura and Harris, 1999; Schikorski and Stevens, 1999). Their large numbers, physical structure, and repertoire of cell-surface receptor proteins make astrocytes uniquely suited to sense and respond to changes in the CNS environment (Hertz et al., 1984; Murphy and Pearce, 1987; Koehler et al., 2006). In order to function properly, neurons must be maintained within a narrow range of ion, oxygen, and glucose concentrations while avoiding the buildup of metabolic waste and released neurotransmitters. One function of astrocytes is to detect environmental changes

and maintain homeostasis for proper neural function (Hertz, 1978; Schousboe and Hertz, 1981; Sykova et al., 1992; Schousboe et al., 1992; Simard and Nedergaard, 2004)

Structurally, astrocytes act as scaffolds during CNS development and allow for neuronal migration (Levitt and Rakic, 1980). They interact with endothelial cells in the formation and function of the blood-brain barrier that separates the cerebrospinal fluid from compounds carried by the blood (Vise et al., 1975; Abbott, 2002; Banerjee and Bhat, 2007). Astrocytes also play a role in establishing the extra-cellular matrix – a network of proteins with direct effects on neuronal migration and the extension of axons (Liesi et al., 1983; Wujek and Akeson, 1987; Ard and Bunge, 1988).

Metabolically, astrocytes condition the cerebrospinal fluid for optimal neuronal efficiency. They are the one of the few cell types in the brain that are able to store glycogen, which they break down into glucose and release to support the high-energy requirements of neighboring cells (Wender et al, 2000). Astrocytes also remove harmful substances such as the neurotransmitter glutamate, which at high concentrations can cause excitotoxicity and neuronal death (Hertz et al., 1978; Choi, 1988; Erecinska and Silver, 1990).

Beyond their role in conditioning the neuronal environment, glia are being studied for their participation in synaptic transmission. In the cortex, synapses are often ensheathed by perisynaptic astrocytes that were once thought to act merely as structural or metabolic support (Ventura and Harris, 1999; Shikorski and Stevens, 1999). More recent studies have demonstrated that these astrocytes can respond to

synaptic transmission through calcium signaling, and also modulate synaptic transmission through the release of their own “gliotransmitters” (Bezzi and Volterra, 2001; Finkbeiner, 1993; Porter and McCarthy, 1997; Newman, 2003).

In addition to these support roles, astrocytes are being examined as a source of stem cells in the adult CNS. After a long debate over the possibility of neurogenesis in the adult brain, several groundbreaking studies demonstrated that, in fact, stem cells are present in the mature brain that can give rise to both neurons and astrocytes in culture (Reynolds and Weiss, 1992; Richards et al., 1992). Follow-up work revealed that glia, including astrocytes, could act as neuronal precursors as well (Doetsch et al., 1999; Laywell et al., 2000; Seri et al., 2001). Thus, while astrocytes support and modulate neuronal function in the CNS they may also play a role in neuronal regeneration or brain remodeling.

1.2 The role of astrocytes in CNS injury

Almost any insult that upsets the delicate balance in the central nervous system will elicit a response from astrocytes, which function to maintain homeostasis. Upon injury, astrocytes are said to “activate” or become “reactive” – terms meant to describe a rapid change in gene expression and morphology that characterize this phenotype. Because of their myriad cell surface receptors and their close proximity to both neurons and the vasculature, astrocytes respond to a wide array of injuries including physical trauma, toxic chemicals, viral infection, hypoxia due to stroke, disruption by tumors, prion associated spongiform

encephalopathies, and certain neurodegenerative diseases including Alzheimer's disease (Norton et al., 1992; Zlotnik, 1968; Beach et al., 1989).

The stereotypical characteristics of a reactive astrocyte are increased proliferation (Koguchi et al, 2002; Kato et al. 2003) and expression of intermediate filament proteins glial fibrillary acidic protein (GFAP) and vimentin (Bignami and Dahl, 1976; Schnitzer et al., 1981; Fedoroff et al., 1983). Morphologically, reactive astrocytes hypertrophy, thickening their processes and becoming migratory. Because many proteins are up or down-regulated, a variety of other markers for reactive astrocytes have been identified (Ridet et al. 1997).

The bulk of changes occurring in a reactive astrocyte are adaptive and prevent further damage to surrounding brain tissue. For example, astrocytes increase their expression of glutamate transporters and the enzyme glutamine synthetase, effectively improving their ability to clear this neurotransmitter from the CSF where it might cause additional damage (Hardin et al., 1994). Reactive astrocytes also protect neurons by releasing a variety of trophic factors including nerve growth factor (NGF) and brain-derived neurotrophic factor (BDNF), among others (Liberto et al., 2004). These factors work to improve neuronal survival and encourage axon regeneration – a critical effect particularly where physical trauma has severed axon fibers.

In many types of non-traumatic injury, or in areas spatially separate from direct trauma, the activated astrocytes revert to their previous "resting" state once the environment is controlled. Because they do not structurally alter their environment, this response is referred to as isomorphic gliosis. In contrast, physical

trauma leads to anisomorphic gliosis, where the astrocytes profoundly modify the lesion site in their efforts at wound healing.

Anisomorphic gliosis is characterized by astrocytes that migrate and interdigitate their processes in an attempt to seal off the area of injury. The reactive astrocytes deposit large amounts of collagen and other ECM proteins to form a basal membrane (Bernstein et al. 1985), which helps to restore the blood-brain barrier (Janzer and Raff, 1987) and contracts to bring the wound edges together. Together, this mass of astrocytes and extracellular matrix is known as the glial scar.

1.3 Controversial effects of the gial scar

This scarring response is another adaptive strategy developed to prevent further damage to areas surrounding the lesion. Scarring restores the integrity of the injury site and fills the space left by dead or dying cells (Faulkner et al., 2004; Myer et al., 2006). The problem arises when axons severed by the trauma attempt to migrate along their previous track to reform the synapses maintained prior to the injury. As observed by Ramon y Cajal as early as 1928, axonal growth cones encountering the glial scar become rounded or club shaped and stall their forward progression. They can remain in this state for years after the injury. Much attention has been given to these “dystrophic end-bulbs” and to the factors that contribute to their formation (Reviewed by Stichel and Muller 1998). Contrary to Cajal’s belief that these end-bulbs were static and quiescent, recent live-cell imaging studies of neurons *in vitro* and *in vivo* revealed that, while stalled in their directed migration, dystrophic growth cones are actually highly dynamic (Tom et al., 2004). When these

growth cones encountered the boundaries of the scar, their forward motion stopped, but the leading edge continually extended membrane veils and retracted them, taking in vacuoles by endocytosis. These results suggest that neurons maintain their ability to extend even dystrophic growth cones, but that the glial scar presents a barrier to extension.

Functional recovery after axotomy requires that the neurons re-extend along a previous pathway to recover their damaged connections, and in this regard, they have proved to be surprisingly resiliant. In the peripheral nervous system where no astrocytes are present to form scar tissue, axons are able to regenerate along previous pathways and form functional synapses (David and Aguayo, 1981; Nguyen et al. 2002). Neurons in the central nervous system transplanted away from the injury site also show a robust ability to extend axons (Davies et al., 1997). It is only when these neurons encounter the perimeter of the glial scar that their growth cones become dystrophic and extension stops (Davies et al. 1999). Axons near the scar may either extend short sprouts into the area where they arrest (Frisen et al. 1993; Li and Raisman 1995), or they turn and migrate by another route, following spans of undamaged tissue or blood vessels (Clemente 1955; Guth et al. 1983; Kruger et al. 1986).

1.4 Inhibitory components of the glial scar

The precise mechanism by which the scar inhibits axon regeneration is unclear, though two general mechanisms appear to play collaborating roles. First, the scar might present a physical barrier that is impenetrable to the growing axons.

The physical blockage may be a result of the thick web of astrocyte processes, the deposition of a dense ECM, or a combination of both. The second factor is that astrocytes and other cell types in the injured area release molecules that are non-permissive for axonal extension. Proposed inhibitory molecules include cytokines, products of metabolism, or extra-cellular matrix proteins that lead to growth cone arrest or turning.

Identification of the cellular components and signaling molecules that cause growth cone arrest has largely been accomplished using *in vitro* assays. Because the majority of these assays utilize embryonic neuronal populations, the results may not represent the effects of inhibitory molecules in the adult central nervous system. In some cases, pharmacological inhibitors are available for *in vivo* studies to measure the effects of pathway activation in injury models.

Some of the factors shown to inhibit axon outgrowth, including components of CNS myelin (Yiu and He, 2006), are present in the uninjured nervous system, and likely serve as guidance cues during development. During injury, these proteins, including Nogo (Prinjha et al., 2000) and myelin associated glycoprotein (MAG) (Mukhopadhyay et al., 1994), may be released from the disrupted myelin and prevent axon extension through the injury site (Tang et al., 2001.)

Reactive astrocytes present another barrier to neurite outgrowth by increasing their production of chondroitin sulphate proteoglycans (CSPGs) (McKeon et al, 1991). CSPGs, including aggrecan, brevican, neurocan and versican, are comprised of sulphated glycosaminoglycan chains attached to a protein core. (Morgenstern et al, 2002). In several studies, these side chains, and in some cases

the protein core itself, presented a non-permissive substrate for axon extension (Snow et al, 1990; Carulli et al, 2005; Ughrin et al, 2003).

1.5 Experimental treatment strategies

Treatment of reactive gliosis is necessarily complicated, and attempts have been made to remove scar tissue through surgical procedures, enzymatic break down, and X-irradiation (Puchala and Windle 1977; Kalderon and Fuks 1996). Few have been successful. Current treatement strategies focus on preventing scar formation so that axons are allowed to extend over their previous tracks to produce active synapses and functional recovery in the shortest time possible. Simple ablation of the reactive astrocytes is not beneficial, as this leads to further damage including long-term failure of the blood-brain barrier, tissue death, severe demyelination of local axons, and poor functional recovery (Faulkner et al. 2004). This study underscores a major trade-off facing the clinical treatment of brain and spinal cord injury: after trauma, reactive astrocytes play a protective role, while their continued presence in the glial scar prevents functional recovery. Clearly, then, effective treatment strategies must support adaptive astrocytic responses while eliminating those that inhibit neural regeneration.

To that end, most current research has focused on either preventing the physical blockade presented by the scar or on identifying and inactivating the chemorepulsive factors present in the injury site. Stichel and colleagues (1999) used injections of collagen synthesis inhibitors to prevent the formation of the basal membrane in a post-commissural fornix injury model. They observed increased

axonal migration through the lesion area when collagen aggregation was inhibited, though these results do not seem to translate well throughout the CNS (Joosten et al. 2000, Hermann et al. 2001). Chondroitin sulfate proteoglycans – the potent inhibitors of axonal extension (Tom et al. 2004) -- are also under investigation because they have been identified in the glial scar *in vitro* and may be the repulsive component adhering to the collagen matrix (Fitch and Silver, 1997; Grimpe and Silver, 2004).

Some of the most promising strategies for preventing reactive gliosis target the signaling molecules that induce the reactive phenotype in the first place. Epidermal growth factor receptor (EGFR), when stimulated by its ligands, has an inhibitory effect on neurite outgrowth by a mechanism that is not well understood. (Koprivica et al., 2005; Schwab et al., 2006). This observation stems from studies showing that the use of EGFR inhibitors improves axon regeneration after optic nerve injury (Koprivica et al., 2005) and a chronic glaucoma model (Liu et al., 2006). In a spinal cord injury model, rats receiving the EGFR inhibitor achieved significant improvement over controls in overall locomoter function, sensation, and coordination (Erschbamer et al., 2007). Histologically, the rats receiving treatment had more spared tissue, and less scar tissue, than controls. Because the expression of EGFR is much higher in astrocytes than in neurons, and because EGFR activation triggers a change to the reactive phenotype, an astrocyte-mediated mechanism for these observations has been proposed (Liu et al., 2006).

One proposed mechanism for EGFR activity in reactive astrocytes is to stimulate proliferation (Levison et al., 2000). Whether through EGFR activation or

other mechanisms, astrocyte proliferation is a commonly described feature of reactive gliosis (Koguchi et al., 2002; Kato et al., 2003; Di Giovanni et al., 2005). Pharmacological inhibition of cell cycle progression after hypoxia decreased astrocyte proliferation *in vitro* and decreased lesion volume in an *in vivo* model of cerebral ischemia (Zhu et al., 2006). These studies also revealed a decrease in neuronal apoptosis, probably as a result of cell cycle inhibition in these post-mitotic cells.

Another strategy to prevent glial scar formation has been to disrupt the intermediate filament cytoskeleton, a direct reversal of the astrocytes' natural tendency to up-regulate GFAP and vimentin in response to injury. Knockout mice which are null for both GFAP and vimentin showed functional motor recovery sooner after spinal cord injury than wild-type animals (Menet et al. 2003). These mice showed a decrease in astroglial reactivity and a greater incidence of axonal sprouting. $GFAP^{-/-}$ $vim^{-/-}$ astrocytes were previously shown to exhibit reduced migratory ability (Lepekhin et al., 2001), which correlates well with the *in vivo* observation of a reduced reactive phenotype and scar formation. Other experiments using $GFAP^{-/-}$ $vim^{-/-}$ mice revealed that the lack of intermediate filaments provided a permissive environment for neuronal migration and extension after retinal transplant (Kinouchi et al., 2003).

Taken together, these data suggest that astrocytes are important in wound healing and minimizing inflammation of a lesion site, but that their migration leads to a physical barrier to neurite extension. Preventing scar formation has been shown to create a permissive environment for axon regeneration. Complete ablation of

reactive astrocytes is harmful, but reducing other aspects of their reactive phenotype may prove to be beneficial in treating injury.

1.6 The actin cytoskeleton regulates cell motility and morphology associated with gliosis

While previous studies have examined the role of intermediate filaments in the pathway to reactive astrocytosis, other targets exist. Data from the studies cited above suggest that it is a change in morphology or cell migration that lead to scar formation and inhibition of axonal extension. Following this line of reasoning leads us to hypothesize that prevention of anisomorphic gliosis would permit axon regeneration and functional recovery.

Though cell morphology and motility are modulated by the intermediate filaments and the microtubule cytoskeleton, the actin cytoskeleton seems to play a much more central role. Rearrangements of the actin cytoskeleton are responsible for many cellular processes including migration, contractility, and cytokinesis.

Understanding the component proteins that make up the actin cytoskeleton is central to asking broader questions about cell morphology or migration. Briefly, actin proteins exist as monomers in the cytosol of all eukaryotic cells. Under certain conditions, these monomers polymerize into long, polarized filaments called F-actin. Individual filaments may be arranged into higher order arrays by proteins that either bind to the growing end or along the length of the filament. For example, α-actinin dimers cross-link actin filaments into thick bundles (Condeelis and Vahey, 1982) while a complex of proteins known as Arp2/3 binds to the side of existing filaments

and produces a branching filament at a fixed angle (Svitkina and Borisy, 1999). These structurally different arrangements give rise to functionally different actin arrays.

A host of other proteins affect the rate of assembly and disassembly of actin filaments. Of note, profilin binds to actin monomers in the cytosol and "charges" them by replacing their spent ADP with ATP, allowing them to be added to the end of a growing chain (Mockrin and Korn, 1980). Capping proteins work just as their name implies, blocking the end of a filament and preventing further addition. A family of proteins including VASP is thought to increase the rate of polymerization by competing with capping proteins and thereby pushing equilibrium toward extension (Barzik et al. 2005). Finally, proteins such as cofilin or gelsolin act to sever filaments and speed their depolymerization (Yin and Stossel, 1979; Nishida et al., 1984). With these basic tools for assembly, organization, and disassembly, a cell can assume complex shapes and move in surprisingly dynamic ways.

In vivo studies have revealed that in addition to increases in intermediate filament proteins, reactive astrocytes exhibit an increase in their F-actin content (Abd-El-Basset and Federoff, 1997). F-actin is all but absent in differentiated, stellate astrocytes of the adult brain, but upon injury, F-actin cables are assembled corresponding with an increase in α-actinin expression. The functional consequence of this actin assembly is unclear, but it supports the hypothesis that a dynamic rearrangement of the actin cytoskeleton contributes to reactive gliosis and the formation of a glial scar.

1.7 Palladin – an actin associated protein that is up-regulated in reactive astrocytes

In 2003, Boukhelifa and colleagues published their observation that a recently discovered actin-associated protein called palladin was undetectable in the astrocytes of adult rat brain, but was rapidly up-regulated in astrocytes after a stab wound was made to lesion the cortex. Palladin was discovered and initially characterized just a few years earlier in the lab of Dr. Carol Otey (Parast and Otey, 2000) where they observed that palladin, a protein related to myotilin and myopalladin (Fig. 1.1 A), is expressed widely in embryonic tissue but is down-regulated in select adult tissues. Immunostaining of cultured cells revealed that palladin decorates actin stress fibers in a punctate pattern and co-localizes closely with α-actinin.

The palladin gene contains a series of nested promoters, and is differentially spliced, giving rise to three major isoforms (Fig. 1.1 B). The most abundant isoform runs as a doublet with an apparent molecular weight of 90-92 kDa. This isoform was the first to be cloned and is the most thoroughly characterized. An examination of the protein structure revealed a canonical binding motif for the actin associated protein VASP in a proline rich region of the N-terminus. This interaction was later confirmed biochemically (Boukhelifa et al. 2004) (Fig 1.2). This same short poly-proline region has also been identified as a binding site for actin associated proteins profilin, Eps8, Spin90, and Src (Boukhelifa et al., 2006; Goicoechea et al., 2006; Ronty et al., 2007)

Because of palladin's close apposition to α-actinin as observed by immunostaining, a binding interaction was sought and mapped to a region near the center of the protein (Ronty et al. 2004). The C-terminal half of palladin is composed of three immunoglobulin-like repeats which are similar to those described for myotilin, the striated muscle protein titin, and others (Fig. 1.1 A). The function of these domains had not previously been elucidated, though homologous regions in other proteins had been shown to bind α-actinin or myosin II (Sorimachi et al. 1997). Other studies, including one on palladin's family member myotilin, showed that regions containing Ig-like domains are able to bind directly to F-actin (Salmikangas et al., 2003; von Nandelstadh et al., 2005).

More recent studies in our lab have shown that astrocytes express another palladin isoform with an apparent molecular weight of 140 kDa. Expressed under the control of an upstream promoter (Fig 1.1 B), this isoform is identical to the 92 kDa protein except for an extended N-terminal region containing two additional VASP binding domains, a region capable of binding to the actin-associated protein Lasp-1 (Rachlin and Otey, 2006) and another Ig-like domain (Fig 1.2).

Over-expression of exogenous 90 kDa isoform in fibroblasts leads to the hyper-bundling of stress fibers (Parast and Otey, 2000), implying that palladin is a bundling protein or an activator of other bundling proteins. The number and diversity of palladin's binding partners identified thus far suggest that it may act as a scaffold – a protein responsible for organizing a cohort of other molecules spatially and temporally. The cell may use scaffolding molecules to ensure that the complex job

of actin assembly, bundling, and breakdown occur in the proper place and order for cell motility to occur.

Palladin's role in other cell types and tissues indicate that it plays an important role in cell migration – a critical process in glial scar formation. During development, palladin is expressed in every embryonic tissue that was tested at a stage when cell migration is most pronounced, though it is down-regulated in many adult tissues (Parast and Otey, 2000). Palladin has been specifically implicated in the migratory potential of neural crest cells that move out of the neural folds during development. In their pre-migratory state, these cells up-regulate the expression of intermediate filament proteins. A sub-population of neural crest cells go on to up-regulate a small subset of actin cytoskeleton components, including palladin, just before they begin to migrate out of the neural fold. (Gamill and Bronner-Fraser, 2002). Indeed, a striking feature of the palladin-null mouse is embryonic lethality at embryonic day 15.5 with neural tube closure defects. This mouse also exhibits facial clefting and herniation of the liver, indicative of a migration defect. (Luo et al, 2004). Fibroblasts cultured from these mice showed aberrant cytoskeletal architecture and a reduced migration rate.

Aside from its role in the neural crest, palladin appears to be critical at other stages of brain development. In the brain of adult rats, a unique 85 kDa isoform was detected by Western blot that is smaller than the more common 90-92 kDa isoform (Hwang et al., 2001). Immunohistochemistry was used to demonstrate that palladin is preferentially localized to excitatory nerve terminals, and has a non-uniform distribution across brain regions. Immunostaining also revealed that the palladin was

preferentially localized to the developing axons, but not to dendrites (Boukhelifa et al., 2001). Using an antisense knockdown approach in cultured cells left them unable to extend neurites after the loss of palladin. These data suggest that palladin has a role in axonal extension and may also contribute to maintenance of the mature synapse.

In studies of cancer metastasis, palladin also appears to play a role in cell migration rates. Observations in our lab indicate that an increase in palladin expression correlates with increased metastatic potential among a group of breast cancer cell lines (unpublished data). A mutated form of palladin was also recently identified as a contributing factor in the development of a highly invasive familial pancreatic cancer (Pogue-Geile et al., 2006). Because the mechanisms for cell migration and actin cytoskeleton dynamics are so conserved over evolution, it is likely that these observations from other cell types will inform current and future studies of astrocyte migration during glial scar formation.

1.8 Astrocyte cell culture for the study of actin dynamics

Since 1980 when McCarthy and deVellis published their landmark paper describing a method for purifying astrocytes from the cortex of neonatal rodents, primary cell culture has been the preferred system for the study of actin dynamics in astrocytes. The goal has long been to create a cell culture model for reactive gliosis and the gial scar, and a wealth of research exists on this subject (reviewed by Wu and Schwartz, 1998). To date, no model perfectly mirrors the phenotype observed in animals, but close approximations exist.

Primary astrocyte cultures are derived from dissociated neonatal cortex and are purified from less adherent cell types by shaking (McCarthy and de Vellis, 1980). At this stage, they have a polygonal, fibroblast-like appearance when grown in plastic dishes. Because they are embryonic astrocytes, they do not possess the morphology or expression profile of the differentiated cells found in an adult. One method for differentiation is the addition of a non-hydrolyzable cAMP analogue that causes the cells to exhibit some of the characteristics of adult astrocytes. The addition of dibutyril cAMP (dBcAMP) leads to disassembly of the actin cytoskeleton and a retraction of the cytoplasm, giving the cells the stellate appearance of adult astrocytes with a small cell body and many thin processes (Safavi-Abbasi et al., 2001). This treatment also converts the embryonic astrocytes to a non-motile phenotype as assessed by migration after implantation in the brain (Chu et al. 1999; Hatton and Hoi, 1993). Other important markers such as GFAP are normally high in the embryonic astrocyte and the addition of dBcAMP does not alter this significantly. Interestingly, differentiation in dBcAMP leads to a down regulation of palladin protein (Boukhelifa et al. 2003).

With these “differentiated” stellate astrocytes, one can begin to ask questions about hypertrophy and migration associated with the reactive phenotype *in vitro*. Several methods exist for inducing gliosis in culture. A popular method is to create a physical scratch wound using a sterile needle or pipette and allowing the astrocytes to migrate into the empty space (Seniuk et al. 1994; Yu et al. 1993). This method leads to astrocyte hypertrophy at the wound edge, an increase in mitosis, and a 70-80% increase in GFAP content, validating it as a model of gliosis. This approach is

suitable for asking questions of migration, but another method is required to perform biochemical studies or semi-quantitative expression analysis.

In order to obtain large numbers of reactive astrocytes for biochemical analysis, it is necessary to mimic injury of a large area. This can be accomplished by supplementing the growing media with one or more cytokines or peptide signals known to activate astrocytes *in vivo.* Factors that have been proposed to mediate a reactive response include IL1-β (Herx et al. 2000; Herx and Yong 2001), IL-6 (Woiciechowsky et al. 2004) and endothelin (Koyama et al., 1999). In primary culture, the addition of inflammatory cytokines leads to the flattening and hypertrophy of astrocyte processes, further supporting the validity of an *in vitro* model.

1.9 Current Study

In summary, astrocytes in the glial scar contribute to the blockade of neuronal regeneration and functional recovery after brain and spinal cord injury. In this study, we seek to deepen our understanding of palladin's role in the reactive phenotype.

In Chapter 2, we utilize a primary astrocyte cell culture models and a traumatic injury model to understand the expression pattern of two palladin isoforms *in vitro* and *in vivo*. We then work to determine the cellular effects of palladin expression on astrocyte migration and adhesion.

In Chapter 3, we work to understand the cellular mechanisms that underlie migration through a complex tissue environment as we explore palladin's role in dynamic actin arrays. We examine the localization and function of palladin in the

highly-dynamic dorsal circular ruffles and podosomes that form after growth factor stimulation. These processes have been implicated in the invasion and migration of cancer cells and fibroblasts, and may be a conserved feature of cells that must migrate through tissue, including reactive astrocytes.

In Chapter 4, we examine palladin's biochemical role in binding and bundling filamentous actin using purified proteins. We identify a novel actin-binding domain in palladin's C-terminus, and describe evidence for a fragment that can both bind and bundle actin filaments.

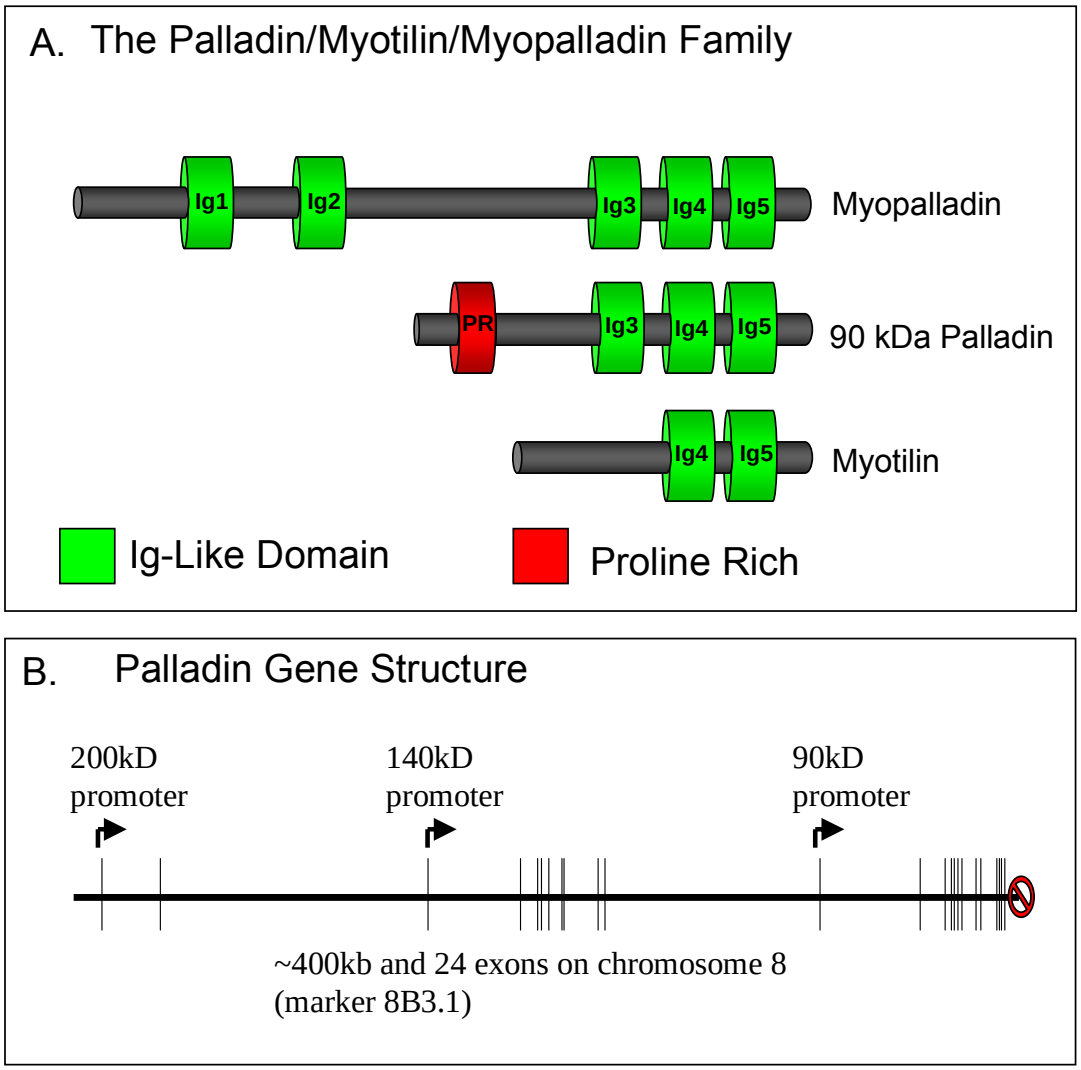

Figure 1.1. The palladin gene. A) Palladin is a member of the same family as striated muscle proteins Myotilin and Myopalladin. All three family members share a similar domain structure containing variable numbers of immunoglobulin-like domains. B) Three common palladin isoforms arise from nested promoters within the same gene.

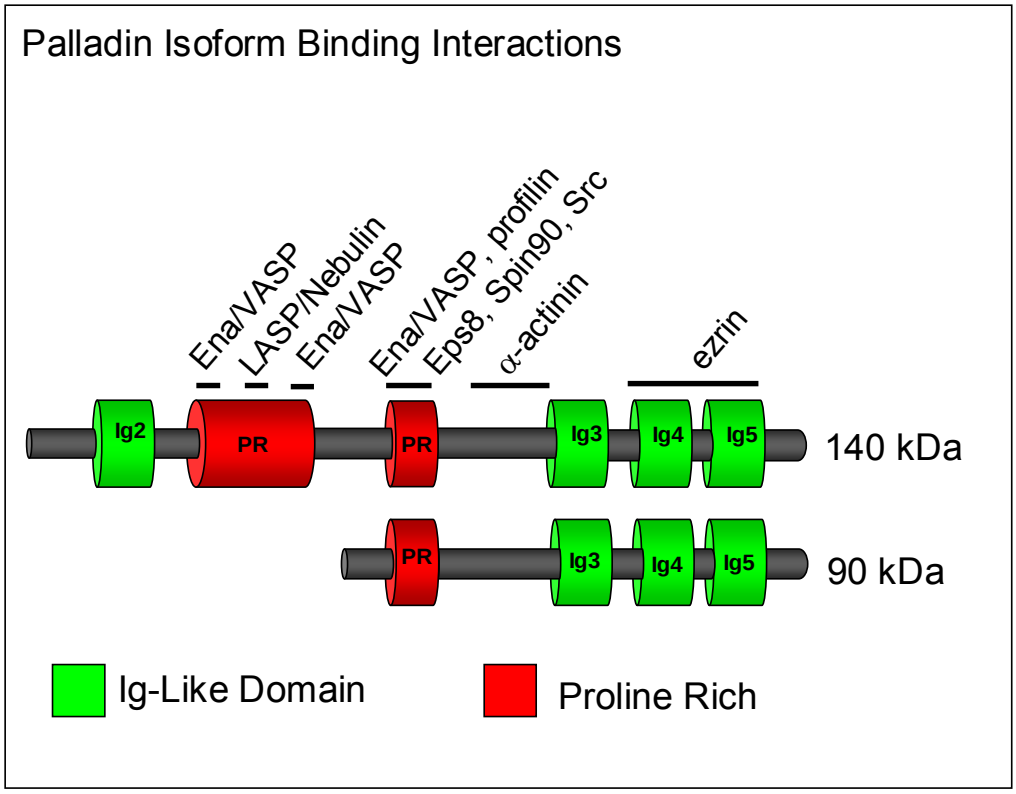

Figure 1.2. Palladin's binding interactions. This schematic shows a subset of palladin's published binding interactions. As the 90 kDa protein is contained entirely within the sequence of the 140 kDa protein, the two share many of the same binding interactions.

CHAPTER 2

PALLADIN EXPRESSION AND FUNCTION IN REACTIVE ASTROCYTES

2.1 INTRODUCTION

After brain and spinal cord injury, astrocytes of the central nervous system undergo a series of well-defined changes including proliferation, hypertrophy, and increased expression of the intermediate filament protein GFAP (Davies et al., 1999). Persistent glial activation results in a dense meshwork of astrocytes and extracellular matrix known as the glial scar. This scar tissue has been shown to inhibit axon outgrowth, thereby preventing functional reconnection of severed axons. The exact mechanism of glial scar formation is not yet known, but it is assumed that activation and migration of astrocytes are involved. The origin of activated astrocytes that contribute to the formation of the glial scar is unclear. One possibility is that activated astrocytes differentiate from multipotential progenitor cells and migrate to the injury site (Moon et al., 2004; Wang et al., 2004). One source for the progenitor cells that has been identified is the area of the gray matter surrounding the central canal of the spinal cord, but whether other periventricular zones of the brain play a similar role is unknown. Alternatively, the existing astrocytes in the area surrounding the injury site may be activated and proliferate (Fawcett and Asher, 1999; Mothe and Tator, 2005).

One of the most distinct morphologic changes in the process of glial scar formation is the increased expression of glial fibrillary acidic protein (GFAP) in cells around the injury site. GFAP is a specific cellular marker for differentiated astrocytes and is the main component of the glial scar. However, it is also present in quiescent, non-reactive astrocytes, and can not be used as a marker for activation of astrocytes.

Contemporary markers for glial cells that undergo activation and migration in several clinical paradigms and experimental models of injury to the CNS and glial scar formation are the embryonic intermediate filaments nestin and vimentin (Calvo et al., 1991; Baldwin and Scheff, 1996; Sahin Kaya et al., 1999). Nestin is a protein transiently expressed in multipotential stem cells and in proliferating progenitor cells in early embryogenesis. In the adult CNS, it is re-expressed in reactive astrocytes surrounding sites of injury. Presumably, this process represents a reversal of the process of differentiation to an immature state that facilitates remodeling after injury (Douen et al., 2004). Vimentin is an embryonic protein that is expressed in cells of mesenchymal derivation with negligible expression in the adult brain. However, it may be significantly re-expressed around the site of injury, and can contribute to the formation of the glial scar (Wang et al., 2004; Alonso, 2005).

Another marker for activated glia that can be detected with immunocytochemistry is A2B5. It is cell surface ganglioside, which was initially detected in neurons, but was later shown to be expressed also in non-neural cells, including glial precursor cells and reactive astrocytes (Drago et al., 1989): the proliferating oligodendrocyte progenitor cells can differentiate into oligodendrocytes or reactive astrocytes, and both of these cell types express A2B5 during

differentiation. The utility of A2B5 as a marker is supported by the fact that it is selective for differentiating glia and is not expressed in non-reactive astrocytes (Scolding et al., 1999).

Palladin is an intracellular protein expressed by neurons throughout the CNS. It is most ubiquitous in the olfactory bulb, cerebral and cerebellar cortex, hippocampus, amygdla, superior colliculus, and the spinal cord (Hwang et al., 2001). Functionally, palladin has been shown to play an essential role in controlling cell shape and cytoskeletal architecture in cell culture models through its association with stress fibers (Parast and Otey, 2000). In the developing CNS, palladin is up-regulated in a population of neural crest cells that migrate out of the neural fold (Gamill and Bronner-Fraser, 2002).

The palladin gene contains a series of nested promoters that give rise to at least three distinct isoforms in rodents. The 90 kDa isoform contains three immunoglobulin-like domains in its C-terminus, whose function we examine in Chapter 4. At its N-terminus, a proline-rich region has been previously shown to bind members of the Ena/Vasp family, Profilin, Eps8, and other proteins (Boukhelifa et al., 2004; Boukhelifa et al., 2006; Goicoechea et al, 2006). Finally, an interaction with the actin bundling protein α-actinin is located near the center of the 90 kDa protein (Ronty et al, 2004). To date, all of palladin's known binding partners are actin-modifying proteins. This suggests that palladin may act as a unique molecular scaffold with the ability to coordinate the interactions and activities of a cohort of proteins that regulate cytoskeletal remodeling.

An additional isoform, with an apparent molecular weight of 140 kDa, is transcribed from an upstream promoter on the palladin gene. This nested pattern of transcription results in a translated protein that contains the entire 90 kDa isoform as its C-terminus. Thus, the 140 kDa isoform likely shares all of the binding interactions described for the 90 kDa isoform. At its N-terminus, the 140 kDa isoform exhibits an extended region which contains an additional Ig-like domain and a large proline-rich region. Binding sites for the actin-binding protein Lasp-1, and additional binding sites for Ena/Vasp proteins have been mapped to this domain (Rachlin and Otey, 2006). Though the 140 kDa isoform is widely expressed in embryonic tissues, it is selectively down-regulated in many adult tissues. In this study, we utilize reagents that uniquely identify the 140 kDa isoform to further understand the expression pattern of palladin isoforms in reactive astrocytes both *in vitro* and *in vivo.*.

Previously, we have utilized a primary astrocyte cell culture model and a rat model of brain injury to demonstrate that palladin immunoreactivity is rapidly increased in reactive astrocytes surrounding the wound, suggesting that palladin may function as a critical inducible scaffold in glial scar formation (Boukhelifa et al., 2003). We here extend this work by describing the expression patterns of two palladin isoforms and by testing whether palladin expression is increased in the astrocytes that also express intermediate filaments in response to injury. By studying the time course and co-expression pattern of palladin and several markers of cell migration, proliferation, and differentiation following injury to the brain, we show that palladin is involved in the process of activation and migration of astrocytes that contribute to glial scar formation.

2.2 MATERIALS AND METHODS

Primary astrocyte cell culture

Brains from E18 rat embryos were removed and transferred to a culture dish containing calcium/magnesium-free (CMF)-Hanks' balanced salt solution (HBSS): The cortex was dissected from each brain, minced, and placed in a 15-ml tube containing 5 ml of CMF-HBSS. Dispase II was added to a final concentration of 2.5 U/ml, the tube was sealed and the tissue was incubated for 15–20 min at 36°C. The tube was transferred to a sterile hood and the tissue pieces were gently triturated with a 10-ml pipette. The tissue pieces were allowed to settle for 2 min and the cells in suspension (three to four ml) were transferred to a sterile culture tube containing 25 ml of complete culture medium (MEM + 10% fetal bovine serum + 20 µg/ml gentamycin). An equivalent volume of CMF-HBSS was added back to the tube and the procedure repeated until most of the tissue was dissociated (five to six cycles). Dissociated cells were diluted in 40–50 ml of complete medium at a concentration of 1–2 × 106 cells/ml. Cells were seeded into poly-lysine-treated Falcon 75 flask at a final density of 20,000 cells/cm^2. When cell density reached confluence (~2 weeks), media was replaced with Dulbecco's MEM and placed in a shaking incubator at 225 RPM overnight. The following day, cells were trypsinized and plated on laminin coated coverslips at densities between 20,000 and 50,000 cells/cm^2. For scratch wound assays, the cells were grown on a 12-mm coverslip coated with poly-lysine. Cells were fed on the following day by a complete medium exchange to eliminate debris, followed by a 50% exchange every 2–3 days thereafter.

Western blot

Astrocytes were sub-cultured in 60 mm dishes and allowed to grow to confluence. Cultures were treated with 500 mM dBcAMP for 48 hours, then supplemented with 200 nM endothelin over the indicated time course. Cells were lysed in Laemmli buffer, boiled, and spun at 150,000 x g to pellet the insoluble fraction, then resolved by SDS-PAGE. Western blot was performed with a palladin polyclonal antibody. Secondary antibodies tagged for infra-red detection were used in combination with the Licor Odyssey imaging system. Tubulin expression was used as a control.

RT-PCR

Astrocyte cultures were differentiated in 500 mM DB cAMP for 48 hours then treated with 200 nM endothelin for 1, 6, 12, or 24 hours. Cells were harvested by scraping in RNALater (Ambion), spun, and frozen at -80° C until further processing. RNA was extracted using the RNEasy mini kit (Qiagen) following the manufacturer's protocol. For each sample, 5 μg of RNA were DNase treated following the manufacturer's protocol (Ambion). A no-template control sample using only water was prepared in parallel. After DNase treatment, the samples were divided in half for the generation of cDNA by reverse-transcription PCR. Half of the sample (2.5 μg) was prepared in buffer with Reverse Transcriptase (RT), while the other half was prepared as a no-RT control.

The cDNA samples were prepared for semi-quantitative Real-Time PCR using the JumpStart SYBR Green ready mix system. Samples were run in triplicate on a RotorGene RG-3000 (Corbett) with no-template and no-RT samples as controls.

The 90 kDa and 140 kDa isoforms were distinguished by designing primers that amplified unique exons. For the 90 kDa isoform, primers were (Forward) 5'-CCTCTTGCTTCGCTGAGAC and (Reverse) 5'-CAGGCGCACTTGGTTCTG. For the 140 kDa isoform, primers were (Forward) 5'-ACCGGGACCCACGTC and (Reverse) 5'-CCTTCCCCTCCAGAACCA.

Adhesion assay and immunofluorescence

Four coverslips were spotted with 2 μL drops of 50 μg/mL Type-1 rat tail collagen (Sigma), mouse laminin (Gibco), and bovine serum fibronectin (Calbiochem) in a 3 X 3 grid and allowed to dry at room temperature. Coverslips were then blocked in 10 mg/mL bovine serum albumin (Sigma) for 30 minutes to prevent non-specific adhesion. Wild-type and palladin knockout cells obtained from E13 mouse embryos were trypsinized, resuspended, and counted with the addition of soybean trypsin inihibitor (Gibco) to obtain equal numbers. Cells were then washed in serum free DMEM and plated on the blocked coverslips for 2 hours at 37°.

After incubation, coverslips were washed thoroughly with 3 X 5 mL of PBS, fixed for 10 minutes in 4% paraformaldehyde, and permeablized in 0.2% Triton. Cells were stained with rhodamine phalloidin (Molecular Probes) and DAPI and visualized by epifluorescence using a Nikon TE200-U microscope with 60x objective lens and a Hamamatsu Orca-ER camera.

DAPI stained nuclei in three random fields per spot were counted and averaged to generate the adhesion rate measured as cells per field.

Migration Assay

Primary astrocytes were grown to confluence, purified by shaking, and split onto laminin coated, photo-etched coverslips at a density of 40,000 cells/cm^2. At the time of plating, cells were transfected with control or palladin knockdown siRNA (Dharmacon) using the Transit siQUEST transfection reagent (Mirus) and following the manufacturer's protocol.

Cells were incubated for 48 hours to allow for palladin knockdown, and media was replaced. Seventy-two hours after transfection, the cell monolayer was wounded with a sterile pipette tip, debris was washed away with fresh media, and the cells were allowed to recover for one hour before imaging. Six regions were imaged per coverslip over the course of 36 hours. After the timecourse was complete, the coverslips were lysed in Laemmli buffer and subjected to SDS-PAGE and Western blot analysis to determine the effectiveness of palladin knockdown.

Using the ImageJ software package, the distance across the denuded area of the coverslip was measured. Two measurements were made along the photoetched grid per image, giving a total of 20-30 measurements per timepoint per culture condition. Migration is plotted as the average wound width over time, plus or minus standard error.

Cortical stab wound and immunohistochemistry

All procedures involving animals were according to the guidelines of the Institutional Animal Care and Use Committee at the University of North Carolina. Twenty five male Sprague-Dawley rats (180-250 g) were used in this study, including 23 rats with cortical cuts and two controls. For surgery, rats were

anesthetized with ketamine (50 mg/kg) and xylazine (8 mg/kg) and placed in prone position in a stereotaxic frame. The body temperature was monitored and maintained with a heating pad. Scalp was incised along the midline and the skull was drilled on both sides 2 mm posterior to bregma and 5 mm lateral to midline. After opening the dura, a 3-4 mm long and 2.5 mm deep cortical cut was made with a steel micro blade with an effort to spare the cortical blood vessels. The scalp was sutured with 4.0 silk and the rats were allowed to survive for 12 hours, 1, 3, 7, or 14 days.

For fixation, rats were anesthetized with sodium pentobarbital (60 mg/kg) and perfused intracardially with 100 ml of normal saline containing 500 units of heparin sodium, followed by 700 ml of freshly depolymerized 4% paraformaldehyde in phosphate buffer (PB, 0.05M, pH 7.2). Brains were removed, post-fixed in the fixative used for perfusion for 3 hours, and stored in cold PB. Blocks containing the sites of cortical cuts were cut on a Vibratome at 50 μm and stored in PB at 4ºC.

For immunohistochemistry, the sections were pretreated with 50% ethanol in phosphate-buffered saline (PBS, 0.05M, pH 7.2) for 30 minutes, to improve antibody penetration, pretreated with 10% normal donkey serum (NDS) in PBS, to mask nonspecific secondary antibody binding sites, and incubated in a mixture of two primary antibodies. We combined our rabbit anti-palladin antibody (1:150) with either of the mouse anti-GFAP (1:1,500, Sigma), anti-nestin (1:200, Chemicon), anti-vimentin (1:200, Sigma) or anti-A2B5 (1:100, Chemicon) antibodies in PBS overnight at room temperature. After several rinses and incubation in 2% NDS for 10 minutes, the sections were incubated for 3 hours with a mixture of fluorescent secondary

antibodies (Cy3-conjugated donkey anti-rabbit and FITC-conjugated donkey anti-mouse; 1:200; Vector). After several rinses, sections were mounted on subbed slides, coverslipped with Vectashield (Vector), and examined on a confocal microscope (Leica TCS; Leica). Confocal images were collected in TIFF format, and contrast and brightness were adjusted with Photoshop (Adobe).

For quantification, the degree of expression of all five markers in cells of gray and white matter within 500 μm of the edges of the wound was scored on a 4-point scale (from "-" to "+++") in 3-5 confocal images per double staining per time point. To eliminate observer bias, sets of images were scored independently by two or three investigators blind to the source image; the variation between scores assigned by different investigators was analyzed by ANOVA (Microsoft Excel).

2.3 RESULTS

In our previous work, we showed that palladin immunoreactivity is undetectable in the astrocytes of adult mice, but that after stab injury, palladin is rapidly and robustly up-regulated in the reactive astrocytes (Boukhelifa et al., 2003). To confirm this response in reactive astrocytes *in vitro*, and to better understand the functional significance of palladin up-regulation, we turned to a primary cell culture model of injury. Using immunofluorescence and western blotting, we showed that palladin protein is down regulated when embryonic astrocytes are treated with dibutyril cAMP, corresponding to a decrease in filamentous actin (F-actin) and a stellate cell morphology. With immunofluorescence, we showed qualitatively that

palladin is up-regulated along the edge of a scratched astrocyte monolayer, mimicking the response we observe in injured animals.

Since that time, our lab and others have advanced in our understanding of palladin's gene structure, defined additional protein binding interactions, and described functional roles for palladin in a variety of cell types (Rachlin and Otey, 2006; Liu et al, 2006; Ronty et al, 2006) . With these advances, and the availability of new reagents and techniques, we sought to describe the expression pattern of palladin isoforms in embryonic, adult, and reactive astrocytes and to probe the functional significance of these changes.

90 kDa and 140 kDa palladin are up-regulated in reactive astrocytes *in vitro*

In previous attempts to show the increase in palladin expression in reactive astrocytes *in vitro,* it was difficult to obtain a large population of reactive cells simply by wounding a monolayer. In addition, immunological reagents had not been developed to detect the 140 kDa isoform efficiently. To overcome these technical difficulties, we experimented with the use of endothelin, a small peptide with the ability to activate astrocytes *in vivo (*Koyama et al., 1999), to create a uniform population of reactive astrocytes. In addiiton, we developed a new key reagent: a polyclonal antibody that specifically detects the extended N-terminal region contained in the 140 kDa isoform, but not the 90 kDa isoform (Characterized by Rachlin and Otey, 2006).

Primary embryonic astrocytes exhibit a flattened, polygonal morphology reminiscent of fibroblasts when grown in culture (Fig. 2.1). The addition of DBcAMP

causes a depolymerization of F-actin and leads to the stellate morphology with a small cell body and complex foot processes. When treated with 200 nM endothelin, the cell processes thicken and become hypertrophic, much like the description of reactive astrocytes *in vivo.*

In addition to these changes in morphology, palladin protein also increases rapidly, as measured by western-blot (Figure 2.2 A). Levels of 90 kDa palladin are low in the presence of DBcAMP, and the 140 kDa isoform is undetectable. By 1 hour after treatment with endothelin, a slight increase is apparent in the levels of the 90 kDa isoform. By six hours, the increase is robust and was sustained over a 48 hour time period. The 140 kDa isoform remains undetectable until about 24 hours after treatment with endothelin, and continues to increase to the 48 hour timepoint.

Though both palladin isoforms appear to be up-regulated in the presence of endothelin, this may be a non-specific response in which all actin-modifying proteins are up-regulated in the reactive astrocyte. To determine the specificity of palladin up-regulation, endothelin-treated astroctyes were prepared for SDS-PAGE and western blotting with antibodies against α-actinin, Mena, and the Arp2/3 sub-unit p-34 Arc (Figure 2.2 B). No change was seen in the expression levels for any of the proteins tested, suggesting that palladin is unique in its response to endothelin treatment.

We next decided to test whether endothelin treatment caused a change in gene transcription using Real Time RT-PCR. Because the coding sequence of the 90 kDa isoform of palladin is contained entirely within the coding sequencing of the

140 kDa isoform, RT-PCR primers were designed to amplify from the 5' untranslated region of the 90 kDa palladin mRNA, making the two isoforms distinguishable.

In the presence of dBcAMP, the mRNA levels of both palladin isoforms are relatively low and were used to establish the baseline to measure the fold-change after treatment. (Figure 2.3) After one hour of endothelin treatment, the level of 140 kDa palladin mRNA remains at baseline levels, while the 90 kDa isoform increases almost 20-fold. After 1 hour, the levels of 90 kDa message decreases, but remains between 5- and 10-fold greater than baseline. 140 kDa palladin message increases approximately 5-fold over dBcAMP treated cells at the 6 hour timepoint and remains at this higher level over the 24 hour timecourse.

Using an isoform-specific antibody (characterized by Rachlin and Otey, 2006), the localization of 140 kDa palladin was explored in cultures of primary rat astrocytes. Astrocytes were differentiated by treatment with 1mM dBcAMP for 48 hours and then scratched with a sterile needle. Immunofluoresence using the 140 kDa specific polyclonal antibody reveals that this isoform is undetectable at the wound edge one hour after injury (Fig. 2.4). By 6 hours, this isoform shows robust expression and localization to actin filaments. This increased expression was maintained over the 48 hour timecourse, mimicking the expression pattern obtained by RT-PCR.

Palladin knock-out cells show reduced adhesion to collagen, but not laminin

Mouse embryo fibroblasts cultured from a palladin knockout mouse were shown to exhibit reduced adhesion to collagen and fibronectin (Luo et al., 2005). Because collagen makes up a significant part of the extracellular matrix of the glial

scar, we sought to determine whether cortical cells from embryonic day 13 knockout mice also exhibit this adhesion defect.

Wild-type and knockout cells were subjected to an adhesion assay using coverslips spotted with collagen, fibronectin, and laminin. While both cell groups adhered equally well to laminin spots, palladin knockout cells showed a dramatic inability to bind the collagen matrix (Fig. 2.5). Fibronectin binding does not appear to be significantly reduced. This indicates that knockout cells are specifically inhibited in their ability to bind collagen, which may be due to an increase in B1 integrin degradation found in knockout MEFs (Liu et al., 2006).

Palladin expression does not alter migration rates in scratch wound assay

We next sought to understand the role of palladin up-regulation in the reactive phenotype. Reactive astrocytes become hypertrophic, migratory, and, with collagen, form a dense network of scar tissue. Our previous results showed that knocking down palladin in astrocytes leads to a reduction in stress fibers (Boukhelifa et al., 2003). In this study, we asked whether a change in palladin expression also affects the migration rate of astrocytes in culture.

Control and palladin knockdown astrocytes were plated on photoetched coverslips to form a monolayer. The monolayer was scratched with a sterile plastic pipette tip to create a single vertical wound and the width of the wound was tracked over 36 hours. There was no significant change in wound closure rate between control and knockdown cells, and closure was complete by about 24 hours after wounding (Fig. 2.6 A). Western blots confirmed that palladin knockdown was

successful (Fig 2.6 B). Morphologically, control and knockdown cells also looked similar throughout the timecourse, extending as a sheet to fill the denuded area (Fig. 2.7).

We hypothesized that this lack of change may be due to the fact that embryonic astrocytes express a host of actin-associated proteins, some of which may functionally overlap with palladin. To test this, control and knockdown astrocytes were differentiated in dBcAMP for 48 hours prior to wounding to convert them to a stellate morphology.

When these cells were wounded and tracked over 54 hours, the rate of wound closure was much slower when compared to embryonic astrocytes (Fig. 2.8). It is also possible to detect a short "lag" period before the cells begin to close the space in earnest. In dBcAMP treated astrocytes, the wound was still visible at the end of the time course, and cell processes were more elongated as they moved to close the space (Fig. 2.9). Measuring the rate of wound closure again revealed that there was no significant difference between control and knockdown cells (Fig 2.8).

Palladin is a marker for reactive astrocytes *in vivo*

A previous study demonstrated that palladin is up-regulated *in* vivo after brain stab injury to rat cortex (Boukhelifa et al., 2003). That study utilized a mouse monoclonal antibody that preferentially recognizes the 90 kDa isoform of palladin. Immunohistochemistry detected palladin expression in as little as 6 hours after injury, and this expression was persistent over the 7 day timecourse. In the current study, we asked whether 140 kDa palladin is also up-regulated *in vivo* and whether this

corresponds with the expression of other established markers of reactive astrocytosis.

In control rats, 140 kDa palladin was expressed in cells throughout the cerebral cortex, including neurons in the gray matter and sparse astrocytes in the white matter (Not shown). After injury, more astrocytes stained for palladin around the lesion, especially in the white matter; the number of 140 kDa palladin-positive cells reached a peak at the 3rd day post-injury, and then decreased (Fig. 2.10). The expression of markers for intermediate filaments GFAP, nestin, and vimentin, and the marker for glial precursor cells A2B5 followed a similar evolution in time (Table 2.1).

We further studied the pattern of co-localization of glial markers around the wound and the glial scar at different time points post-injury. The majority of 140 kDa palladin-positive astrocytes in the vicinity of the lesion expressed all other markers for activated astrocytes (Fig. 2.11). At 12 hours post-injury, palladin was expressed in numerous GFAP-positive astrocytes around the lesion (Fig. 2.11 A). When necrosis around the wound was pronounced, palladin immunoreactivity was detected along the edge of the wound, where immunoreactivity for GFAP was very weak. At one day post-injury, the expression of 140 kDa palladin, GFAP, vimentin, and A2B5 was increased, and nestin was detected for the first time in the area surrounding the wound (Fig. 2.11 B-D). At 3 days post-injury, 140 kDa palladin expression was increased along the edge of the wound, and was expressed not only in the area adjacent to the lesion, but also within the cortical gray matter up to several millimeters away from it. At 7 days, the glial scar at the edge of the wound

had strong stain for nestin, vimentin, and A2B5 and weaker stain for palladin. At 14 days, the staining for all markers subsided, and in most animals, the cortical wound was entirely replaced by a glial scar (Table 2.1).

Even though the wound was confined to the gray matter, proliferation and activation of astrocytes occurred also in the white matter underlying the lesion, frequently causing the glial scar to appear more pronounced in the white matter than in the gray matter. Palladin-positive cells in the white matter in the vicinity of the cortical lesion progressively increased 1-7 days post-injury and co-expressed GFAP, nestin, vimentin, and A2B5 (Fig. 2.12).

2.4 DISCUSSION

Palladin is an actin-associated phosphoprotein that exhibits dramatic effects on cytoskeletal architecture. Its ability to bind to a cohort of actin-modifying proteins suggests that palladin acts as a molecular scaffold by arranging and modulating the activities of its binding partners.

Palladin expression is developmentally regulated in astrocytes, showing robust expression in the highly plastic embryonic brain and down-regulation at maturity. After injury this pattern is reversed, as reactive astrocytes were shown to rapidly up-regulate palladin near the wound edge both *in vitro* and *in vivo* (Boukhelifa et al., 2003). This suggested that palladin expression is a conserved feature in the reactive phenotype. The observation that other actin modifying proteins are not specifically regulated in the reactive cell (Safavi-Abbasi et al., 2001; Kalman and Szabo, 2001; Fig 2.2 B, present study) suggests that the resting cell contains all the

necessary components for rapid cytoskeletal rearrangement, but that specific scaffolding or signaling molecules may be necessary for the assembly and coordination that result in migration or stress fiber formation.

In the present study, we have extended our previous understanding of palladin expression by demonstrating that palladin is transcriptionally regulated in a cell culture model of reactive gliosis. Message level of the 90 kDa isoform increases almost 20-fold within an hour after endothelin treatment, underlining not only the magnitude, but the speed with which the cell alters its expression. The observed increase is not sustained, though, and expression levels drop to approximately 5-times baseline. This expression pattern, if correlated *in vivo*, would support the use of palladin as a very early marker of reactive astrocytes after brain and spinal cord injury. That palladin expression is so rapidly increased after injury suggests that it has a critical role in the astrocytes' response to injury.

Our observations indicate not only that individual palladin isoforms exhibit temporally regulated expression, but also that each isoform appears to be independently regulated. Consistent with this observation, previous efforts to characterize palladin's developmental regulation demonstrated that palladin isoforms are differentially expressed during development (Parast and Otey, 2000), and that the larger isoforms exhibit a tissue-specific expression pattern. This suggests both that palladin's internal promoters are regulated by separate transcription factors and that individual isoforms may have unique functions within the cell.

In order to understand the basis of palladin's transcriptional regulation, computer analysis of palladin's promoter regions may be used to identify candidate

transcription factors. This analysis is necessarily complex due to the nested structure of palladin's promoters and the relative abundance of transcription factor binding sites. Efforts to identify conserved sequences among vertebrate species should help narrow a genome based search, but understanding the signaling pathways that lead to palladin up-regulation may provide more informed targeting. For example, a recent study by Jin et. al (2007) showed that palladin expression is decreased in cells when actin is pharmacologically depolymerized, and that its low expression in focal adhesion kinase null cells can be rescued by the expression of paired-related homeobox gene-1 protein. These observations place palladin within well-characterized transcriptional regulation pathways and narrow the number of candidate transcription factors that must be screened.

Another compelling question raised by the observation that palladin isoforms are differentially regulated concerns the functional consequence of the individual isoform expression patterns. As the 90 kDa isoform is contained entirely within the 140 kDa isoform, there is likely some functional overlap between the two. Both contain binding sites for α-actinin, Ena/Vasp family proteins, profilin, ezrin, etc. The extended N-terminal region of the 140 kDa isoform contains additional binding sites for the Ena/Vasp family of proteins, as well as a binding site for Lasp-1. Lasp-1 is a membrane associated protein that contains two copies of an actin binding domain and a C-terminal SH3 domain that facilitates its binding to palladin, as well as zyxin, lipoma preferred partner (LPP), and VASP (Keicher et al, 2004; Li et al, 2004; Rachlin and Otey, 2006). Though some of Lasp-1's cellular functions remain to be elucidated, recent reports indicate that Lasp-1 expression is critical for cancer cell

proliferation and migration (Grunewald et al, 2006). As reactive gliosis is also characterized by a change in proliferation and migration, it may be informative to examine the role of the 140 kDa palladin/Lasp-1 interaction in reactive astrocytes.

That mouse embryo fibroblasts (Luo et al., 2005) and cortical cells from knockout mice (present study, Fig. 2.5) have shown a reduced ability to bind collagen suggests a functional role for palladin up-regulation in the glial scar. Scar tissue, both in skin and CNS injuries, is characterized by dense deposits of collagen in the extracellular matrix. Likewise, in both tissues, cells near the injury site up-regulate palladin. Taken together, these results suggest that palladin expression may be necessary for adhesion to the collagen matrix, possibly through the stabilization of β1 integrin (Luo et al., 2005). Functionally, this may aid migration or contribute to the cell's ability to contract and draw together the wound edges. Attempts to measure astrocyte contractility were unsuccessful, as the astrocytes were unable to dimensionally distort collagen gels (data not shown). Further experiments in a tissue-specific, inducible palladin null mouse would help to elucidate some of these mechanisms. Inducing brain injury in this mouse would allow us to measure the *in vivo* migration rate of reactive astrocytes and determine the effects of palladin on wound occlusion and scarring.

We also show that knocking down palladin in embryonic and stellate astrocytes does not significantly alter their migration rates *in vitro*. This result was surprising, as Luo et al. (2005) showed that palladin knockout fibroblasts exhibit reduced migration rates. While astrocytes and fibroblasts are clearly different, this discrepancy is more likely due to the extremely long time-course required to

measure astrocyte migration. Scratch wound assays of astrocytes are a measure not only of migration, but also of proliferation (Zhu et al., 2006), and the long intervals used in our experiments likely amplify the effects of cell division. Indeed, there are some who suggest that the wound closing response is primarily a result of proliferation of astrocytes along the wound edge as a result of the loss of contact inhibition (Lanosa and Columbo, 2007). These studies showed that BrdU incorporation is high along the wound edge in the presence of serum, but is negligible in serum deprived cells, and is not affected *in vitro* by the age of the culture or the extent of wounding. This lack of proliferation by serum starved cells may explain the results we obtained in our wound closure experiments using cells grown in serum containing, or serum free plus dBcAMP containing media. In the serum starved, differentiated astrocytes, wound closure rate was reduced and the wound closure was marked by increased membrane protrusion without obvious cell-body translocation or "wound filling." These observations are consistent with the published observations that serum starved cells do not proliferate as rapidly as those in the presence of serum. In the future, single cell tracking models will therefore be more helpful in determining the effect of palladin expression on astrocyte migration in a two-dimensional culture. Perhaps more instructive would be the measure astrocyte migration through a three-dimensional matrix or transwell chamber.

In naive rats, 140 kDa palladin was expressed in neurons throughout the cerebral cortex, and in a few astrocytes in the subcortical white matter. In a previous study, using a different anti-palladin antibody, we reported that palladin expression in the mature brain is limited to a subpopulation of nerve terminals, and is not detected

in astrocytes (Hwang et al., 2001). The anti-palladin antibody used here (4IgNT) was raised against an epitope common for two larger forms of palladin (140 kDa and 200 kDa).

In rats with cortical wounds, 140 kDa palladin was significantly upregulated in astrocytes surrounding the lesion, particularly in the white matter, at the early stages of glial scar formation. In an earlier study, using a model of wounding a glial cell monolayer *in vitro*, we reported that palladin concentrates at the leading edge of the wound in the early stage, followed by a decline at later stages, while the staining for GFAP does not reach the edge of the wound (Boukhelifa et al., 2003). In the present study, following a similar spatial and temporal pattern of expression *in vivo*, 140 kDa palladin immunoreactivity increased along the edge of the wound 12 hours post-injury, and began to decrease after 7 days. The change in palladin expression was followed by a similar change in GFAP expression, suggesting that this palladin isoform is upregulated during an earlier, presumably more active, phase in the process of glial scar formation, and thus may have an important role in its initiation.

Palladin immunoreactivity was increased in astrocytes that expressed the intermediate filaments nestin and vimentin in the early phase of glial scar formation. Nestin and vimentin are expressed in multipotential stem cells during embryonic development and are normally undetectable in mature brain (Schnitzer et al., 1981; Wislet-Gendebien et al., 2005). However, they can be upregulated in glial cells following injury to the CNS and are thought to play a major role in the formation of glial scar through promoting activation and migration of astrocytes (Baldwin and Scheff, 1996; Douen et al., 2004; Moon et al., 2004). Although the origin of reactive

astrocytes is not unequivocally established, it is clear that these cells proliferate, migrate into the injury site, and contribute to the formation of glial scar. Since palladin has been associated with the control of migration of various cell types, its expression in reactive astrocytes supports its role in cellular proliferation and migration during the formation of glial scar.

While both nestin and vimentin were expressed in the gray matter surrounding the injury, vimentin was also expressed in the underlying white matter. The role of vimentin-positive astrocytes in the white matter is unclear, but recently it has been shown that vimentin can serve as a source of cytokines or as a physical conduit for migrating cells from remote sites, and can thus be associated with astrocytes migration (Wang et al., 2004). Since palladin was expressed by vimentin-positive astrocytes in white matter underlying the site of cortical injury, we suggest that it may be associated with migration of astrocytes from white matter into injury site during the process of glial scar formation.

A2B5 is expressed in glial precursor cells and reactive astrocytes (Rao et al., 1998). We observed increased immunoreactivity for palladin in astrocytes that expressed A2B5 following injury. Since palladin has been shown to control the cell shape following injury, and the process of differentiation inevitably includes changes in cell morphology, the observation that palladin is significantly upregulated in A2B5-positive astrocytes suggests that palladin is involved in the process of differentiation of glial precursor cells or reactive astrocytes in response to injury.

Even though in our model, the injury was confined to the gray matter, 140 kDa palladin expression was increased significantly more in the whiter matter than in

gray matter, coinciding with the apparently larger size of the glial scar in the white matter underlying the wound. Palladin expression was also increased throughout the injured cortex, at a considerable distance from the lesion. Similarly, nestin expression was detected around the lesion but also throughout the cortex in a model of cortical ablation (Douen et al., 2004). The mechanism of upregulation of proteins like palladin and nestin in cells far from a site of injury to the CNS is unknown.

Palladin up-regulation after injury is not confined to astrocytes of the CNS, as palladin expression has also been identified as a consistent feature in other cell types after tissue injury. These cells are often more plastic and migratory as a function of the wound-healing response. Similar to the astrocyte response, palladin was shown to be rapidly up-regulated as fibroblasts were differentiated into the highly-contractile myofibroblasts after TGF-β1 treatment (Ronty et al, 2006). TGF-β1 increased the expression of the 90 kDa palladin isoform, and led to the *de novo* expression of the 140 kDa form. The investigators were able to observe the same response using *in vivo* models of rat dermal wounds and human tissue samples. In each case, palladin was observed in myofibroblasts near the wound site, often before the expression of the classic myofibroblast marker α-Smooth Muscle Actin (SMA).

Palladin was also found to be up-regulated downstream of angiotensin II treatment in vascular smooth muscle cells (SMCs). SMCs become highly migratory after vascular injury, inducing the vessel remodeling that occurs throughout chronic hypertension. Not only was palladin detected in SMCs of the tunica media and

neointima of injured rat aorta, its expression was also shown to increase migration rate of SMCs in vitro. (Jin et al, 2007).

Based on these observations, palladin expression appears to be a highly conserved response to injury in a variety of tissues. Its role in these systems remains to be identified, but on the cellular level, palladin has been shown to modulate the higher-order structures of the actin cytoskeleton. How this modulation contributes to the cell's ability to migrate through a complex matrix or to increase the contractility of the wound edges will be the subject of future studies.

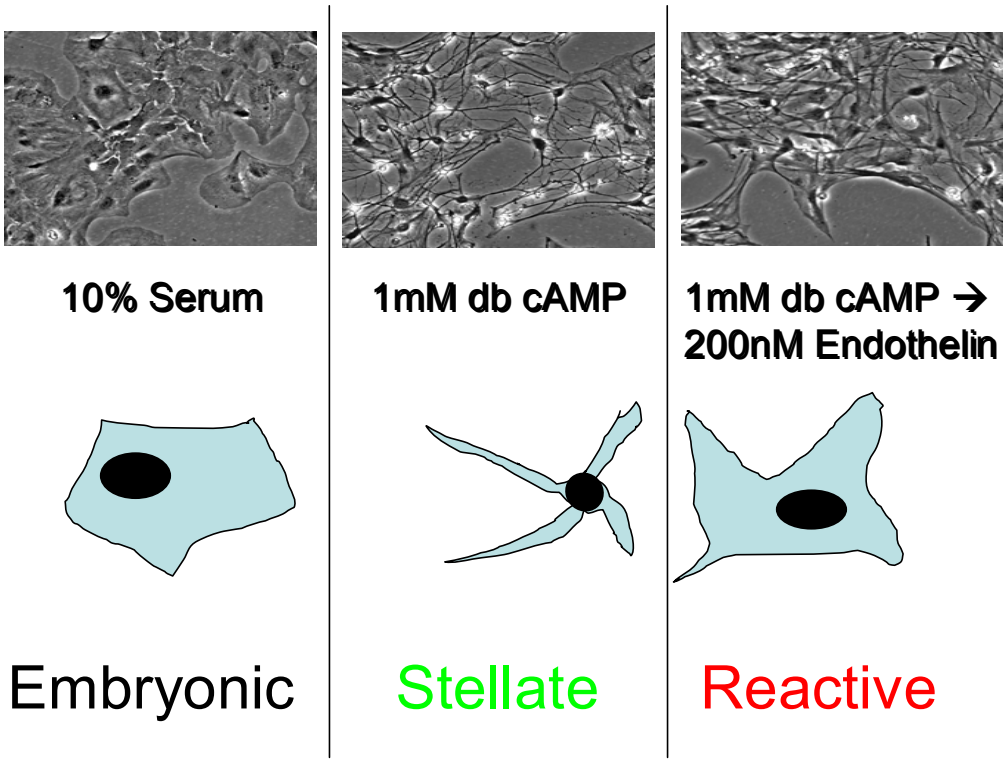

Figure 2.1 Endothelin treated astrocytes undergo a morphological change. Primary embryonic astrocytes are maintained in culture in the presence of serum, and exhibit a flattened, polygonal morphology. dBcAMP treatment causes the cell periphery to retract, inducing a stellate morphology reminiscent of mature astrocytes in the adult CNS. The addition of 200 nM endothelin to stellate astrocytes causes them to thicken their processes and hypertrophy, morphologically resembling the reactive phenotype.

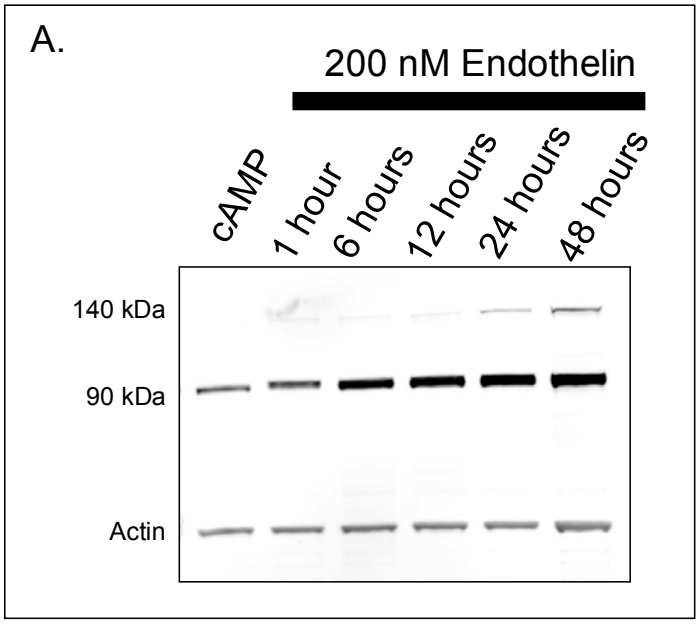
A.
200 nM Endothelin
cAMP
1 hour
6 hours
12 hours
24 hours
48 hours
140 kDa
90 kDa
Actin

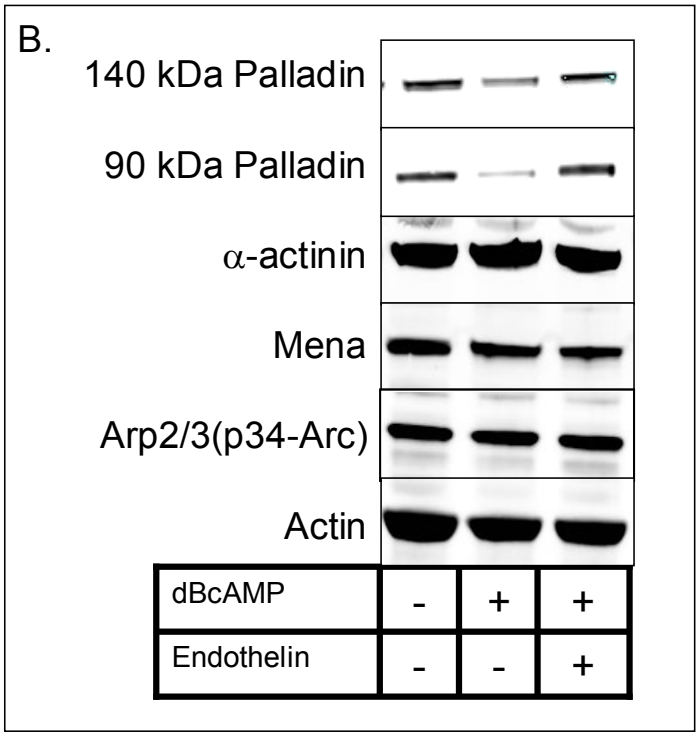
B.
140 kDa Palladin
90 kDa Palladin
α-actinin
Mena
Arp2/3(p34-Arc)
Actin
dBcAMP - + +
Endothelin - - +

Figure 2.2 Endothelin increases astrocyte expression of two palladin isoforms. (A.) Primary rat astrocytes were differentiated in dBcAMP containing medium and then treated with 200 nM endothelin over 48 hours. After 1 hour, protein levels for 90 kDa palladin increase noticeably, and continue to rise over 24 hours, where they plateau. 140 kDa palladin levels remain below the detection limit until 24 hours. (B.) Western blots reveal that the expression levels other actin binding proteins do not change in the presence of either dBcAMP or endothelin.

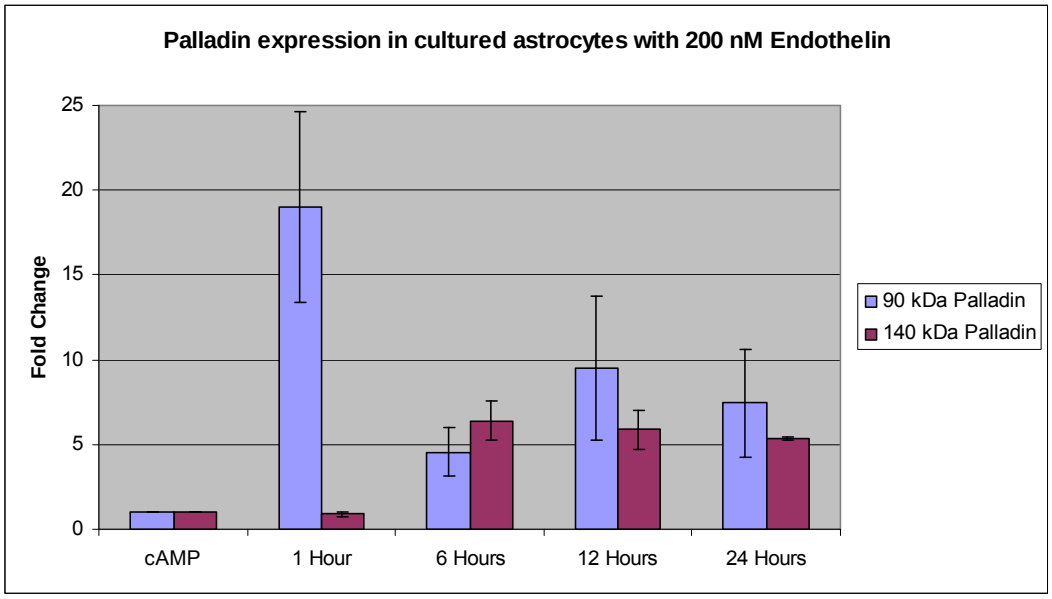

Figure 2.3 Transcriptional regulation of palladin after endothelin treatment. Primary rat astrocytes were differentiated in dBcAMP containing medium and then treated with 200 nM endothelin over 24 hours. After 1 hour, mRNA levels for 90 kDa palladin spike to almost 20 times the level of quiescent astrocytes. 140 kDa palladin levels increase over 5-fold at six hours and remain at this level over the timecourse.

Figure 2.4

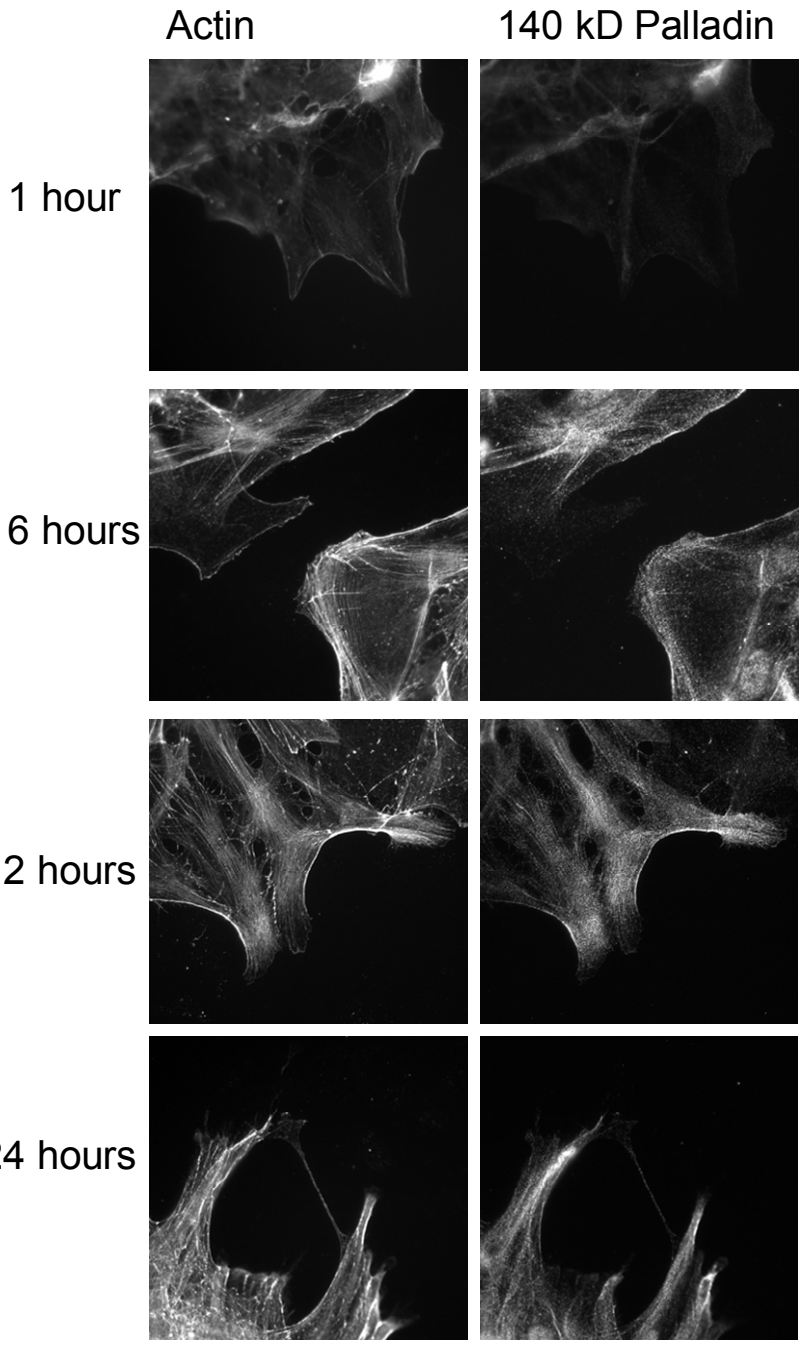

Figure 2.4 Immunoreactivity timecourse of 140 kDa palladin in scratch wound model. Primary astrocyte cultures were differentiated in dBcAMP for 48 hours and scratched with a sterile pipette tip. Cells were fixed over a 48 hour timecourse and stained with a polyclonal antibody that recognizes the N-terminal domain of 140 kDa palladin, but not the 90 kDa form. Palladin is undetectable after 1 hour, but shows robust expression after 6 hours and throughout the timecourse.

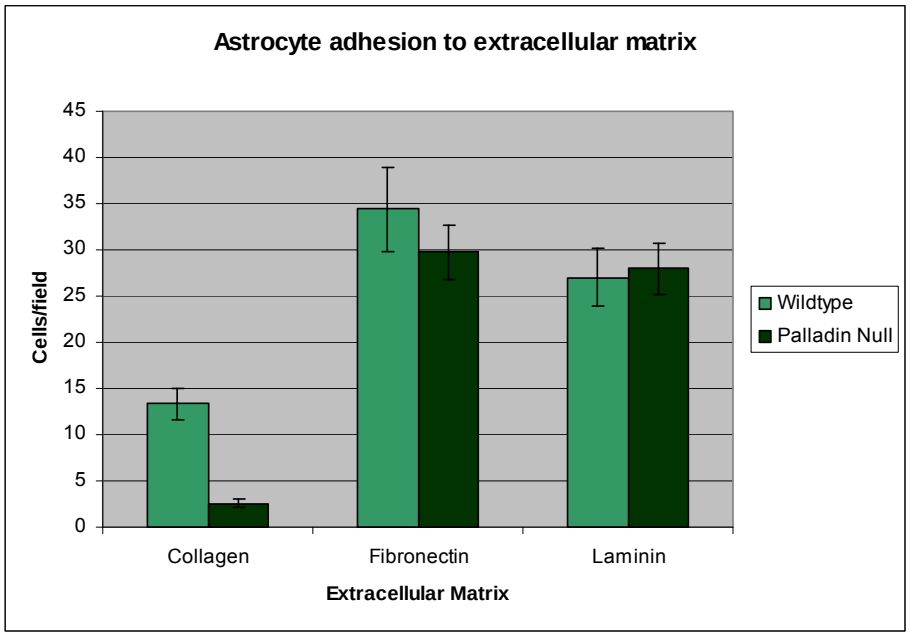

Figure 2.5 Palladin null cells show decreased adhesion to collagen. Cells cultured from the cortex of day E13 wild-type and palladin null mice were allowed to adhere to coverslips dotted with collagen, fibronectin, and laminin. Palladin null cells show a dramatic reduction in their ability to bind collagen, while fibronectin and laminin binding do not appear to be affected.

A.

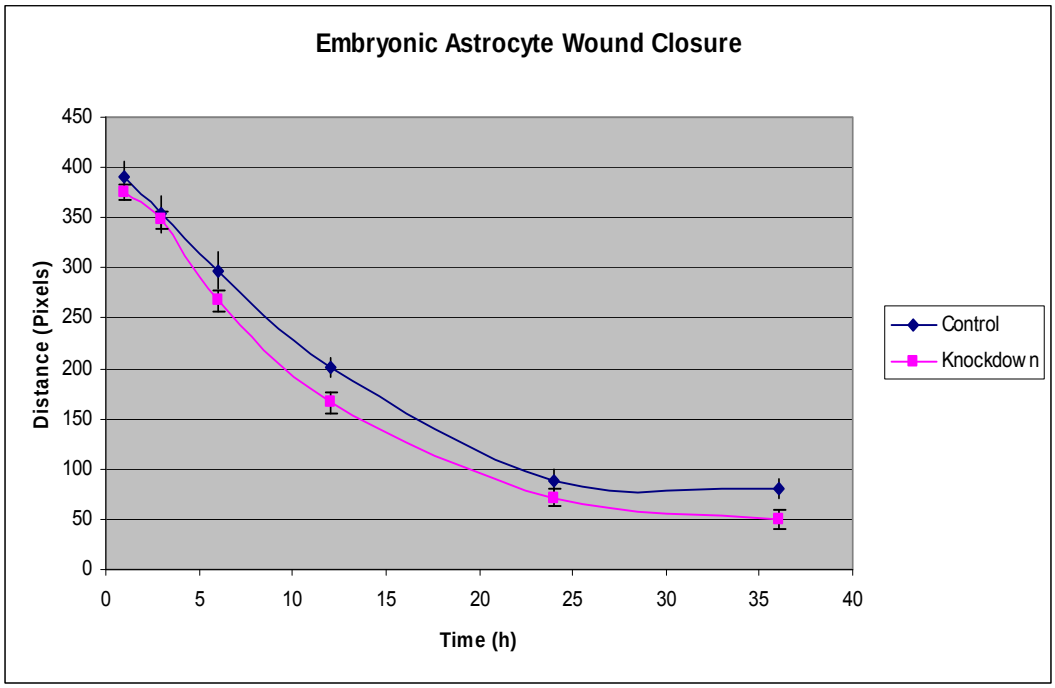

B.

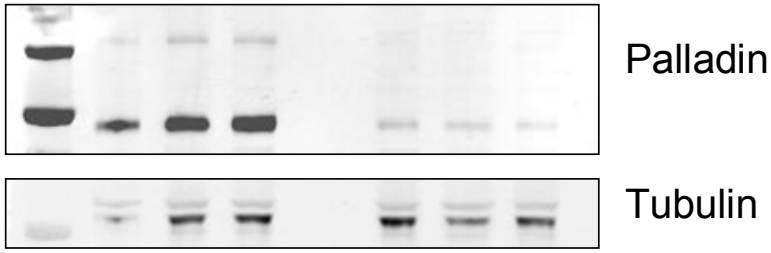

Figure 2.6 Palladin knockdown does not affect wound closure rate of embryonic astrocytes. (A.) A monolayer of control or palladin siRNA treated cells were scratched with a sterile pipette tip and tracked over time. Cells quickly begin to fill the denuded area, and complete wound closure can be observed at approximately 24 hours. Palladin knockdown does not seem to affect closure rate. (B.) Western blot confirms that siRNA treated cells show nearly complete knockdown of both palladin isoforms.

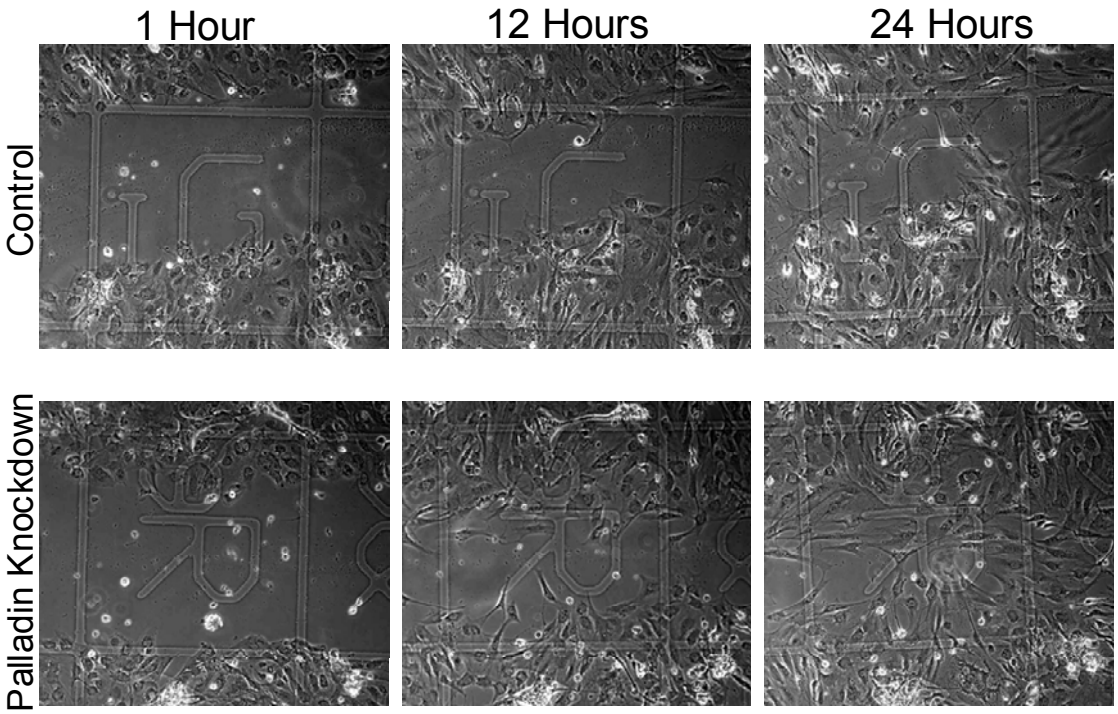

Figure 2.7 Morphology of migrating embryonic astrocytes. A monolayer of control and palladin siRNA treated embryonic astrocytes were scratched with a sterile pipette tip and tracked over time. The cells extend as a sheet and migrate to fill the denuded area over 24 hours. No difference could be observed between palladin knockdown cells and control cells.

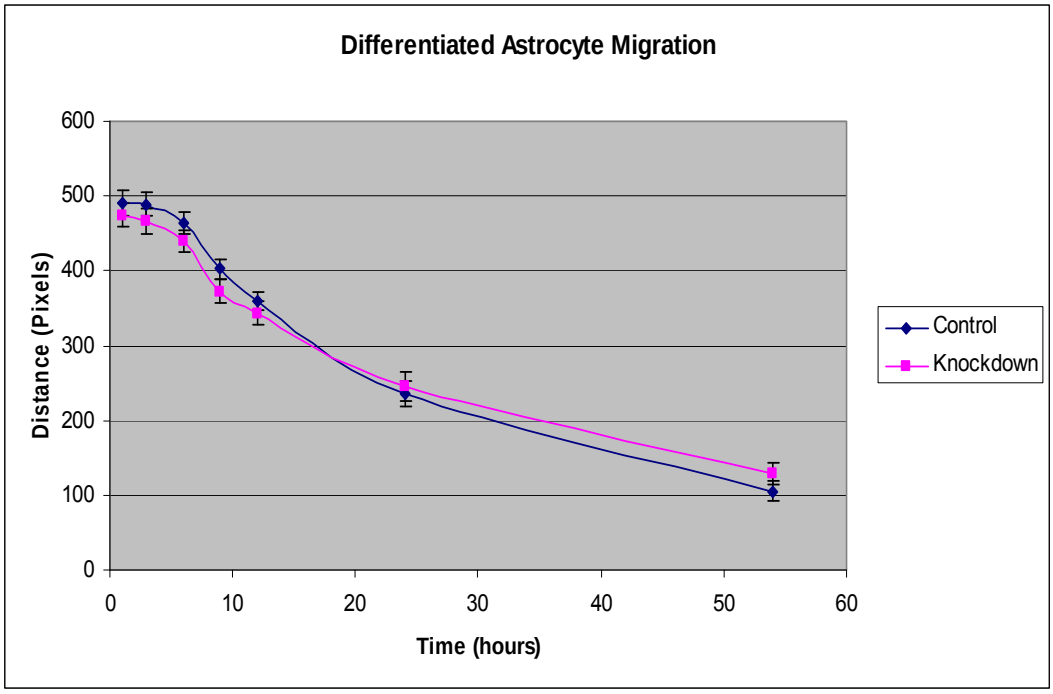

Figure 2.8 Palladin knockdown does not affect wound closure of stellate astrocytes. Control and palladin siRNA treated cells were differentiated in dBcAMP for 48 hours and subject to a scratch wound assay. After a brief lag period, cells begin to fill the denuded area, though at a slower rate than cells grown in serum. Palladin knockdown does not seem to affect closure rate.

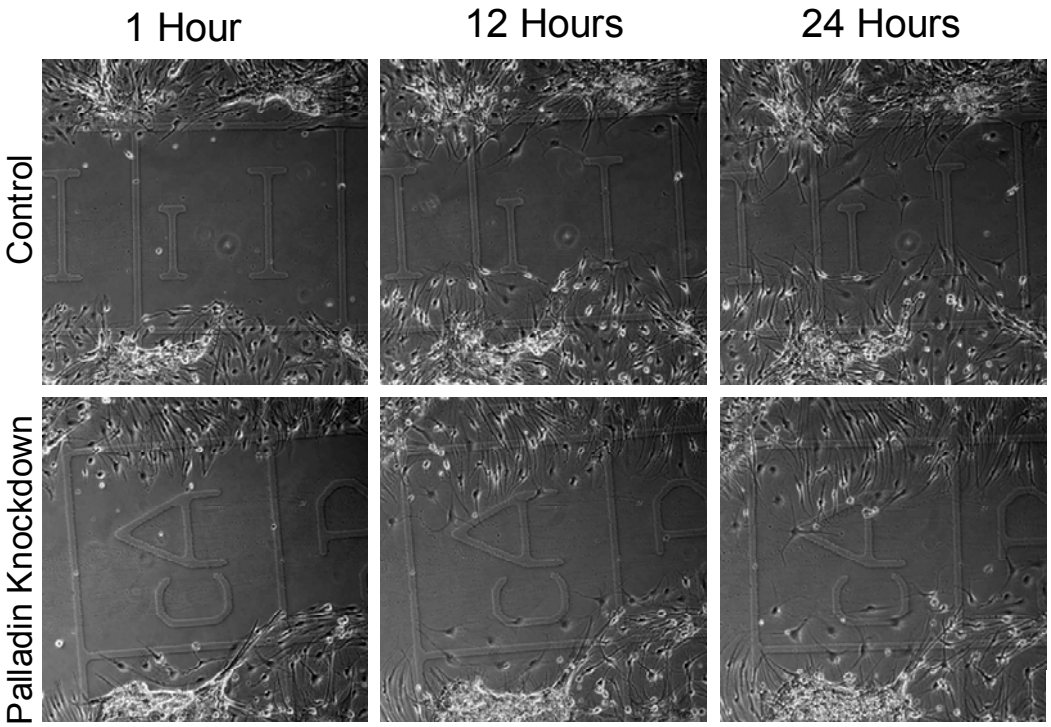

Figure 2.9 Morphology of migrating differentiated astrocytes. Control and palladin siRNA treated cells were differentiated in dBcAMP for 48 hours and subject to a scratch wound assay. Morphologically, the cells extend thinner processes and migrate more slowly than cells grown in serum. No difference could be observed between palladin knockdown cells and control cells.

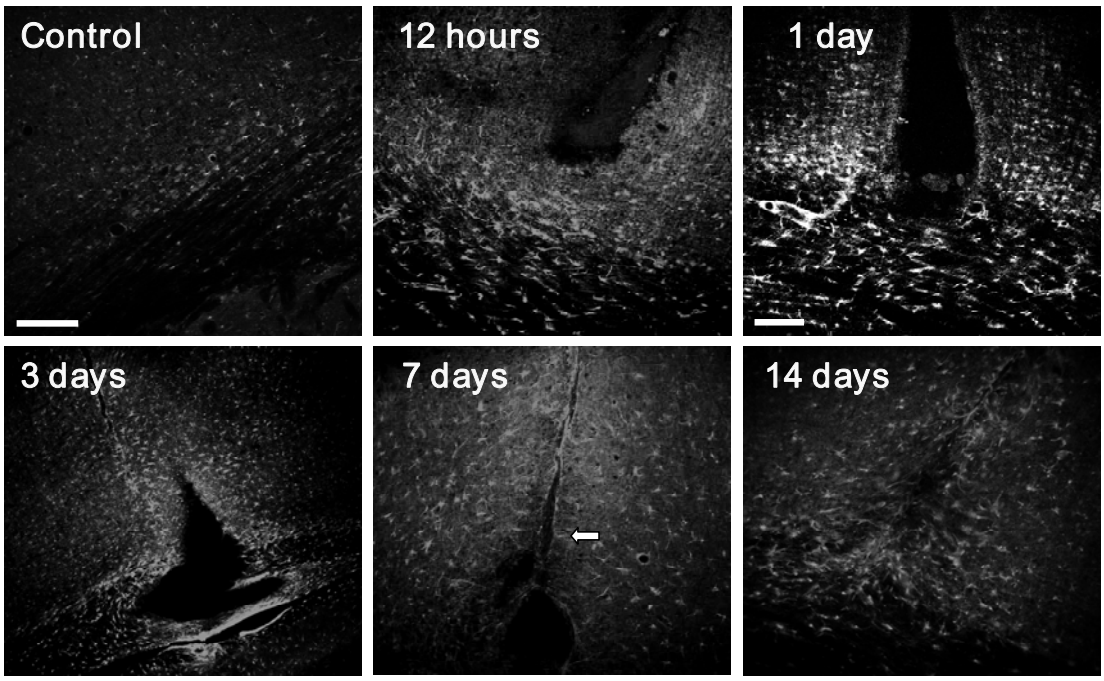

Figure 2.10 Timecourse of 140 kDa palladin immunoreactivity *in vivo.* 140 kDa Palladin immunoreactivity is increased along the edge of the wound at 12 hours post-injury, reaches maximum at 3 days, and then decreases. At 7 days, in cortex, the glial scar along the the edge of the wound has weaker stain for palladin (arrow). Scale bar = 100μm.

Table 2.1 Upregulation of glial markers in response to cortical injury

	12 hrs		24 hrs		3 days		7 days		14 days	
	Gray matter	White matter	Gray matter	White matter	Gray matter	White matter	Gray matter	White matter	Gray matter	White matter
Palladin	+	+	++	++	+++	+++	+	++	+	+
GFAP	±	+	+	++	++	+++	+++	+++	++	+
Nestin	-	-	+	-	+++	+	++	+	+	-
Vimentin	+	+	++	++	+++	+++	+++	+++	+	+
A2B5	+	±	++	±	+++	+	+++	+++	+	+

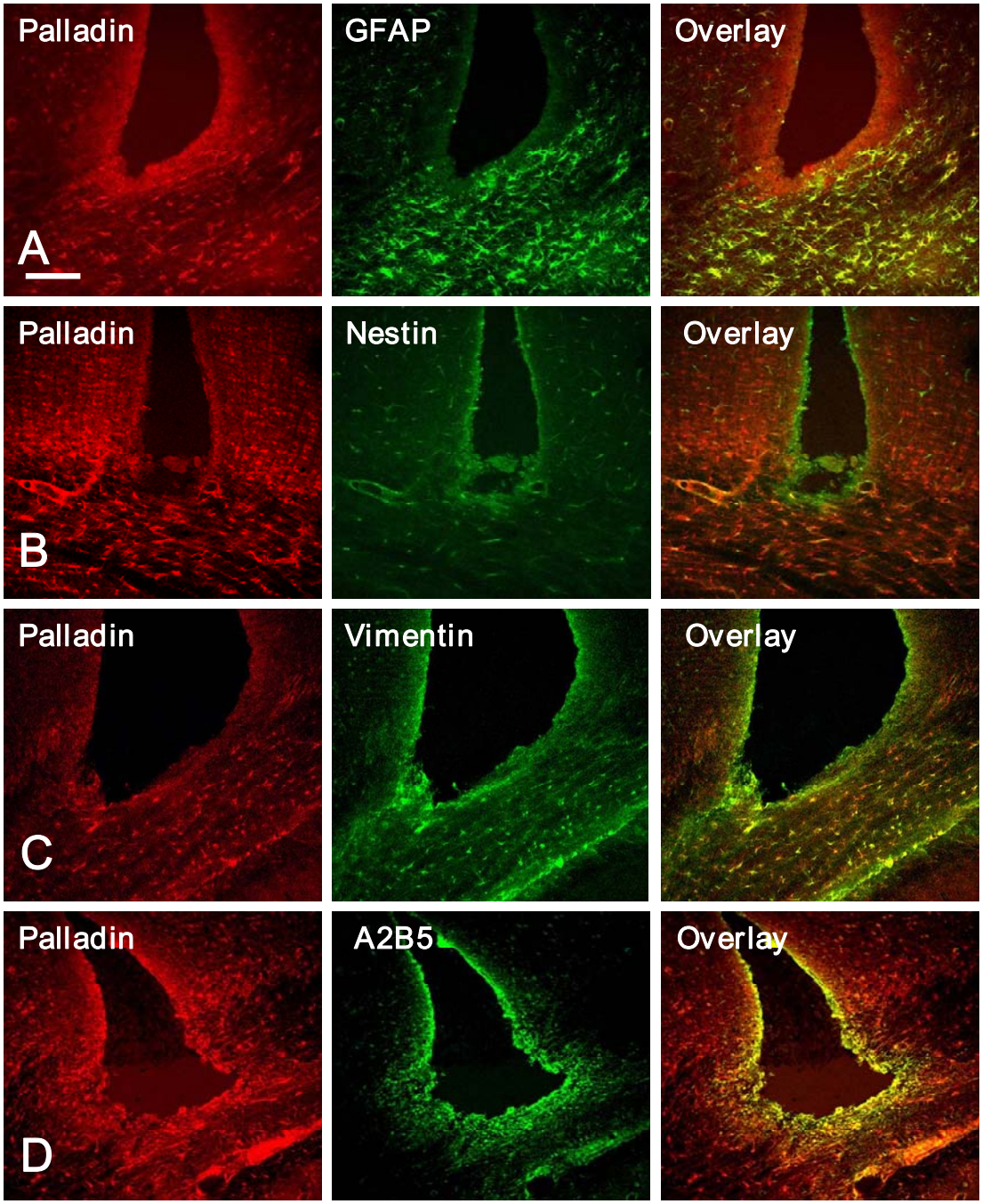

Figure 2.11 (A.) At 12 hours post-surgery, the immunoreactivty of 140 kDa palladin begins to increased at the wound edge prior to that of GFAP. (B-D) Immunoreactivity of Nestin, Vimentin, and A2B5 were observed 24 hours after injury. .Scale bar = 100 μm.

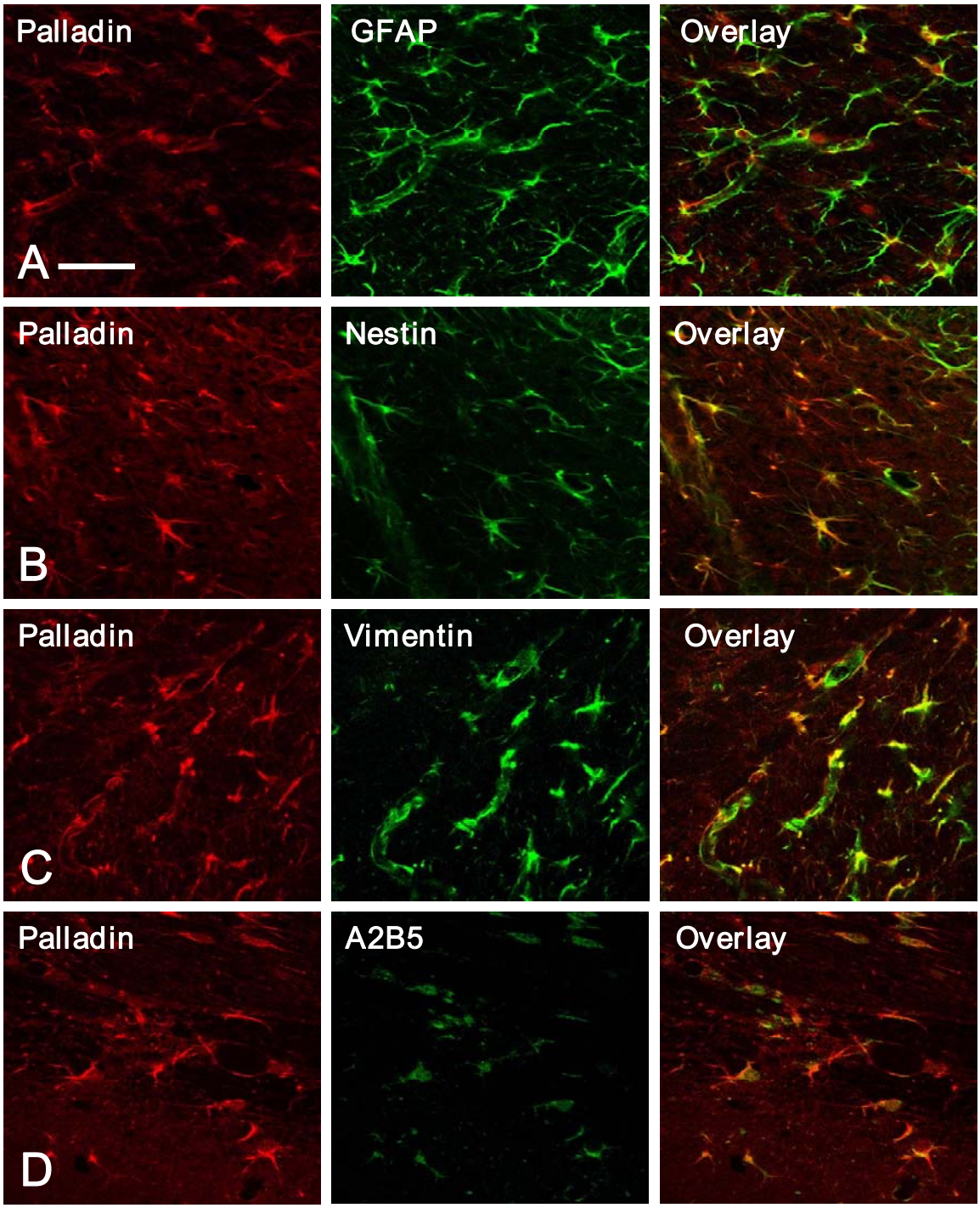

Figure 2.12 140 kDa Palladin co-localizes with markers of reactive astrocytosis. High magnification images show that 140 kDa palladin is colocalized with GFAP(A), nestin(B), vimentin(C), and A2B5(D) in reactive astrocytes. Scale bar = 50 μm.

CHAPTER 3

THE ROLE OF PALLADIN IN INVASIVE CELLULAR PROTRUSIONS

3.1 INTRODUCTION

Reactive astrocytes in the central nervous system must migrate through a complex three-dimensional environment near the injury site, and this cell motility is dependent on the dynamic remodeling of the actin cytoskeleton. Inside the cell, actin-binding proteins promote filament growth and organize actin filaments into functionally specialized arrays that support the well-studied surface specializations including lamellipodia, filopodia and the phagocytic cup. While most of these studies examine cells attached to a two-dimensional, rigid substrate, cells *in vivo* encounter a very different environment.

Of recent interest, many motile cells frequently form membrane surface structures such as highly dynamic ruffles on the dorsal surface, and podosomes on the ventral surface. Essential for the motility and invasion of both normal, highly differentiated cells and neoplastic cells, these structures also use an actin-based machinery to distort the plasma membrane. Dorsal ruffles and podosomes share common architectural features and functions but, depending on the cell types, vary

in their molecular components and regulation (Buccione et al., 2004; Linder and Aepfelbacher, 2003).

It is now well established that activation of receptor tyrosine kinases (RTKs) by growth factors often results in the formation of peripheral membrane ruffles or circular dorsal ruffles (Buccione et al., 2004). Circular dorsal ruffles (also called waves or ring ruffles) are highly dynamic, and form transiently on the dorsal plasma membrane. Although the precise function of dorsal ruffles is a matter of debate, these structures are believed to be important in cytoplasmic remodeling, the establishment of polarity in motile cells, and cell surface receptor down-regulation (Dowrick et al., 1993; Krueger et al., 2003; Orth and McNiven, 2003; Swanson and Watts, 1995; Warn et al., 1993). Active RTKs induce the formation of dorsal ruffles through the activation of the small GTPases Ras and Rac; however, the detailed molecular events leading to the formation of circular ruffles are not clear (Eriksson et al., 1992; Hall, 1998).

Podosomes are also highly dynamic actin-based protrusive structures first described for Rous sarcoma virus-transformed fibroblasts (Gavazzi et al., 1989). Podosomes are adhesive structures that form transiently in the ventral surface of the membrane in response to Src and phorbol ester stimulation (Fultz et al., 2000; Gimona et al., 2003; Hai et al., 2002; Moreau et al., 2003; Osiak et al., 2005). A core of actin filaments and actin-associated proteins is surrounded by a ring of vinculin, talin, and paxillin (Gavazzi et al., 1989), together with proteins associated with the actin polymerization machinery such as gelsolin, cortactin, dynamin, WASP/NWASP and Arp2/3 (Buccione et al., 2004; Linder and Aepfelbacher, 2003).

Podosomes also contain metalloproteases (Sato et al., 1997), supporting the concept that podosomes may serve to spatially restrict sites of matrix degradation.

Palladin appears to be a unique molecular scaffold that interacts with a subset of proteins involved in actin polymerization and crosslinking. Palladin localizes to many actin-containing structures, including stress fibers, focal adhesions, cell-cell junctions, and embryonic Z-lines (Mykkanen et al., 2001; Parast and Otey, 2000). Analysis of the palladin sequence revealed a number of consensus motifs that function as binding sites for known actin-regulating proteins. The N-terminal half of palladin contains polyproline stretches that bind to members of the Ena/Mena/VASP family of proteins (Boukhelifa et al., 2004). Within its N-terminal half, palladin also contains a binding site for the filament crosslinking protein, α-actinin (Ronty et al., 2004). It has recently been shown that palladin also binds via its N-terminal polyproline sequences to ArgBP2 and profilin, two proteins that are involved in the regulation of cytoskeletal dynamics (Ronty et al., 2005; Boukhelifa et al., 2006). Palladin is required for normal actin organization, as demonstrated by knockdown studies in cultured cells (Parast and Otey, 2000) and in cells cultured from a palladin-knockout mouse, both of which displayed reduced actin organization (Luo et al., 2005).

Another molecule that plays a role in generating both dorsal ruffles and podosmes is Eps8. Eps8 is a signaling molecule that was originally identified as a substrate for the epidermal growth factor receptor (EGFR) (Fazioli et al., 1993; Provenzano et al., 1998). Eps8 belongs to a family of proteins that link growth factor stimulation to actin dynamics, participating in the transduction of signals from Ras to

Rac (Offenhauser et al., 2004). It has been reported that Eps8 binds directly to several proteins, including F-actin, EGFR, IRSp53, RN-tre and Dvl1 (Castagnino et al., 1995; Funato et al., 2004; Inobe et al., 1999; Matoskova et al., 1996). Eps8 participates in the formation of a trimeric complex that also includes the scaffold protein Abi-1 and the guanine nucleotide exchange factor (GEF) Sos-1. This macromolecular complex is one of the signaling pathways that activates the small GTPase Rac, which regulates actin assembly and promotes lamellipodia and dorsal ruffle formation (Innocenti et al., 2003; Scita et al., 1999; Scita et al., 2001). Eps8 participation in this complex is essential, as demonstrated by the lack of Sos-1-dependent Rac–GEF activity, Rac activation and remodeling of actin cytoskeleton that occurs in Eps8-null fibroblasts (Scita et al., 1999).

In the present study, we show that palladin localizes not only to the highly dynamic dorsal ruffles that form transiently in response to growth factor stimulation, but also to podosomes. Palladin expression enhances the formation of both the dorsal ruffles and podosomes and co-localizes in these structures with its recently identified binding partner, Eps8.

3.2 MATERIALS AND METHODS

Materials

The following antibodies were used: Eps8 (BD Biosciences); Rac (Transduction Laboratories) and palladin (polyclonal antibody and monoclonal 1E6 antibody previously characterized by Parast and Otey (Parast and Otey, 2000).

Human recombinant platelet-derived growth factor BB (PDGF-BB) and protease inhibitor cocktail for mammalian tissues were from Sigma. MATCHMAKER GAL4 Two- Hybrid System 3 and MATCHMAKER mouse embryonic pACT2 cDNA library were from BD Biosciences. Secondary antibodies conjugated to either IRdye700 or IRdye 800 were from Rockland Immunochemicals. TransIT siQuest transfection reagent was from Mirus, and the Fugene6 transfection reagent was from Roche. Alexafluor-488- and Alexafluor-568 anti-mouse IgG and anti-rabbit IgG-conjugated secondary antibodies were from Molecular Probes.

Stimulation and immunofluorescence staining

Rat vascular smooth muscle cells A7r5 cells were grown in DMEM, containing 10% fetal bovine serum (FBS) and supplemented with 1% penicillin/streptomycin (all from Gibco BRL). Cells were grown on glass coverslips and fixed in 4% paraformaldehyde in PBS, then permeabilized in 0.2% Triton X-100 and incubated with the specific primary antibodies for 1 h. Primary antibodies were detected with Alexafluor-488 and Alexafluor-568 anti-mouse IgG and anti-rabbit IgG conjugates. Coverslips were examined with a Nikon TE200-U microscope with 20X phase (NA 0.7) and 60X phase (NA 1.4) objective lenses, an optional 1.5 X tube lens and a Hamamatsu Orca-ER camera. Images were processed using Adobe Photoshop 7.0 (Adobe Systems). Where indicated, cells were treated with PDGF (20 ng/ml) for 3 minutes. Podosome formation was induced by the addition of 1 μM phorbol-12,13-dibutyrate (PDBu; Sigma-Aldrich), as previously described (Gimona et al., 2003; Hai et al., 2002).

For live-cell imaging, A7r5 cells were plated on 22 mm square coverslips and transfected with GFP-90 kDa palladin using Transit-LT1 transfection reagent and following the manufacturer's protocol. After 24 hours, cells were serum starved for 2 hours and then the coverslips were assembled into a live-cell imaging chamber. During imaging, cells were maintained at 37° C in a heated tent and imaged for 5 minutes before infusing the chamber with media containing PDGF to induce ruffle formation.

siRNA experiments

To knock down the expression of the 90-92 kDa palladin isoform by RNA interference, two 21-base oligonucleotides were purchased from Dharmacon Research. The RNA sequences were as follows: sense, 5'-CUACUCCGCUGUCACAUUAUU- 3' and antisense, 5'-UAAUGUGACAGCGGAGUAGUU- 3'). As a control we used si*CONTROL* Non-Targeting siRNA #1 from Dharmacon. HeLa cells were transfected using the TransIT siQuest transfection reagent following manufacture's instructions. Cells were assayed 86 hours after transfection. In some experiments, the pSuper RNAi system (Oligoengine) was used to knockdown expression of palladin in A7r5 cells. Generation of the RNAi vector followed manufacturer's protocols. Forward and reverse oligos containing the anti-palladin short hairpin RNAi sequence were generated, and were the following: forward, GATCCCCCAAACGTCTTCAACATCCATTCAAGAGATGGATGTTGAAGACGTTTG TTTTTA; reverse, AGCTTAAAAACAAACGTC

TTCAACATCCATCTCTTGAATGGATGTTGAAGACGTTTGGGG. A7r5 cells were passaged the day before the experiment. Cells were transfected using Fugene6 transfection reagent following manufacturer's instructions. Cells were assayed 72 hours after transfection.

3.3 RESULTS

Dorsal ruffle formation in A7r5 cells after PDGF stimulation

To date, palladin has been detected in many actin-containing structures, such as stress fibers, cell-cell junctions and focal adhesions (Parast and Otey, 2000). In recent years, much attention has been paid to another type of dynamic structure implicated in cell motility: dorsal membrane ruffles. Growth factor stimulation of quiescent cells typically results in a transient increase in membrane ruffling that precedes motility and mitogenic effects. The vascular smooth muscle cell line A7r5 has been used previously in the study of membrane ruffles and podosomes after PKC stimulation (Brandt et al, 2002; Zhou et al, 2005). Platelet derived growth factor (PDGF) and other growth factors are often used to generate membrane ruffles in serum starved fibroblasts (Hedberg et al, 1993; Wyman and Acaro, 1994; Anton et al, 2003). For our studies, we decided to stimulate A7r5 cells with PDGF in order to induce cytoskeletal rearrangement including dorsal circular ruffles.

To determine the time-course of ruffle formation after PDGF treatment, we used live-cell microscopy. Serum starved A7r5 cells were assembled in a live-cell imaging chamber and imaged on a heated stage by phase contrast. Media containing PDGF was infused, and Supplemental Movie 3.1 shows that ruffling

begins approximately 5-10 minutes after treatment. Ruffling continues for 20-30 minutes after growth factor stimulation, and the dynamic membrane protrusions can be seen taking up large vacuoles of media by macropinocytosis (See Fig. 3.1 and Supplemental Movie 3.2 for higher magnification.) To further characterize these membrane protrusions, ruffles were imaged by scanning electron microscopy. The micrographs reveal the ultrastructure of membrane protrustions on the dorsal surface of the cells, some of which have a circular arrangement, consistent with our observations by phase contrast imaging (Fig. 3.2).

Palladin localizes to membrane ruffles after PDGF stimulation

Because dorsal ruffles are also actin-rich structures, we asked whether palladin is a component of these structures. To determine whether palladin is recruited to these dynamic actin-based protrusions, immunostaining was used to visualize endogenous palladin in A7r5 cells after stimulation with PDGF. Interestingly, although some palladin is still detected in its characteristic punctuate pattern along actin stress fibers in PDGF-stimulated cells, endogenous palladin is also recruited to circular membrane protrusions or ruffles along with filamentous actin (Fig. 3.3). It is worthwhile to note that palladin localizes to dorsal ruffles with a variety of shapes, ranging from small circular to larger elongated ruffles.

To analyze the dynamics of palladin recruitment to dorsal ruffles, GFP-tagged palladin was transiently transfected into A7r5 cells, which were then serum-starved for 2 hours prior to imaging. The addition of PDGF induced the extension of dynamic ruffles (Figure 3.4 and supplementary movies 3 and 4) and revealed that GFP-

palladin is rapidly recruited to these structures on a similar time scale to that reported for other proteins (Anton et al., 2003; Dharmawardhane et al., 1997; Hedberg et al., 1993)

Palladin knockdown decreases ruffle formation induced by PDGF

To determine the role of palladin in PDGF induction of ruffles, we examined the effect of downregulation of palladin expression on the cellular response to PDGF. Short hairpin RNAi (shRNAi) constructs were used to knockdown the expression of palladin. Fig. 3.5 shows that palladin expression was suppressed in shRNAi-transfected cells. When transfected cells were treated with PDGF, dorsal ruffle formation was found to be inhibited in the palladin-knockdown cells (Fig. 3.6 A). Quantification of these results showed that palladin knockdown reduces the percentage of cells with ruffles from 50% to 10% (Fig. 3.6 B). These results suggest that palladin plays an important role increasing the efficiency of dorsal ruffle formation induced by PDGF.

Palladin localizes to PDBu-induced podosomes and enhances podosome formation after phorbol ester stimulation

Treatment of the rat vascular smooth muscle A7r5 cells with the phorbol ester phorbol-12,13-dibutyrate (PDBu) induces podosome formation (Hai et al., 2002). When cultured in serum, A7r5 cells displayed a robust actin cytoskeleton, highlighted by contractile actin stress fibers. Upon stimulation with the phorbol ester PDBu, the actin cytoskeleton of A7r5 cells undergoes the dissolution of stress fiber

and focal adhesions, with the concomitant formation of dynamic podosomes (Hai et al., 2002). To determine whether palladin is recruited to these actin-based structures, immunostaining was used to visualize endogenous palladin in A7r5 cells after stimulation with PDBu. Fig. 3.7 shows that palladin was clearly enriched in the podosomes and co-localized with actin in cells doubly stained with anti-palladin antibodies and phalloidin. To determine the role of palladin in PDBu induction of podosomes, we examined the effect of palladin-knockdown on the cellular response to PDBu. Short hairpin RNAi (shRNAi) constructs were used to knockdown the expression of palladin. Fig. 3.8 A shows that when palladin shRNAi transfected cells were treated with PDBu, a significant percentage of the siRNA transfected cells were unable to form podosomes. The number of cells that formed podosomes after phorbol ester stimulation was determined, showing that palladin knockdown reduces the percentage of cells that form podosomes from 42% to 20% (Fig. 3.8 B). These results suggest that, similarly to what we observed for dorsal ruffles, palladin plays an important role increasing the efficiency of podosome formation induced by PDBu.

Palladin co-localizes with Eps8

Eps8 is a signaling molecule that was originally identified as a substrate for the epidermal growth factor receptor (EGFR) (Fazioli et al., 1993; Provenzano et al., 1998). Eps8 belongs to a family of proteins that link growth factor stimulation to actin dynamics, participating in the transduction of signals from Ras to Rac (Offenhauser et al., 2004). It has been reported that Eps8 binds directly to several proteins, including F-actin, EGFR, IRSp53, RN-tre and Dvl1 (Castagnino et al., 1995; Funato

et al., 2004; Inobe et al., 1999; Matoskova et al., 1996). Eps8 participates in the formation of a trimeric complex that also includes the scaffold protein Abi-1 and the guanine nucleotide exchange factor (GEF) Sos-1. This macromolecular complex is one of the signaling pathways that activates the small GTPase Rac, which regulates actin assembly and promotes lamellipodia and dorsal ruffle formation (Innocenti et al., 2003; Scita et al., 1999; Scita et al., 2001). Eps8 participation in this complex is essential, as demonstrated by the lack of Sos-1- dependent Rac–GEF activity, Rac activation and remodeling of actin cytoskeleton that occurs in Eps8-null fibroblasts (Scita et al., 1999). Recently, Eps8 was identified by yeast-two hybrid screen as a binding partner for palladin's N-terminal proline-rich region. (Goicoechea et al., 2006).

In previous reports, palladin has been localized to regularly-spaced puncta along the stress fibers of well-spread fibroblasts and in cell-cell junctions (Parast and Otey, 2000). The observations described above demonstrate that antibodies to palladin also label dorsal ruffles in cultured A7r5 cells (Fig. 3.3). In addition to its localization in phagocytic cups, comet tails and cell-cell contacts, Eps8 has been detected in circular, dorsal ruffles (Disanza et al., 2004; Provenzano et al., 1998), and so we next investigated the degree of co-localization of palladin and Eps8 in ruffles. A7r5 vascular smooth muscle cells were serum-starved for 2 hours and then treated with PDGF for 5 minutes. Immunofluorescence staining shows a high degree of overlap of palladin and Eps8 staining in PDGF-induced dorsal ruffles (Fig. 3.9 A). These results demonstrate that both palladin and Eps8 are recruited to circular ruffles in response to PDGF stimulation. Eps8 has also been detected in

podosomes (Provenzano et al., 1998), and so we also explored whether palladin and Eps8 co-localized to these actin-based structures. A7r5 vascular smooth muscle cells were treated with 1 μM PDBu for 30 minutes. Immunofluorescence staining shows a high degree of overlap of palladin and Eps8 staining in PDBu-induced podosomes (Fig. 3.9 B).

3.4 DISCUSSION

Previously, it was shown that palladin is required for the maintenance of normal stress fibers and focal adhesions in cultured fibroblasts and trophoblasts (Parast and Otey, 2000). More recently, palladin was shown to play a critical role in embryonic development, as the palladin-knockout mouse had an embryonic lethal phenotype and exhibited defects in body wall closure (Luo et al., 2005). Fibroblasts cultured from the palladin null embryos showed impaired stress fiber formation, reduced adhesion to fibronectin, and reduced cell migration (Luo et al., 2005). These results are consistent with the hypothesis that palladin functions as a key regulator of actin organization in a wide variety of cell types. In the current study, we identified two additional actin-based structures that contain palladin: podosomes formed on the ventral surface of the cell after exposure to phorbol esters and the highly dynamic dorsal membrane ruffles that form in response to PDGF. Membrane ruffling is significantly decreased in palladin knockdown cells, which suggests an important role for palladin in the life cycle of these transient structures.

These observations led us to hypothesize that palladin may be directly or indirectly involved in any of the following stages of ruffle formation: (1) intracellular

signaling pathways after growth factor stimulation; (2) actin filament nucleation or stability at sites of protrusion; or (3) structural organization of actin filaments leading to the formation of higher-order actin arrays that support membrane protrusion. In support of hypotheses 2 and 3, palladin has been shown to bind to a host of actin-associated proteins that may alter nucleation rates, stability and bundling. Notably, binding interactions have been described between palladin and α-actinin, ezrin, ENA/VASP proteins, LPP and ArgBP2, each of which plays a role in actin organization (Boukhelifa et al., 2004; Mykkanen et al., 2001; Ronty et al., 2005; Ronty et al., 2004, Jin et al, 2006).

In our published report, we provide the first evidence that palladin may also play a role in the signaling pathways leading to ruffling through its interaction with a novel binding partner, Eps8 (Goicoechea et al., 2006). It is interesting to note that Eps8, like all the other binding partners for palladin identified to date, is a protein that regulates the actin cytoskeleton; thus, these results place palladin within a known biochemical pathway that links growth factor stimulation to dynamic actin changes that are involved in cell motility and morphological plasticity. Moreover, these and previous results support the hypothesis that palladin might function as a highly potent scaffolding molecule, with the potential to influence both actin polymerization and the assembly of existing actin filaments into bundles and other higher-order arrays involved in adhesion and migration.

The mechanism by which palladin alters Rac activity (Goicoechea et al. 2006) and ruffling will require further study, but interaction with Eps8 may prove to be an essential link. Eps8 integrates different signaling pathways by participating in: (1)

actin remodeling through Rac, forming a complex with Abi-1 and Sos-1; (2) receptor endocytosis modulating Rab5 activity, forming a complex with RN-tre; and (3) actin-based motility processes by capping the barbed ends of actin filaments (Disanza et al., 2004; Innocenti et al., 2003; Lanzetti et al., 2000). Our results showed that neither the over-expression of palladin nor the knockdown interfere with the ability of Abi-1 to bind to Eps8 or Sos-1, which suggests that palladin binding to Eps8 does not trigger a ligand-dependent association with Abi-1 and Sos-1 (Goicoechea et al., 2006). It remains to be determined whether palladin forms part of the Eps8/Abi-1/Sos-1 complex; however, our results suggest that palladin might be stabilizing the Eps8/Abi-1/Sos-1 complex, thus promoting Rac activation and actin reorganization. Alternatively, palladin could be involved in regulating the actin capping activity of Eps8. It has been recently reported that full length Eps8 is auto-inhibited and does not cap barbed ends, while the binding of Abi-1 alters the conformation of Eps8 and releases its barbed-end actin capping activity (Disanza et al., 2004). The binding of palladin to Eps8 could be involved in a similar mechanism, modulating Eps8 barbed-end capping activity. These possibilities will be explored in future studies.

Our results suggest that palladin and Eps8 participate together in a pathway that leads to the formation of dorsal ruffles. Thus, our future efforts will focus on exploring how the interactions of these two proteins are regulated by cellular signaling pathways. In our published study we investigated whether palladin/Eps8 interaction is regulated by growth factors (Goicoechea et al. 2006). We performed coimmunoprecipitation analysis with lysates from growth factor-stimulated or non-stimulated cells; however, we did not see any significant difference in the amount of

immunoprecipitated proteins. If the palladin/Eps8 interaction is being regulated dynamically *in vivo*, it is possible that an intact cytoskeleton may be necessary to maintain the interaction. Additional experiments will be needed to address this possibility.

Eps8 is tyrosine-phosphorylated by a variety of tyrosine kinases, of both the receptor (RTKs) and non-receptor type (Fazioli et al., 1993). Palladin is also a phosphoprotein and it contains clusters of serine-rich sequences next to the Eps8-binding site, which suggests that serine phosphorylation could play a role in regulating palladin's binding to Eps8. It remains to determined whether palladin and Eps8 are phosphorylated downstream of the same kinase pathways, and whether their binding interactions are regulated by their phosphorylation state.

Our observation of palladin in membrane ruffles led us to examine another actin-based structure involved in motility, the podosome. These structures have been described in several human cancer cell lines, particularly invasive breast carcinomas and melanomas, and their presence has been correlated with invasiveness *in vitro* (Bowden et al., 1999; Kelly et al., 1998; Monsky et al., 1994). It has been reported that palladin levels are increased in cancer cell lines, including invasive breast carcinomas and an agressive form of familial pancreatic cancer (Wang et al., 2004; Pogue-Geile et al., 2006). Localization of palladin to structures resembling podosomes in immature dendritic cells was reported earlier by Carpen and collaborators (Mykkanen et al., 2001). In this report, we show not only that palladin localizes to podosomes in A7r5 cells but also that palladin expression enhances the formation of podosomes after phorbol ester stimulation.

One possible role for palladin in podosome formation may be that it functions as a scaffolding molecule to recruit proteins known to be required for podosome formation. For example, palladin binds to α-actinin, which is localized to podosomes (Fultz et al., 2000; Linder and Aepfelbacher, 2003). Here, we show that palladin associates with Eps8, which has also been reported to localize to podosomes (Provenzano et al., 1998). Future studies will examine the role of palladin in the signaling pathways leading to podosome formation, and will address palladin's role in invasive motility.

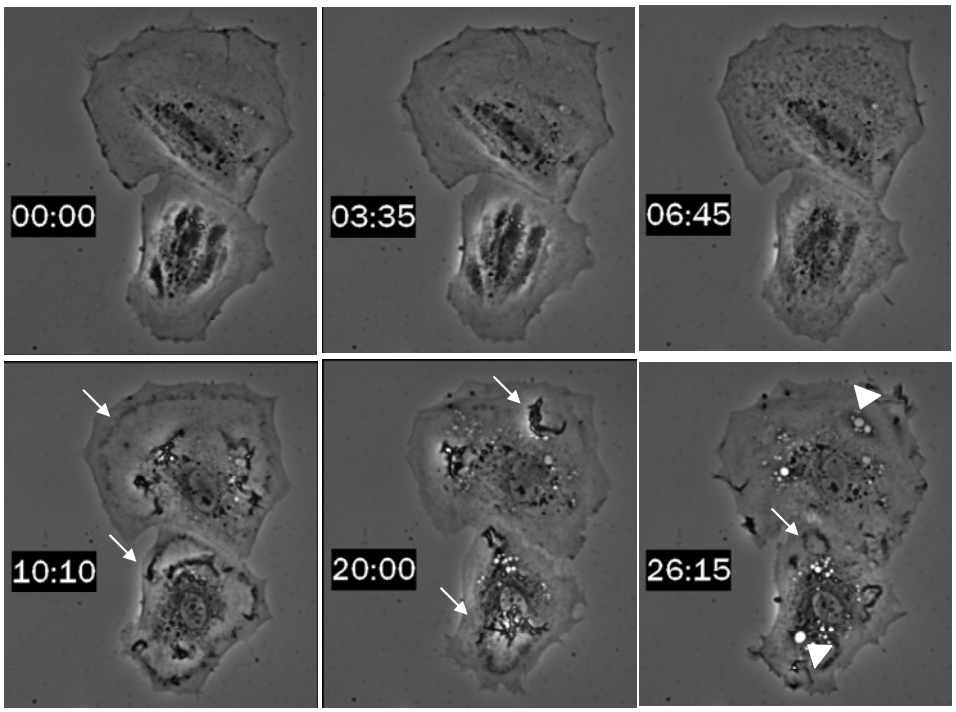

Figure 3.1. A7r5 cells form dorsal ruffles in response to PDGF. A7r5 cells were plated on fibronectin overnight and serum-starved for 2 hours prior to growth factor treatment. The addition of PDGF at time 6:00 led to the induction of dynamic, actin-based membrane protrusions (indicated by arrows). Ruffles also induce the uptake of vacuoles (arrowheads) Time is given in Minutes:Seconds.

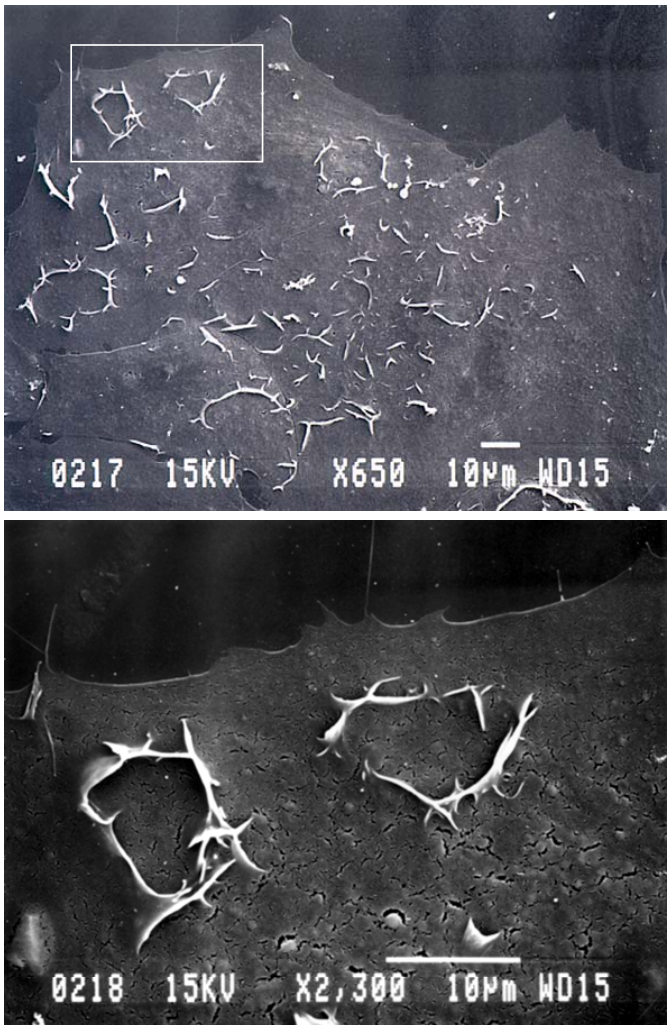

Figure 3.2 Dorsal ruffles imaged by scanning electron microscopy. A7r5 cells were serum starved and treated with PDGF for 5 minutes before fixation and preparation for scanning EM. (A.) Micrographs reveal the ultrastructure of dorsal membrane ruffles. (B.) Magnification of highlighted region from (A.).

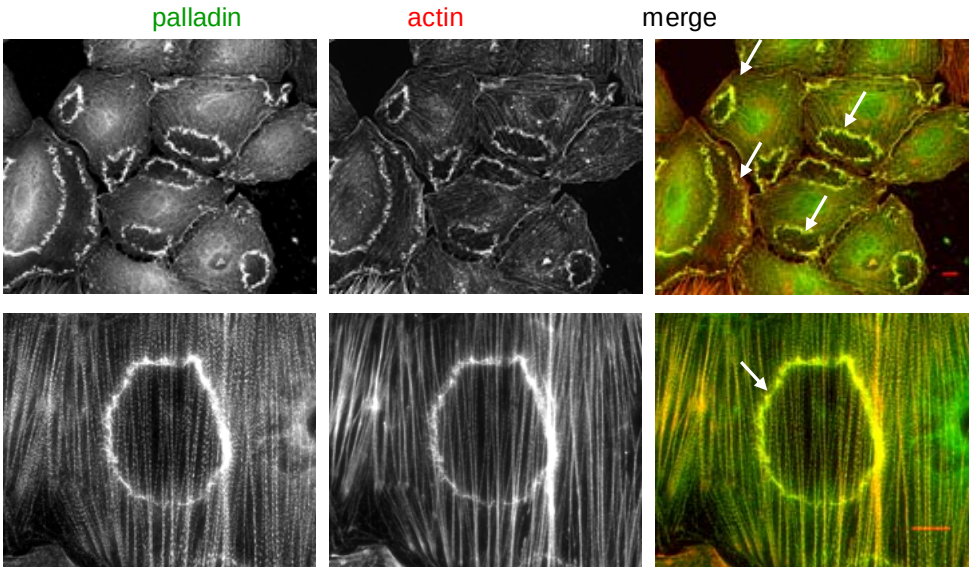

Figure 3.3. Palladin localizes to PDGF-induced membrane ruffles. A7r5 cells were plated on fibronectin overnight and serum-starved for 2 hours prior to growth factor treatment. The addition of PDGF led to the induction of dynamic, actin-based membrane protrusions (indicated by arrows). After fixation, endogenous palladin was detected in these structures by immunofluorescence. Co-labeling with TRITC-phalloidin and polyclonal anti-palladin antibody reveals that palladin co-localizes with filamentous actin in ruffles and along stress fibers. Top: Low magnification image. Bottom: High magnification image to show detail. Scale Bar = 10μm

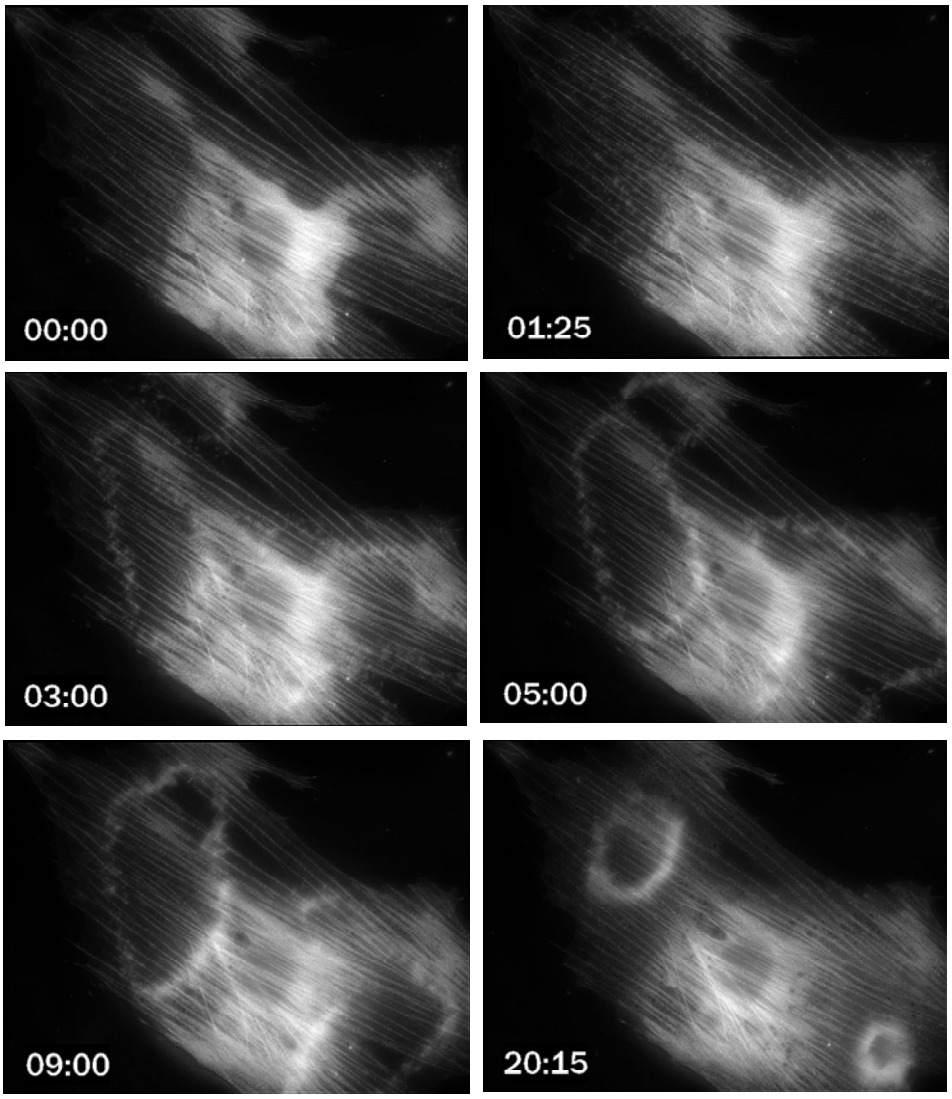

Figure 3.4. Live-cell imaging of palladin recruitment to dorsal ruffles. A7r5 cells were transfected with GFP-90 kDa palladin and prepared for live cell imaging of dorsal ruffles. PDGF treatment was administered before the start of the movie. At T=0, palladin can be seen decorating the stress fibers and in the thickened perinuclear region. At 1:25, palladin localization diffuses before coalescing into membrane ruffles at 3:00. Ruffles continue throughout the timecourse, continually growing narrower. Time given in Minutes:Seconds.

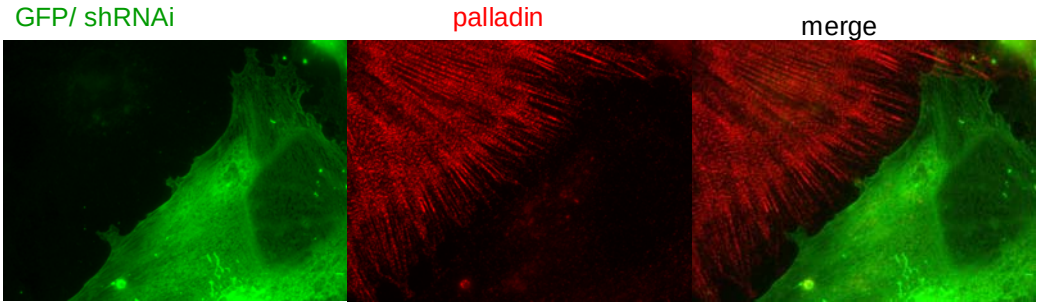

Figure 3.5. Palladin staining of shRNAi-transfected cells**.** A7r5 cells transfected with pSuper RNAi targeting palladin were fixed after 48 hours, permeabilized and stained with polyclonal anti-palladin antibody. Transfected cells (green fluorescence), exhibited undetectable palladin staining.

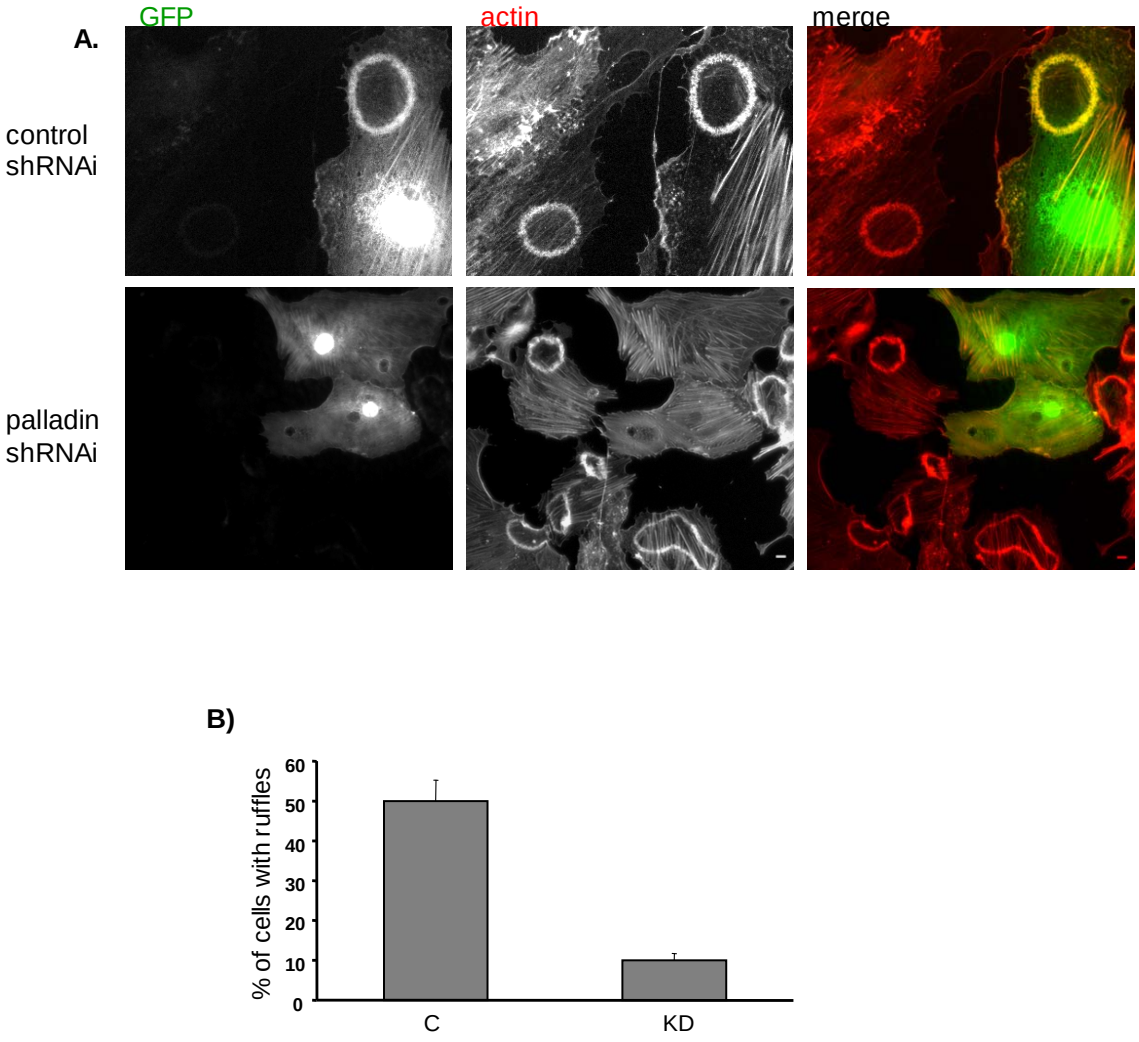

Figure 3.6. Palladin knockdown decreases PDGF-induced ruffle formation. A) A7r5 cells transfected with control pSuper RNAi and pSuper RNAi targeting palladin were plated on fibronectin overnight and serum-starved for 2 hours prior to PDGF treatment. Cells were fixed, permeabilized and stained with TRITC-phalloidin. Transfected cells (green fluorescence) were detected by the presence of GFP encoded in the pSuper vector. B) The proportion of cells developing ruffles after PDGF stimulation is shown for cells transfected with palladin siRNA (KD, 10 ± 2 %) and transfected with control siRNA (C, 50 ± 5 %). Results are representative of three independent experiments in which at least 100 transfected cells were counted. Scale Bar = 10µm

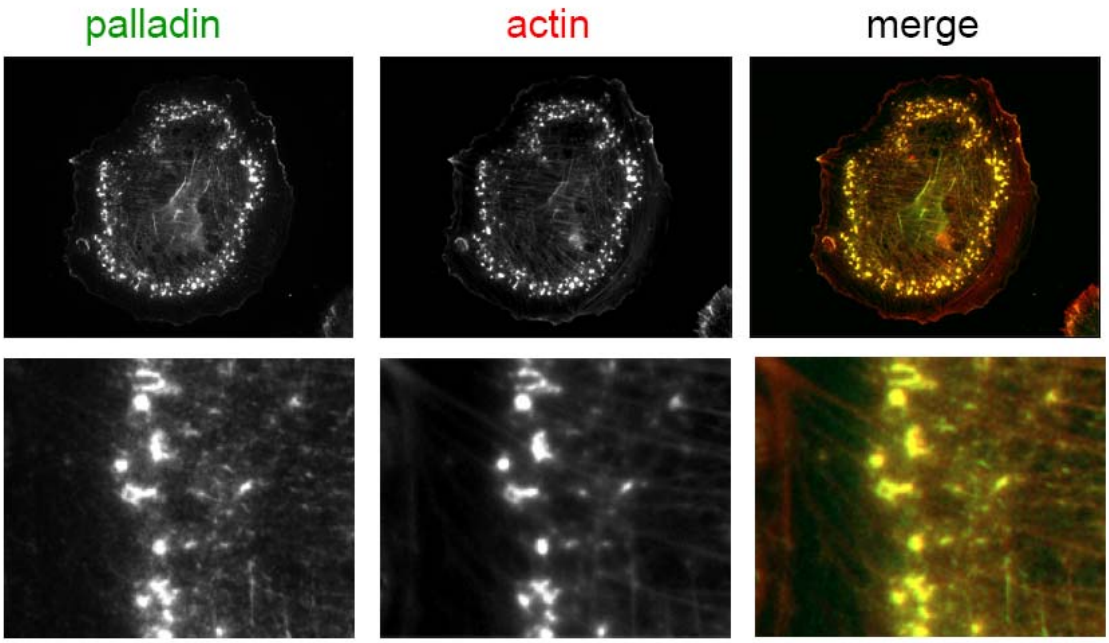

Figure 3.7. Palladin localizes to PDBu-induced podosomes. A7r5 cells were plated on fibronectin and treated with the phorbol ester PDBu. After fixation, endogenous palladin was detected by immunofluorescence. Co-labeling with TRITC-phalloidin and polyclonal anti-palladin antibody reveals that palladin co-localizes with actin. Top: Low magnification image. Bottom: High magnification image to show detail.

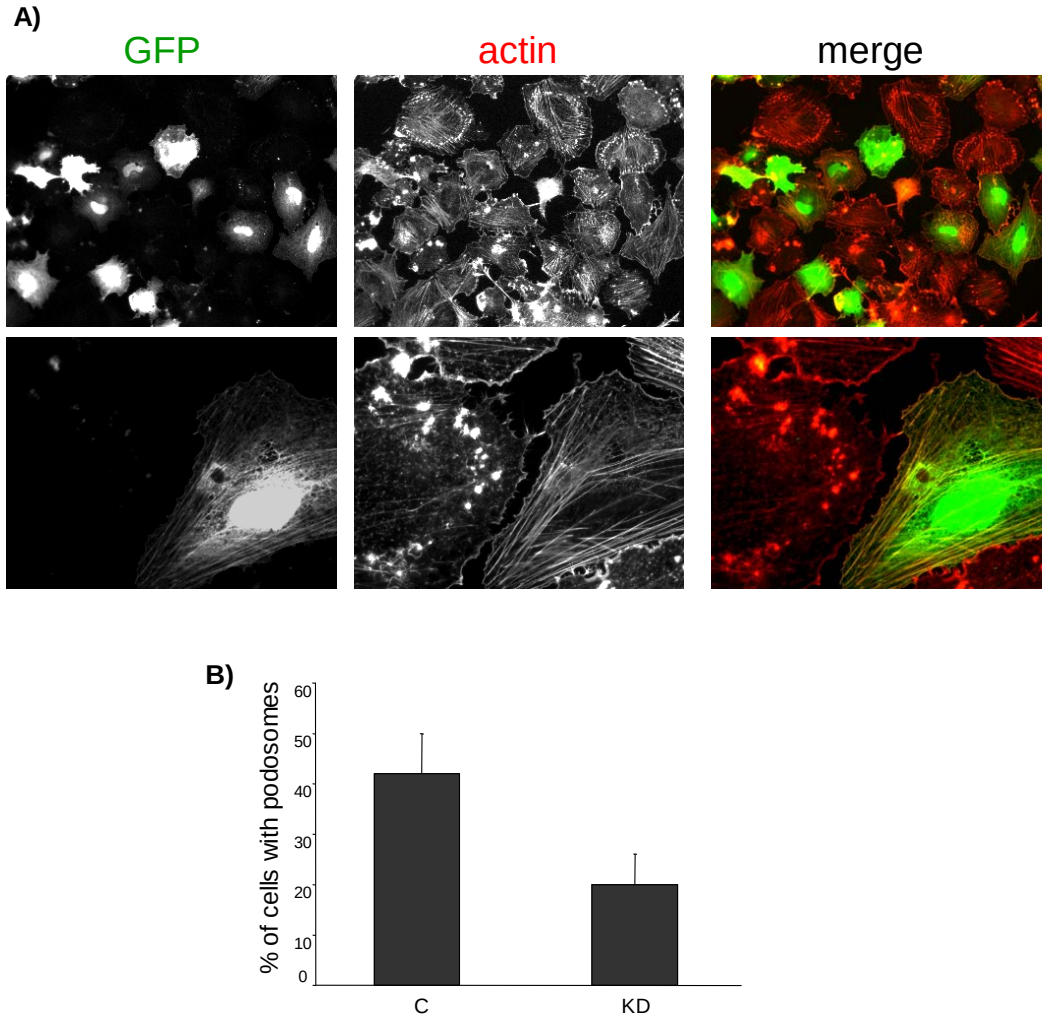

Figure 3.8. Palladin knockdown decreases PDBu-induced podosome formation. A) A7r5 cells transfected with control pSuper RNAi and pSuper RNAi targeting palladin were plated on fibronectin overnight and treated with PDBu. Cells were fixed, permeabilized and stained with TRITC-phalloidin. Transfected cells (green fluorescence) were detected by the presence of GFP encoded in pSuper. Top: Low magnification image. Bottom: High magnification image to show detail. B) The proportion of cells developing podosomes after PDBu stimulation is shown for cells transfected with control siRNA (C, 36 ± 3 %) and transfected with palladin siRNA (KD, 19 ± 5 %). Results are representative of three independent experiments in which at least 300 transfected cells were counted.

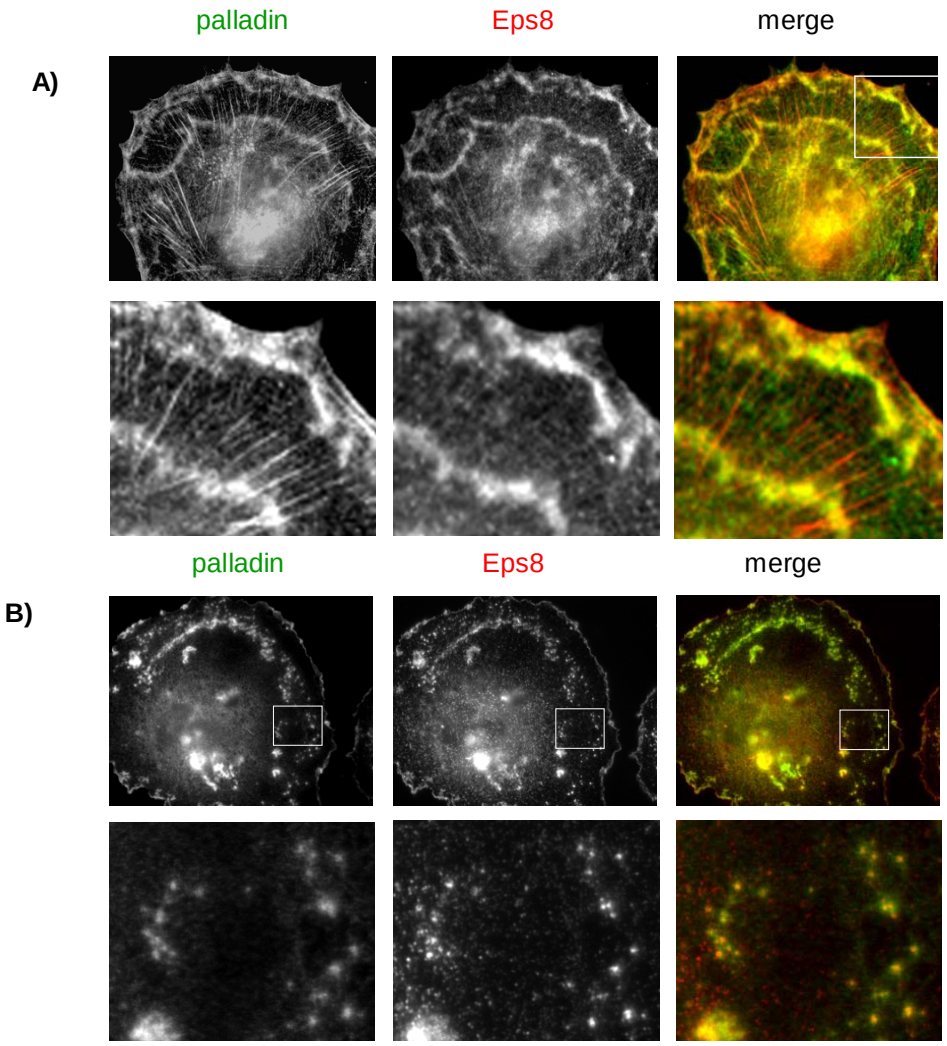

Figure 3.9. Palladin co-localizes with Eps8. A7r5 cells were plated on fibronectin-coated coverslips and were either incubated for 2 hours in serum-free media prior to treatment with PDGF (A) or treated with the phorbol ester PDBu (B). Cells were fixed and immunolabeled with polyclonal anti-palladin antibody and monoclonal anti-Eps8 antibody. The two images were merged (overlay) to show the relative localization of palladin (green) and Eps8 (red). Top: Low magnification image. Bottom: High magnification image to show detail.

CHAPTER 4

PALLADIN IS AN ACTIN CROSSLINKING PROTEIN THAT USES IMMUNOGLOBULIN-LIKE DOMAINS TO BIND FILAMENTOUS ACTIN

4.1 INTRODUCTION

The actin cytoskeleton is a dynamic assembly that provides the cell with mechanical support and elasticity (Heidemann et al., 1999; Heidemann et al., 2004), participates in cell locomotion through the formation and disassembly of protrusions (Welch et al., 1997), and provides a scaffold for the trafficking of cellular components (Langford, 1995; Bassel and Singer, 1997) and organization of signaling complexes (Mahoney et al, 1997). The organization of actin networks within the cell is tightly controlled by a variety of regulatory proteins that either crosslink actin filaments into robust bundles or regulate the assembly and disassembly of actin filaments by 1) capping/uncapping or severing the filament ends or 2) promoting the polymerization of actin at specific sites (dos Remedios et al., 2003). To date, more than twenty-three classes of proteins have been shown to crosslink actin filaments into tight parallel bundles, loosely spaced bundles, or flexible networks (Kreis and Veil, 1999). Actin-crosslinking proteins such as filamin (Popowicz et al., 2006; van der Flier and Sonnenberg, 2001), α-actinin (Blanchard et al., 1989), and fascin (Edwards and Bryan, 1995) play important roles in maintaining cell shape and allowing cells to move and to adhere to a substrate. In addition, in differentiated cells *in vivo*, actin-

crosslinking proteins have a critical function in generating specialized actin-based structures such as sarcomeres, microvilli and stereocilia (reviewed in (Adams, 2004; Bartles, 2000). Thus, the extraordinary diversity of actin-binding proteins provides cells with a wide variety of molecular tools for constructing both dynamic and stable arrays of actin filaments.

Palladin is a phosphoprotein that is widely expressed in vertebrate cells and tissues (Parast and Otey, 2000; Rachlin and Otey, 2006; Mykkanen et al., 2001). Palladin exists as three major isoforms, which display apparent molecular weights of 90, 140 and 200 kDa by SDS-PAGE (Parast and Otey, 2000; Rachlin and Otey, 2006). Palladin is the most widely expressed member of a novel subfamily of actin-associated proteins (Otey et al., 2005). The two other members of this family of proteins, myotilin and myopalladin, are primarily expressed in striated muscle (Salmikangas et al., 1999; Bang et al., 2001). Palladin has been detected in structures that contain contractile bundles of actin filaments, such as stress fibers and sarcomeres (Parast and Otey, 2000; Mykkanen et al., 2001). Palladin also localizes to anchoring structures such as focal adhesions and podosomes, and motile structures such as neuronal growth cones and dorsal ruffles (Parast and Otey, 2000; Rachlin and Otey, 2006; Boukhelifa et al., 2001; Goicoechea et al., 2006). Palladin is ubiquitously expressed in embryonic organs but is down-regulated in some adult tissues (Parast and Otey, 2000). Within smooth muscle and non-muscle cells, palladin localizes to actin filaments in regularly spaced puncta that have also been found to contain α-actinin (Ronty et al., 2004) and vasodilator-stimulated phosphoprotein (VASP) (Boukhelifa et al., 2004). Palladin possesses a

large number of molecular partners, including a cohort of proteins that bind directly to actin: α-actinin (Ronty et al., 2005), VASP (Boukhelifa et al., 2004), profilin (Boukhelifa et al., 2006), ezrin (Mykkanen et al., 2001), and Eps8 (Goicoechea et al, 2006). Palladin also binds to a second cohort of proteins that indirectly influence actin organization: ArgBP2 (Ronty et al., 2005), LPP (Jin et al., 2007), and SPIN90 (Ronty et al., 2007). The larger isoforms of palladin also bind to the actin-binding protein Lasp-1 (Rachlin and Otey, 2006). The observation that palladin binds to an unusually large number of actin-binding proteins suggests that it may function as an actin-associated scaffolding molecule.

Although palladin's precise cellular function and mode of sub-cellular localization is still under investigation, results to date indicate that palladin plays an important role in organizing the actin arrays needed for normal cell adhesion, motility, and changes in morphology during cell development. Palladin expression has been explored in a variety cell types and a mouse model organism. With antisense and siRNA knockdown approaches, loss of palladin expression is associated with a failure of cells to assemble stress fibers, focal adhesions, dorsal ruffles and podosomes (Parast and Otey, 2000; Goicoechea et al., 2006). Up-regulation of palladin correlates with changes in cell morphology and the formation of the actin cytoskeleton in maturing peripheral blood monocytes (Mykkanen et al., 2001). Decreased palladin expression correlates with the loss of filamentous actin as polygonal astrocytes become stellate (Boukhelifa et al., 2003). However, up-regulation of palladin and increased stress fibers are both seen in stellate astrocytes in response to injury.

Palladin's function has also been explored in a knockout mouse model. The palladin null mice die at about embryonic day 15, demonstrating that palladin is essential for normal mammalian embryonic development (Luo et al., 2005). Palladin null embryos exhibit striking defects in body wall closure, both dorsally and ventrally, which supports the view that cell motility is impaired in the absence of palladin expression. In addition, palladin null mouse embryo fibroblasts are defective in their ability to move, adhere and assemble stress fibers (Luo et al., 2005; Liu et al., 2006). Together, these results suggest that palladin is required for normal assembly and remodeling of the actin cytoskeleton.

A common feature of the palladin family of proteins is the presence of multiple immunoglobulin-like (Ig) domains. The three isoforms of palladin are transcribed from a series of nested promoters within a single gene; consequently, the three C-terminal Ig-like domains (Ig3, Ig4, and Ig5) are present in all three isoforms (Rachlin and Otey, 2006). The 140 kDa and 200 kDa isoforms contain an additional fourth Ig domain (Ig2) near the N-terminus, while the 200 kDa isoform contains a total of 5 Ig domains (Ig1-Ig5). Myotilin has two Ig domains that are homologous to the Ig4 and Ig5 domains of palladin (Bang et al., 2001), while myopalladin has five Ig domains that are in the same relative positions and homologous to the five Ig domains of the 200 kDa isoform of palladin (Rachlin and Otey, 2006; Bang et al., 2001).

The Ig fold is a modular domain that appears in both extracellular and intracellular proteins and is often involved in protein-protein interactions (Barclay, 2003; Williams and Barclay, 1988). Ig domains typically contain about 100 amino

acids and consist of seven to nine beta strands that adopt a sandwiched beta sheet fold (Bork et al., 1994). In addition to being a signature domain of this protein family, Ig domains have been described in a small number of other intracellular proteins that are associated with actin and myosin in vertebrates, including myosin light chain kinase (MLCK), myomesin, titin, MyBP-C and MyBP-H (Linke, 2000; Okagaki et al., 1993; Vaughan et al., 1993; Holden et al., 1992). The majority of these Ig-containing proteins are specifically expressed in striated muscle, suggesting that this particular type of Ig domain may play a special role in creating the highly ordered cytoskeleton of the sarcomere (Vaughan et al., 1993; Gilbert et al., 1999). It is interesting to note that inherited forms of heart disease are associated with mutations affecting the Ig domains of either titin or MyBP-C, suggesting that the Ig domains have a key role in maintaining sarcomere integrity (Gerull et al., 2006; Gerull et al., 2002; Oakley et al., 2004; Watkins et al., 1995).

Currently, the precise molecular function of palladin family Ig domains is a matter of debate. The binding site of ezrin has been mapped to a region containing the Ig4 and Ig5 domains of palladin (Mykkanen et al., 2001). However, a number of recent reports suggest the interesting possibility that certain Ig domains can function as actin or myosin-binding modules. Isolated protein fragments containing Ig domains and flanking sequence derived from the palladin relative myotilin have been shown to bind directly to F-actin (Salmikangas et al., 2003; von Nandelstadh et al., 2005). Myotilin even appears to function as an actin-bundling protein *in vitro*, as purified myotilin promotes the formation of large, multi-filament aggregates that have been imaged by electron microscopy and also detected in differential sedimentation

assays (Salmikangas et al., 2003). In certain invertebrate species, skeletal muscle also contains a protein called kettin, which has 31 copies of a similar Ig-like domain (Hakeda et al., 2000). Recently, a fragment containing four of kettin's Ig domains were shown to bind directly to F-actin (Ono et al., 2006). This suggests, first, that binding of actin by Ig domains may be a highly conserved molecular mechanism shared by both vertebrate and invertebrate proteins, and second, that Ig domains within the same molecule may be specialized for different functions. Yet, although these results strongly suggest that certain Ig domains could function as F-actin binding sites, no previous study has shown this conclusively using isolated Ig domains.

The high degree of homology between palladin and myotilin in their Ig domains raises the possibility that palladin may also function as a direct binding partner for F-actin, and we undertook to test this idea using a combination of biochemical and microscopy-based assays. In this report, we show that purified 90 kDa palladin generates actin bundles directly *in vitro* and that one of its Ig domains possesses actin-binding activity. These results support the view that Ig domains can function as conserved actin-binding modules, and add further support to accumulating evidence that multiple Ig domains within the same protein can have specialized functions.

4.2 MATERIALS AND METHODS

Identification and cloning of palladin immunoglobulin domains.

The three tandem Ig domains of the 90 kDa palladin isoform were identified using a BLAST search and were initially characterized as C2-type Ig domains.

However, secondary structure prediction using PSIPredict (Bryson et al., 2005; McGuffin et al., 2000) and ClustalX (Thompson et al., 1997) alignment with telokin (1TLK), titin I1 (1G1C), and twitchin (1WIT) indicated that the three Ig domains of the palladin 90 kDa isoform are members of the I-type immunoglobulin-like domains (Harpaz and Chothia, 1994). Domain boundaries of the palladin Ig domains were determined from the secondary structure prediction using PSiPredict. The DNA sequences and the translated protein sequences for the palladin Ig domains are included in the Supplemental section.

Expression and purification of palladin fragments.

Full-length 90 kDa palladin was expressed as 6xHis fusion protein in Sf9 insect cells using a commercially-generated baculovirus (BD Biosciences), and purified using a commercial affinity purification kit (BD Biosciences) (Boukhelifa et al., 2006).

DNA sequences encoding 1) the individual Ig3, Ig4, and Ig5 domains, 2) a fragment containing the linker sequence between the Ig3 and Ig4 domain, and 3) the tandem Ig3-Ig4, and Ig4-Ig5 domains of palladin were inserted into a modified pMAL-c2x (New England Biolabs) expression vector with the sequence ENLYFQG encoding a TEV protease cleavage site inserted between the maltose-binding protein (MBP) affinity tag and the palladin inserts. The plasmids were transformed into BL21(DE3) CodonPlus-RIPL E.coli (Stratagene) and colonies were selected from agar plates containing 75 mg/mL ampicillin. Cell cultures were grown in Luria broth supplemented with 10 g/L glucose at 37° C to OD_{600} = 0.6-0.8 and induced

with 0.5 mM IPTG. Following induction, cells were grown at 30° C for four hours, then harvested by centrifugation for 20 minutes at 3000 RPM. Cells were resuspended in lysis buffer (50 mM Tris-Cl pH 7.4, 150 mM NaCl, 1 mM EDTA, 10 mM DTT, 1 mM PMSF, and 1X BAL (1000X BAL = 10 mg/mL benzamidine, 2 mg/mL antipain, and 1mg/mL leupeptin)) and the cell membranes were lysed by sonication using a Fisher Scientific Model 550 Sonic Dismembrator. The cell lysate was centrifuged at 17,000 RPM for one hour to pellet any insoluble contents. The soluble contents of the cell lysate were loaded at ~2 mL/min on a column of amylose-functionalized agarose resin (New England Biolabs). The column was washed with 50 mL of column buffer (50 mM Tris pH 7.4, 200 mM NaCl, 2 mM DTT, 1 mM EDTA) after which the fusion protein was eluted with an elution buffer (column buffer + 10 mM maltose) and collected in 3 mL fractions. Fractions containing protein were identified by Bradford assay (BioRad) and checked by SDS-PAGE. The fractions containing the fusion protein were combined, the affinity tag was cleaved overnight at room temperature in the elution buffer with 1X BAL, and 0.6 mg tobacco etch virus (TEV) protease (pRK793, Addgene, Inc) added. The following day, the cleaved protein was diluted three-fold with a dilution buffer (25 mM KH_2PO_4 (pH = 5.5), 2 mM DTT, and 0.1% NaN_3) in order to lower the pH and salt concentration. The diluted protein sample was purified by ion-exchange on an ÄKTA*FPLC* (GE Healthcare) with a HiPrep™ SP XL column. The protein was loaded on the column with Buffer A (25 mM KH_2PO_4 (pH = 5.5), 25 mM NaCl, 2 mM DTT, and 0.1% NaN_3) with a flow rate of 0.5 mL/min. The column was washed with two column volumes and then the protein was eluted using a gradient with a target

concentration of 100% Buffer B (25 mM KH_2PO_4 (pH = 5.5), 1 M NaCl, 2 mM DTT, and 0.1% NaN_3) over 10 column volumes. Fractions containing protein were determined by UV absorbance at 280 nm and confirmed by SDS-PAGE. Reagents were purchased from Sigma, unless otherwise indicated.

Actin co-sedimentation assay.

A solution of 6.4 mg/ml actin purified from rabbit muscle acetone powder was diluted two-fold with an equal volume of 2x F-actin buffer (20 mM Tris pH 8.0, 200 mM KCl, 5 mM $MgCl_2$, and 4mM DTT) and allowed to polymerize at room temperature for thirty minutes. Purified palladin was centrifuged at 150,000 x g for twenty minutes to pellet any insoluble protein immediately before the co-sedimentation samples were prepared. Samples were prepared that contained 10 μM of the polymerized actin and 10 μM of the palladin proteins in a total volume of 200 μL. A control sample was prepared substituting the palladin protein solution with an equal volume of buffer. The samples were incubated for one hour at room temperature and centrifuged at 150,000 x g for thirty minutes. Supernatants were collected and boiled in Laemmli sample buffer. The pellets were washed quickly with 1x F-actin buffer and re-suspended in 200 μL of water, which was also boiled in Laemmli sample buffer. Twenty-five microliters of each sample was loaded onto a Bis-Tris 4-12% gradient polyacrylamide gel and separated by electrophoresis in MES running buffer. The gels were stained with SimplyBlue SafeStain (Invitrogen) and destained with water. Gel images were acquired by scanning the gels with Licor's Odyssey infrared scanner, which allows for quantitative measurements.

For the differential sedimentation assay of actin bundle formation, one additional centrifugation step was added. The samples were first centrifuged at 5,000 x g for ten minutes. The 5,000 x g pellets were washed quickly with 1x M buffer and re-suspended in 100 µL of water before being boiled with Laemmli buffer. The supernatants were collected and centrifuged at 150,000 x g for thirty minutes and treated as described above.

Electron microscopy of actin filaments.

A solution of 6.4 mg/ml actin purified from rabbit muscle acetone powder was polymerized at 74 µM concentration by adding an equal volume of 2x F-actin buffer (20 mM Tris pH 8.0, 200 mM KCl and 5 mM $MgCl_2$). After polymerizing for one hour, the F-actin gel was diluted to 10 µM actin in 1x F-actin buffer. Baculovirus-purified palladin was added to 1 µM in the actin gel. Palladin buffer was added to the control. The samples were allowed to incubate for 30 minutes before being diluted, first to 1 µM actin with 2.0 µM Alexafluor-488 phalloidin (Molecular Probes) and then to 100 nM actin. Samples were pipetted onto a carbon-coated, copper-mesh grid and stained with 1% uranyl acetate for thirty seconds, blotted and then allowed to dry. Negative stain images were acquired using an FEI-Philips Tecnai 12 (FEI Company, Hillsboro, OR) transmission electron microscope. Images were collected at 80 kV with a 1k x 1k CCD camera (Gatan, Pleasanton, CA).

Fluorescence microscopy of actin filament bundles.

A solution of 6.4 mg/ml actin purified from rabbit muscle acetone powder was polymerized at 74 μM concentration by adding an equal volume of 2x F-actin buffer (20 mM Tris pH 8.0, 100 mM KCl and 5 mM $MgCl_2$). After polymerizing for thirty minutes, the F-actin gel was diluted to 10 μM actin in 1x F-actin buffer. Baculovirus-purified palladin was added to 1 μM in the actin gel. Palladin buffer was added to the control. The samples were allowed to incubate for 30 minutes before being diluted first to 1 μM actin with 1.5 μM Alexafluor-488 phalloidin, and then to 100 nM. Five microliters of each sample was placed in between a coverslip and glass slide and visualized by epifluorescence using a Nikon TE2000-U microscope with 60x objective lens, an optional 1.5x tube lens and a Hamamatsu Orca-ER camera.

Size exclusion chromatography – multiple angle light scattering (SEC-MALS).

The purified 90 kDa palladin isoform and Ig3-Ig4 fragment were buffer-exchanged into a solution of 20 mM Tris (pH 7.4), 150 mM NaCl, 2 mM DTT and 0.01% NaN_3. Samples were also repeated in a similar buffer containing 100 KCl in place of the 150 mM NaCl. The samples were loaded onto a Superdex 200 column (GE Healthcare) with a flow rate of 0.5 mL/s and the elution was sampled every 0.5 s. The laser wavelength was set at 690 nm and data were analyzed using ASTRA 4.90.08 (Wyatt Technology).

Homology modeling of the palladin Ig3 domain.

Suitable templates for the homology modeling of the palladin Ig3 domain were chosen using a BLAST search (Altschul et al., 1997) and the Inub server at the

University of Buffalo Center of Excellence in Bioinformatics (Fischer, 2003). Both search queries identified Ig domains of titin and the C-terminal domain of myosin light chain kinase, also called telokin, as good candidates. After examining a sequence alignment with the palladin Ig3 domain using Clustal X (Thompson et al., 1997), X-ray structures of the titin I1 domain (pdb 1G1C) and telokin (1F1G) were chosen as templates for homology modeling of the palladin Ig3 domain. The homology model was built for the Ig3 construct that we have been able to express and purify, namely residues 277-381 of the murine 90 kDa palladin sequence. The protein sequence for the 90 kDa isoform of mouse palladin is given in Supplemental Section 1 of Rachlin, et al. (Rachlin and Otey, 2006). Both templates required the addition of a residue at the position occupied by P323 of the palladin sequence. Insight II (Accelrys) was used to build the homology model using the Biopolymer module to add the additional residue to the templates and the Homology module to construct the homology model. Both templates produced excellent homology models, however the homology model based on the titin I1 domain produced a higher sequence-structure self consistency score (0.74) and was therefore selected as the better template to generate the homology model.

4.3 RESULTS

Purification of the palladin 90 kDa isoform.

After previous unsuccessful attempts to generate purified palladin from bacterial hosts, we cloned the 90 kDa palladin isoform into baculovirus and expressed the protein in insect cells in high yield (Boukhelifa et al., 2004). The

ability to over-express and purify palladin provided us with the opportunity to investigate the molecular mechanisms of palladin *in vitro*, without the complication of other actin-associated proteins that may co-purify with palladin. Palladin is known to co-localize with α-actinin and VASP to dense regions along actin stress fibers (Ronty et al., 2004); however, whether palladin is able to interact with F-actin directly has not been previously determined. Palladin over-expression in Cos-7 cells is correlated with the rearrangement of actin into super-robust bundles (Rachlin and Otey, 2006; Ronty et al., 2004), but whether palladin can bundle actin directly or is able to regulate other proteins which bundle actin is not clear. Palladin in mouse embryonic fibroblast (MEF) lysate has been shown to co-sediment with F-actin when centrifuged at 14,000 rpm (Parast and Otey, 2000); we now have the opportunity to investigate whether purified palladin co-sediments with F-actin in the absence of other binding partners.

Palladin binds directly to F-actin and crosslinks filaments into bundles.

Palladin's recruitment to stress fibers and other filamentous actin arrays may be achieved in one of two ways: (1) palladin may bind directly to actin filaments or (2) palladin may be associating with actin indirectly through one of its binding partners (e.g. α-actinin or VASP). To determine if palladin binds to F-actin directly, we performed an actin co-sedimentation assay using purified actin and purified 90 kDa palladin. After incubating palladin with filamentous actin, the samples were spun at high speed to pellet the insoluble actin fraction. Approximately 40% of the palladin co-sedimented with the F-actin fraction, indicating that palladin can bind

directly to actin (Figure 4.1 A). In a control sample containing palladin alone, the protein remained soluble and did not sediment by itself (data not shown).

Previous studies have shown that modifying palladin expression in Cos-7 cells results in dramatic changes in cytoskeletal architecture (Rachlin and Otey, 2006; Ronty et al., 2004). We reasoned that if palladin is binding to actin directly, it could also be acting as a filament crosslinking protein, which could give rise to the observed hyper-bundling phenotype when palladin is over-expressed. To test this, we repeated the co-sedimentation assay, this time adding an initial low speed (5000 x g) spin to pellet the actin bundles before using a high-speed spin (150,000 x g) to pellet the remaining actin filaments. Only a small fraction of the actin filaments sedimented at low speed in the absence of palladin, while about half of the actin pelleted in the presence of palladin (Figure 4.1 B). This indicates that palladin is crosslinking individual filaments into actin bundles.

To confirm these results, actin bundles were visualized using electron microscopy. When actin is incubated with full-length palladin, robust multi-filament bundles were seen (Figure 4.1 C). The bundles were closely-spaced and often slightly curved, suggestive of flexible crosslinking.

Palladin's Ig3 domain binds to actin.

We next sought to identify the specific region(s) of palladin that is responsible for actin binding. Analysis of palladin's sequence did not reveal any of the canonical actin binding domains described for other actin-modifying proteins (dos Remedios et al., 2003). However, palladin's C-terminal half contains three immunoglobulin-like

domains, similar to those that have been implicated in F-actin binding in palladin's relatives myotilin and kettin (von Nandelstadh et al., 2005; Ono et al., 2006), so we undertook to test the ability of isolated Ig domains derived from palladin to bind directly to F-actin. As shown in Figure 4.2 B, the Ig3 domain was the minimum fragment necessary for binding to filamentous actin. This is a novel result, because in no previous case has a single Ig domain been shown to be sufficient for actin binding. The Ig4 and Ig5 domains showed no actin-binding activity, demonstrating that although the domains appear to be structurally similar on the basis of secondary structure prediction and sequence alignments, the actin-binding ability of palladin's Ig3 domain is unique. The tandem Ig4-Ig5 fragment also did not bind to F-actin. Although the isolated Ig4 domain did not bind to F-actin in this assay, a palladin fragment containing both Ig3 and Ig4 exhibited much greater affinity for actin than the Ig3 domain alone. The residues in the Ig3/Ig4 linker region that are near the C-terminus of Ig3 contain a high incidence of basic residues (eight of the first eighteen residues are basic). Since basic residues have been implicated in a number of actin-binding interfaces (Amann et al., 1998; de Arruda et al., 1992; Huttelmaier et al., Janssen et al., 2006; Lee et al., 2004; Li et al., 1998; Tang et al., 1997; Yarmola et al., 2001), it is reasonable that the linker region may enhance an electrostatic interaction between the Ig3 domain and F-actin. However, neither the Ig4 domain nor the Ig3/Ig4 linker region alone is able to bind to actin.

While both the 90 kDa and 140 kDa palladin isoforms share the three C-terminal Ig domains tested in this assay, the 140 kDa isoform contains an additional Ig domain (Ig2) at its N-terminus. In Cos-7 cells, expression of this larger isoform

increases the density of stress fibers, leading us to hypothesize that Ig2 may also bind to actin, thereby promoting bundle formation. This is not the case, however, as Ig2 showed no binding to actin filaments in these assays (Fig. 4.3).

Determination of the binding affinity of the 90 kDa isoform and palladin fragments with F-actin.

The concentration of F-actin was held constant and increasing amounts of palladin protein were used in co-sedimentation assays to determine the binding affinity for the Ig3 and Ig3-4 fragments as well as the full-length 90 kDa isoform. We could not determine a value for the Ig3 fragment, as the binding did not completely saturate within the concentration range we could achieve with the purified fragment. We estimate that the K_d is between 60-80 μM, based on repeated attempts to determine this binding affinity. The data were fit to a hyperbolic curve, assuming a 1:1 stoichiometry and specific binding only. We determined K_d values to be 2.1 ± 0.5 μM for the full-length 90 kDa isoform (Figure 4.2 C) and 8.7 ± 1.5 μM for the Ig3-4 fragment (Figure 4.2 D).

Identification of the binding interface between Ig3 and F-actin

We sought to determine the dependence of F-actin binding to palladin Ig fragments as a function of salt concentration, as a number of other actin-binding proteins have been shown to bind actin in a salt-dependent manner (Amann et al., 1998; Huttelmaier et al., 1999; Lee et al., 2004; Li et al., 1998; Tang et al., 1997). An increase in the ability to bind actin as the salt concentration is lowered is usually

an indication that the binding is driven by electrostatic interactions. To test this idea, we performed F-actin co-sedimentation assays at KCl concentrations of 25, 50, 100, and 200 mM. We found that the interaction between F-actin and the palladin Ig3 domain was strongly salt-dependent and that binding greatly increased as the salt concentration was lowered (Fig. 4.4). Additionally, we confirmed that the Ig4 domain of palladin exhibited no interaction with actin at lower salt concentrations (data not shown).

Since basic residues have been implicated in a number of actin-binding interfaces (Harpaz and Chothia, 1994; Altschul et al., 1997; Fisher, 2003; Amann et al., 1998; de Arruda et al., 1992; Huttelmaier et al., 1999; Janssen et al., 2006; Lee et al., 2004), we hypothesized that these regions may confer an electrostatic interaction between the Ig3 domain and F-actin. To further elucidate the binding interface a homology model of the Ig3 domain based on titin's I1 domain was used to reveal two basic patches (Fig. 4.5). One is on the surface of the folded domain, and the other lies in the Ig3/Ig4 linker region near the C-terminus of Ig3. We identified the basic residues in each patch were that were not likely to be involved in salt-bridges, and therefore were not necessary for domain folding to occur. These residues were changed to alanine, and cosedimentation assays were performed on each mutant.

Compared with wild-type Ig3, the K15A,H16A,K18A mutant showed a dramatic reduction in its ability to bind F-actin (Fig. 4.6). Mutations in the other basic patch (K36A, K38A) caused no change the ability of Ig3L (a fragment comprising Ig3

plus the Ig3-Ig4 linker region) to bind F-actin. Ig4 was used as a negative control for binding.

Next, sequential mutations in Basic Patch 1 were used to assess the relative contribution of each residue to actin binding. Compared with wild-type Ig3, the K15A showed a slight decrease in actin binding, which was not changed in the K15A-H16A mutant (Fig 4.7). The triple mutant, K15A-H16A-K18A, shows the greatest decrease in its affinity for F-actin. This suggests that the basic patch comprised of K15, H16, and K18 is responsible for actin binding. NMR analysis of the mutated fragments reveals that the domain structure is still folded and that these mutations affect only one face of the protein (Fig. 4.8).

The tandem Ig3 and Ig4 domains of palladin are required to bundle actin.

The palladin fragments were then used in a differential sedimentation assay to identify the smallest fragment of palladin that is capable of bundling actin filaments. While Ig3 continued to sediment with actin in the high-speed centrifugation, we did not detect a significant amount of actin bundle formation when F-actin was incubated with the Ig3 domain (Fig. 4.9 A). The previous co-sedimentation experiments indicated that the fragments Ig4, Ig5, Ig4-5, and the Ig3/Ig4 linker sequence do not bind F-actin so it is not unexpected that they also fail to bundle F-actin. We did, however, detect actin bundles when F-actin was incubated with a fragment containing both Ig3 and Ig4 (Figure 4.9 A, B).

Because the concentration of Ig3-Ig4 used in the differential sedimentation assay was enough to completely bundle the F-actin present in the sample, we

sought to determine the critical concentration at which Ig3-Ig4 can maximally bundle actin. Increasing concentrations of Ig3-Ig4 were added to 10 μM actin, and densitometry of the coomassie stained gel revealed that between 2 and 5 μM Ig3-Ig4 was sufficient to pellet all of the F-actin in a low speed spin (Fig. 4.10). This implies that the fragment is a highly efficient actin bundling domain.

We used fluorescence microscopy to visualize the bundles formed by 90 kDa palladin and the Ig3-Ig4 construct (Fig. 4.11). As expected, bundles were not observed when F-actin was incubated with Ig3 or the tandem Ig4-Ig5 fragment. Bundles formed by α-actinin served as a control. Actin bundles generated by Ig3-Ig4 were also imaged at high-resolution by electron microscopy, as shown in Fig. 4.12.

In order to bundle actin filaments, palladin must either bind two filaments simultaneously, or bind single filaments and dimerize. To test the second hypothesis, we subjected full-length palladin and the Ig3-Ig4 fragment to size-exclusion chromatography, coupled with multi-angle light scattering to determine the molecular weight of palladin in solution. These analyses detected only monomers at physiological salt, indicating that neither the full-length protein, nor the Ig3-Ig4 fragment dimerize in this assay (Fig. 4.13).

Palladin Ig3 mutant localizes to stress fibers

To determine whether palladin's sub-cellular localization to actin arrays is dependent on Ig3's ability to directly bind actin, a GFP tagged 90 kDa palladin construct was prepared with the introduction of the K15A and K18A mutations that

resulted in the greatest reduction in actin binding. In Cos-7 cells, which lack robust stress fibers and express undetectable levels of palladin, GFP-palladin over-expression leads to the formation of dense actin bundles (Rachlin and Otey, 2006). Over time, these stress fibers detach from their focal contacts and contract, leaving large and small aggregates of actin, GFP-palladin, and other stress-fiber associated proteins (Fig. 4.14 A, Supplementary movie 4.1).

To determine whether the Ig3-Actin binding region participates in this phenotype, we expressed a GFP-tagged wild-type 90 kDa palladin or K15A,K18A Ig3 palladin in Cos-7 cells. After 24 hours, wild-type palladin appears to decorate stress-fibers, and actin bundles are denser than in untransfected cells (Fig. 4.14 A). The GFP tagged mutant still localizes to stress fibers, and is also capable of inducing the formation of robust actin bundles in Cos-7 cells (Fig. 4.14 B). This implies either that actin binding is not completely eliminated in the mutant or that palladin is capable of targeting actin stress fibers by some other means. It may do so by an additional cryptic actin-binding domain, or through its interaction with other described actin-binding proteins.

Disruption of Ig4 domain alters palladin localization in Cos-7 cells

Genetic comparisons between a non-migratory cancer cell line and derivative cell line that had become highly metastatic revealed that the metastatic cells contained a single amino acid mutation in palladin's Ig4 domain (Fig. 4.15 A) (Terri Brentnall, personal communication). This mutation, named Patu2 after the cell line in which it was discovered, changes a highly-conserved, packed tryptophan in the

core of Ig4 to cysteine (Fig. 4.15 B,C). Because this tryptophan is a consistent feature of palladin's Ig domains, it is likely necessary for proper domain folding.

When the Patu2 GFP-palladin mutant is introduced into Cos-7 cells, the phenotype is noticeably different from wild-type palladin expression (Fig 4.16). At low levels, Patu2 palladin may be observed in puncta along the Cos-7 cell's typically weak actin filaments, but the dense bundles observed with wild-type palladin are absent. Furthermore, while wild-type palladin ultimately leads to the contraction and aggregation of stress fibers, Patu2 palladin forms aggregates that are smaller and lack filamentous actin. Thus, an intact Ig4 domain is necessary for palladin's ability to form dense bundles in Cos-7 cells, but not for its association with actin filaments.

4.4 DISCUSSION

Our results show that the widely-expressed, actin-associated protein palladin functions as an actin-crosslinking protein *in vitro*, and that the Ig3 domain of palladin is involved in F-actin binding. These results indicate that palladin occupies an unusual functional niche: since the proline-rich domains in palladin's N-terminal half have been shown previously to be docking sites for multiple actin-binding proteins, it appears that palladin is essentially a cytoskeletal-scaffolding protein fused to an actin-crosslinking protein. This distinctive molecular function is likely to underlie the dramatic effects on actin organization that result from palladin over-expression (Rachlin and Otey, 2006; Ronty et al., 2004). It is interesting to note that palladin binds to three other proteins that have been shown to crosslink actin filaments *in vitro*: α-actinin, VASP and Eps8 (Goicoechea et al., 2006; Ronty et al., 2004;

Boukhelifa et al., 2004). This observation raises some interesting questions about the evolution of actin-bundling proteins in vertebrate cells: do these multiple actin-crosslinking proteins function synergistically or redundantly, or do they possess subtle functional differences in their ability to generate multi-filament arrays? In the case of *Drosophila* proteins forked and fascin, both crosslinkers are required for the formation of robust, mature actin bundles, and their functions seem to be temporally regulated (Tilney et al., 1998). Fascin and α-actinin in mammalian cells can individually crosslink actin, though together they function synergistically to enhance cell stiffness and elasticity and alter the geometry of actin filament bundles (Tseng et al., 2005). Recently, Disanza et al. describe their work on the actin crosslinking pair Eps8 and IRS-p53, which, when bound to one another, releases auto-inhibition of IRS-p53 and unmasks its actin binding domain (Disanza et al., 2006). Similar to these examples, palladin and α-actinin may co-regulate their activities, crosslink synergistically, or contribute to different phases of stress fiber formation.

While it is not clear whether palladin and α-actinin may be functioning cooperatively as actin-bundling proteins, there is evidence to suggest that the region of palladin that is responsible for its binding interaction with α-actinin is particularly important for palladin's cellular function. A recent report has linked a point mutation in palladin to a form of familial pancreatic cancer, and has also shown that palladin RNA levels are increased in familial and sporadic precancerous and cancerous pancreatic tissues (Pogue-Geile et al., 2006). The disease-causing mutation occurs in the α-actinin binding region of palladin, and HeLa cells transfected with the mutated form of palladin showed cytoskeletal abnormalities, altered localization of

palladin, and increased motility (Pogue-Geile et al., 2006). In addition to pancreatic cancer, other human diseases and conditions in which palladin has been implicated include pre-eclampsia (Gultice et al., 2006; Jarvenpaa et al., 2007) invasive breast cancer (Wang et al., 2004), and increased risk of heart attack (Shiffman et al., 2005). Clearly, additional studies will be necessary to determine the relative importance of palladin's bundling activity, actinin-binding activity, and other molecular activities, to its cellular function and its precise role in these diverse pathologies.

The results of the F-actin differential centrifugation experiments (Fig. 4.9 A) indicate that the Ig3 domain is an actin-binding domain that is not capable of bundling actin. The isolated Ig3 domain's binding affinity constant for actin is outside of the physiological range (Kd > 60 μM), suggesting that additional palladin sequences may contribute to create a stable binding interaction when the intact palladin protein binds to F-actin. The Ig3-Ig4 fragment binds to F-actin almost as well as the full-length protein (see Figs. 4.2 C and 4.2 D) and is also capable of bundling actin filaments (see Figs. 4.9 A, 4.10, and 4.11). For palladin to crosslink actin, it must bind two actin filaments simultaneously (Puius et al., 1998). This can be achieved if palladin has one actin binding site and forms dimers, or if palladin contains two actin-binding sites per monomer. We have not been able to find a second actin-binding site within the Ig3-Ig4 construct; neither the Ig4 domain nor the region linking the two Ig-like domains appears to bind actin in the co-sedimentation assays (see Fig. 4.2 B). We have also been unable to detect the presence of a dimer in either the full-length molecule or the Ig3-Ig4 fragment using size exclusion chromatography combined with multiple-angle light scattering (SEC-MALS) (Fig.

4.13). One possibility is that filament cross-linking by palladin is a two-step process, similar to the mechanism that has been demonstrated previously for vinculin in which F-actin binding activates a cryptic dimerization site within the vinculin tail domain (Janssen et al., 2006; Johnson and Craig, 2000). Our data are consistent with a model in which binding of F-actin induces a conformational change in palladin that promotes or stabilizes dimer formation. Future work will focus on the structural basis for Ig3's interaction with F-actin and elucidation of mechanisms by which paladin promotes F-actin bundling through its Ig domains.

Our results agree with a general pattern that has been reported previously: Ig domains often occur as multiple copies within one protein and different Ig domains often have specialized functions within the same molecule. For example, MyBP-C possesses three fibronectin type III (Fn3) domains and seven or eight Ig domains, depending on the isoform (Bennett et al., 1999). Only four of the Ig domains bind to myosin, two at the C-terminus (Okagaki et al., 1993; Welikson et al., 2002) and two near the N-terminus (Ababou et al., 2007). Additionally, interactions between domains of MyBP-C have been found for two of the Ig domains and one Ig domain with a Fn3 domain (Moolman-Smook et al., 2002), while the functions of three of the Ig domains have not been clearly defined. Similarly, the functions of the N-terminal Ig domains found in the 140 and 200 kDa isoforms of palladin remain to be determined, and these could turn out to be the same or different from the C-terminal domains. Based on our results and others, the Ig domains found within cytoskeleton-associated proteins may fall into the following functional groups: actin-binding (von Nandelstadh et al., 2005; Ono et al., 2006), myosin-binding (Okagaki et al., 1993;

Welikson et al., 2002), ezrin-binding (Mykkanen et al., 2001), dimer-forming (Fucini et al., 1997), or regulators of molecular spacing (Fucini et al., 1997) and elasticity (Bullard et al., 2006; Bullard et al., 2005; Improta et al., 1996; Politou et al., 1996). As more structural information on different Ig domains becomes available, it may be possible to determine structural specializations that correspond to each of these functional categories.

To begin structural analysis of the palladin Ig domains, we have constructed a homology model of the Ig3 domain based on the I1 domain of titin (1G1C) (Fig. 4.17 A). We predict that the Ig domains of palladin are I-type immunoglobulin-like domains and will have the common features of the I-frame (Fig. 4.17 B). We expect that the actin-binding ability of the Ig3 domain is due to the interaction surface created by the amino acid sequence, rather than a large-scale difference in the protein fold compared to other I-set Ig-like domains. We are in the process of determining the solution structure of Ig3 by NMR spectroscopy. The homology model will aid in both structure determination efforts and in guiding further mutagenesis efforts to identify the site of F-actin binding. Although Ig domains are present in a number of actin/myosin-associated proteins and have been suggested to be involved in actin-binding, the palladin Ig3 domain is the first isolated Ig domain shown to bind F-actin. It will be interesting to determine the structural basis for how, in palladin, the Ig fold has been adapted for actin-binding and other functions, e.g.: dimer formation and interaction with ezrin. These questions will be the focus of additional future experimental efforts.

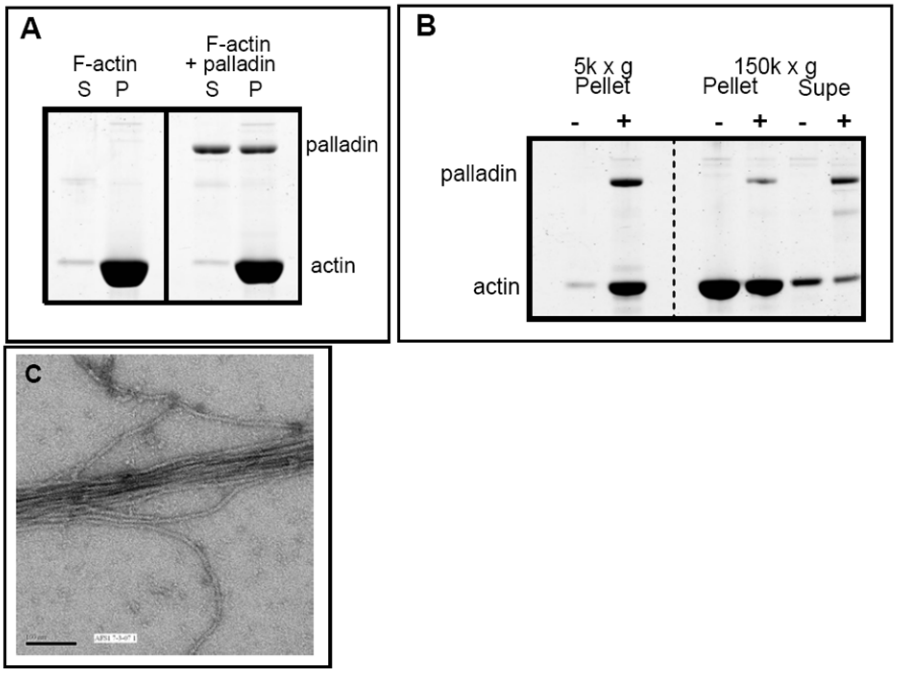

Figure 4.1. Palladin binds and crosslinks F-actin. *A,* 90 kDa palladin binds F-actin. Purified F-actin and palladin were incubated separately or together and then subjected to a high speed centrifugation (150,000 x g). After spinning, supernatants and pellets were separated and resolved by SDS-PAGE. F-actin alone sediments at high speed (left lanes), while palladin does not (not shown). When incubated together, ~40% of palladin co-sediments with the actin filaments (right lanes). *B,* 90 kDa palladin crosslinks F-actin. An actin co-sedimentation assay was performed as in *A,* with one added step. Crosslinked actin was first pelleted in a low-speed spin by centrifuging the samples at 5,000 x g for ten minutes. Pellets from this spin were collected and prepared for SDS-PAGE, while the supernatants were collected and centrifuged at 150,000 x g for thirty minutes, to pellet the remaining F-actin. The samples were resolved by SDS-PAGE, stained and analyzed by scanning densitometry. Palladin crosslinked approximately 50% of the filamentous actin, causing it to sediment in the low speed spin. *C*, Actin bundles visible by EM. Purified 90 kDa palladin was added to F-actin and prepared for imaging by negative stain transmission electron microscopy. Micrographs show thick actin bundles in the presence of palladin, while only individual filaments appear in control samples (not shown).

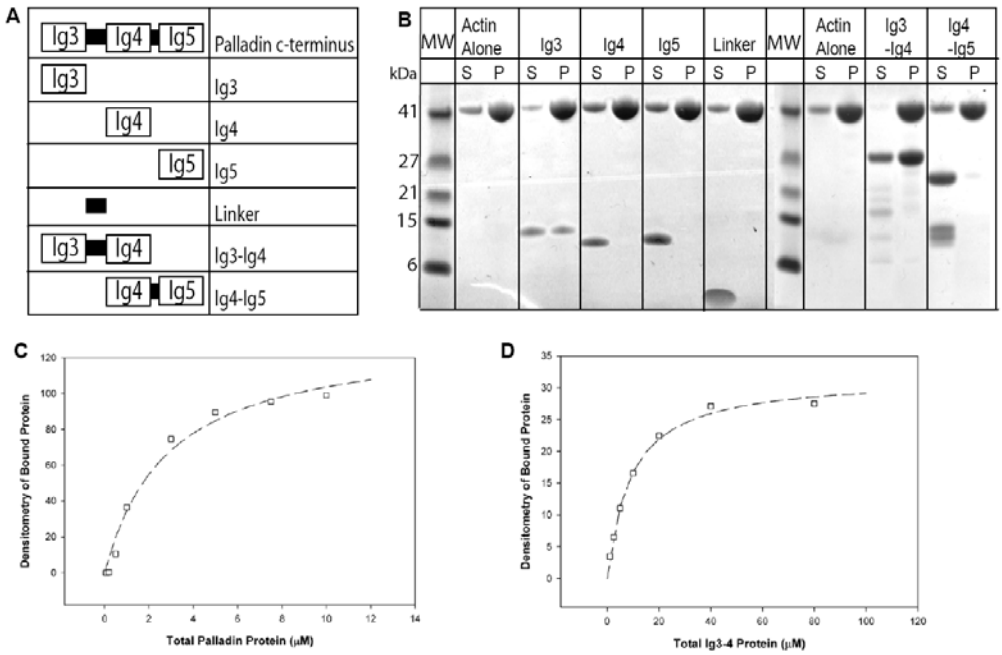

Figure 4.2 Characterization of actin binding within the palladin Ig domains. *A,* Schematic of c-terminal constructs. *B,* Ig3 binds F-actin. Fragments of palladin's C-terminus were purified and assayed for actin binding by co-sedimentation. Ig3 binds filamentous actin, while Ig4 and Ig5 do not. The addition of the linker region and Ig4 in conjunction with Ig3, seem to enhance F-actin binding. *C*, The co-sedimentation assay was performed with variable amounts of 90 kDa palladin and 1 μM F-actin. The fraction of palladin that co-sediments with F-actin was monitored by densitometry of the SDS-PAGE gel. A hyperbolic curve was used to fit the data, assuming a 1:1 stoichiometry and specific binding only, which gives a dissociation constant for full-length palladin with F-actin of 2.1 ± 0.5 μM. *D*, The same assay described in C was performed on the Ig3-4 fragment with 5 μM F-actin. A similar fitting of the data gives a dissociation constant for the Ig3-4 fragment and F-actin of 8.7 ± 1.5 μM.

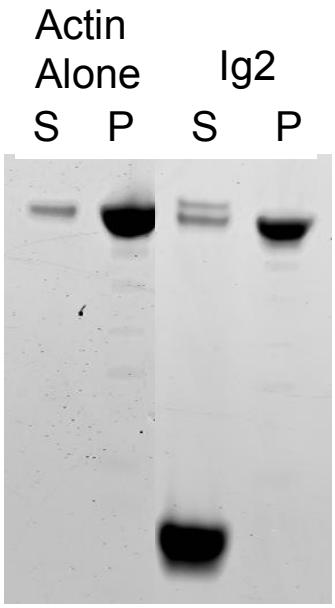

Figure 4.3 Ig2 does not bind actin filaments. Purified Ig2, cloned from the N-terminus of 140 kDa palladin, shows no ability to bind actin filaments, as it segregates with the supernatant (S), and not the pellet (P).

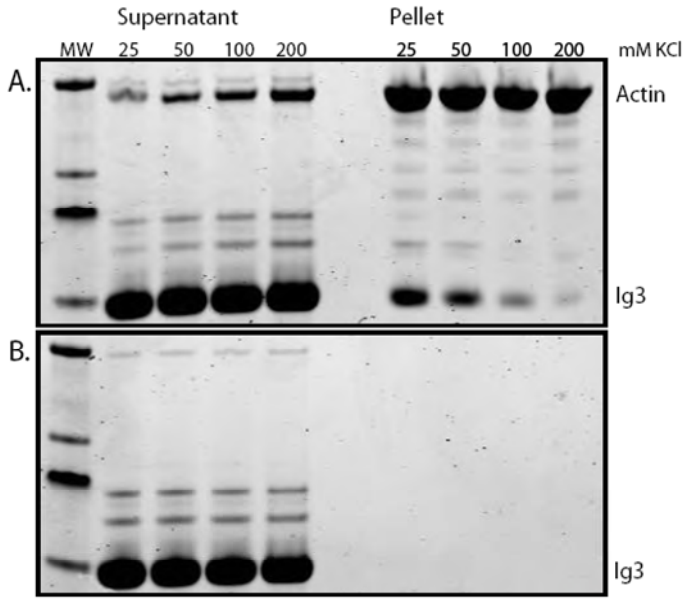

Figure 4.4. *A.* Salt dependence of Ig3-actin interaction. 20 mM Ig3 was incubated with 5 mM actin in buffer containing increasing concentrations of KCl at 25 mM, 50 mM, 100 mM, or 200 mM. The samples were then subjected to centrifugation at 150,000 x g to pellet F-actin. The affinity of Ig3 for actin varies inversely with salt concentration. *B.* Parallel samples without actin were prepared to demonstrate that the protein remains soluble at low salt concentrations.

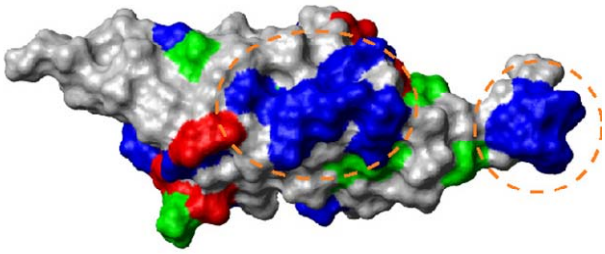

Basic patch 1: Residues Lys15, His16, Lys18

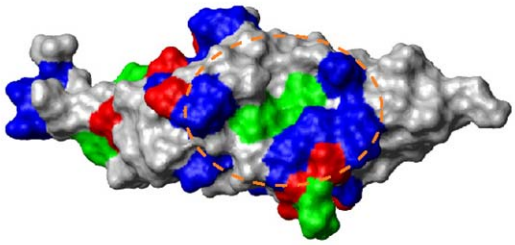

Basic patch 2: Residues Lys36, Lys38

Figure 4.5. Ig3 domain contains two basic patches. Homology modeling of the Ig3 domain revealed two basic patches on the face of the domain that could participate in actin binding. Patch 1 consists of Lys15, His16, and Lys18, while Patch 2 consists of Lys36 and Lys38. Residues are counted from the N-terminus of the Ig3 domain. Color code: blue – basic residues; red – acidic residues; green – polar residues; grey – other.

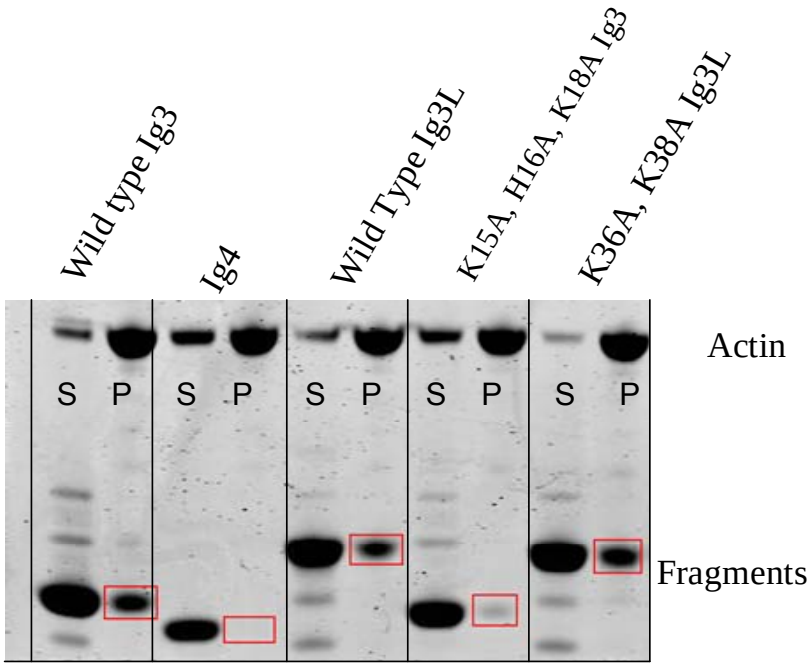

Figure 4.6. Basic Patch 1 is necessary for actin binding. Wild-type and mutant Ig domains were subjected to an actin co-sedimentation assay. Wild-type Ig3 and Ig3L bind F-actin while Ig4 does not. Mutation of Basic Patch 1 (K15A, H16A, K18A) drastically reduces the ability of Ig3 to bind F-actin, while mutation of Patch 2 (K36A, K38A) has no obvious effect on the binding of Ig3L.

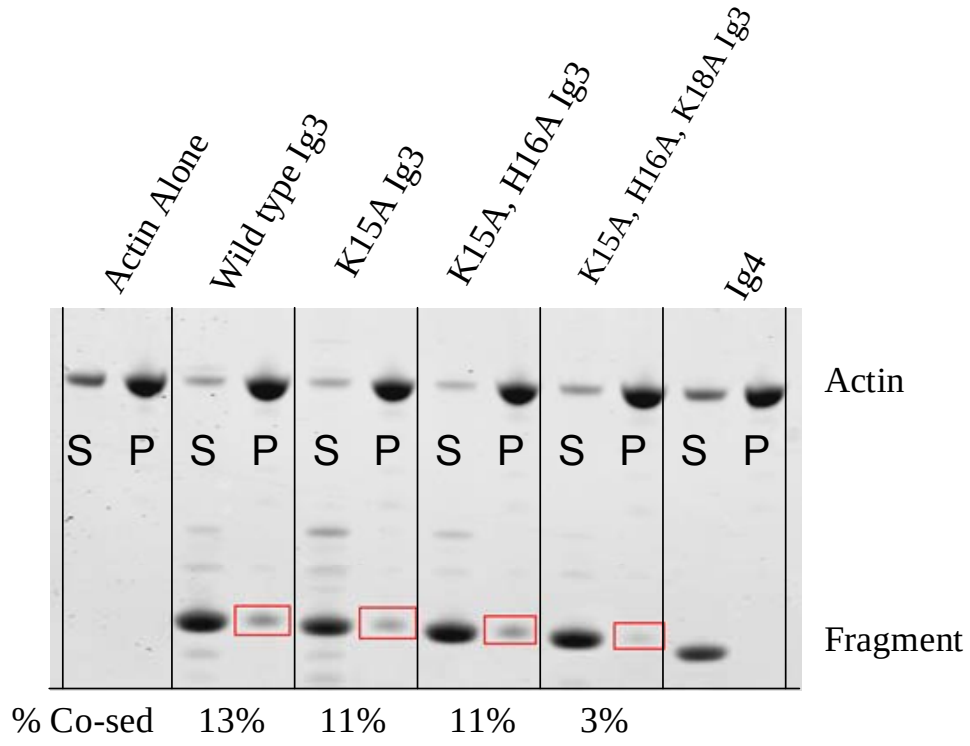

Figure 4.7. Sequential mutation of Basic Patch 1 reduces actin binding. Wild-type and mutant Ig3 domains were subjected to an actin co-sedimentation assay. Wild-type Ig3 binds F-actin while Ig4 does not. Sequential mutation of Basic Patch 1 (K15A, H16A, K18A) gradually reduces the ability of Ig3 to bind F-actin, with the K15A and K18A mutations playing the largest apparent role in binding.

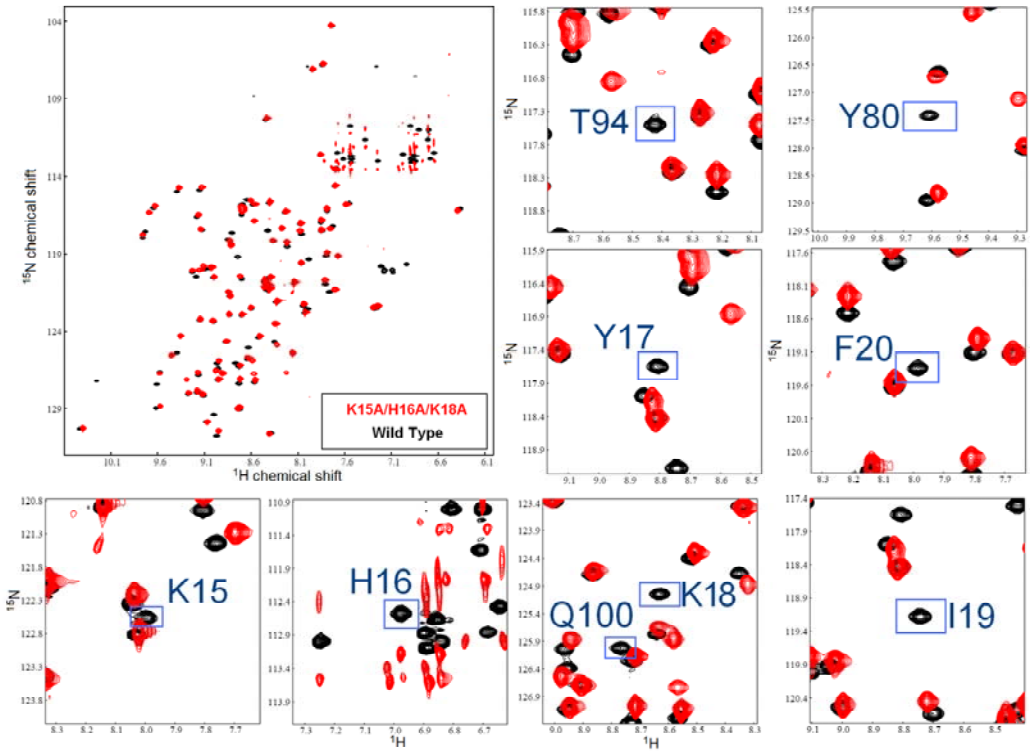

Figure 4.8. Backbone structure of Ig3 is conserved in the triple mutant. Overlay of the 15N-1H HSQC spectrum of K15A/H16A/K18A Ig3 (**Red**) over Wild type Ig3 (**Black**). Over 75% of the backbone amide peaks are unchanged. Peaks corresponding to mutated residues 15, 16 and 18 shift completely, and spatially close residues of 17, 19, 20, 80, 94, 98 and 100 also shift completely. The overlay shows that the overall fold and the backbone structure of the Ig3 domain remains largely unperturbed by the mutations.

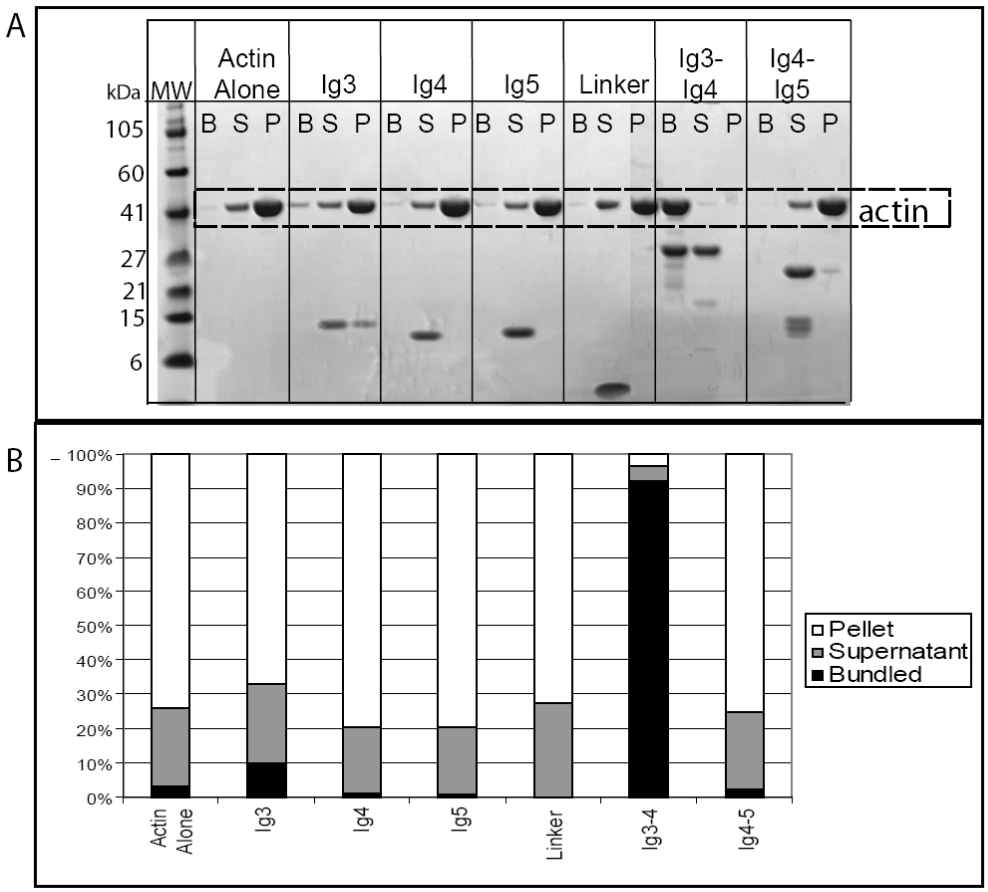

Figure 4.9 Identification of an actin bundling fragment. *A,* Ig3-Ig4 is a fragment capable of bundling actin. Fragments of palladin's c-terminus were used in a differential centrifugation assay to assess their ability to crosslink actin. Samples were subjected to a low speed spin, and actin bundles (B) in the pellet were collected before sedimenting the remaining F-actin by ultra-centrifugation and resolving the supernatant (S) and pellet (P) from these spins by SDS-PAGE. *B,* Quantification of actin bundling. Actin bands from *A.* were analyzed by densitometry to estimate the ability of each construct to bundle actin. Individually, Ig3, Ig4, Ig5, and the linker domain showed no ability to bundle actin, bringing down < 2% of the F-actin in the low speed spin. Ig3-Ig4 exhibited robust actin bundling activity, pulling down 95% of the actin filaments.

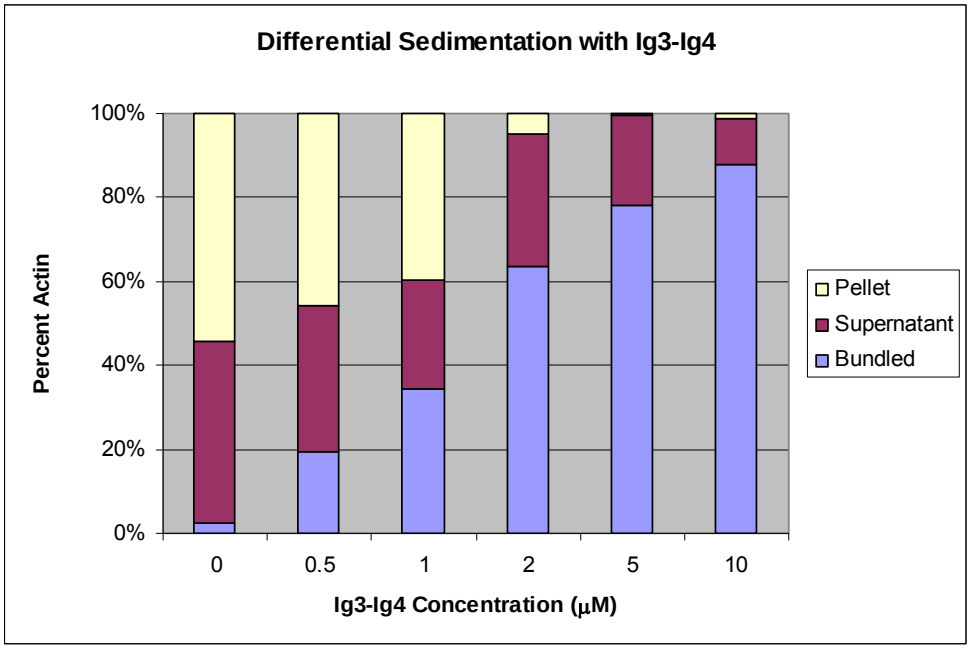

Figure 4.10 Ig3-Ig4 bundles actin in a dose-dependant manner. Increasing concentrations of Ig3-Ig4 fragment were combined with 10 μM F-actin to determine the effective concentration at which maximum bundling occurs. Densitometry of the coomassie stained bands from a differential sedimentation assay revealed that between 2 and 5 μM Ig3-Ig4 fragment is capable of completely bundling 10 μM F-actin.

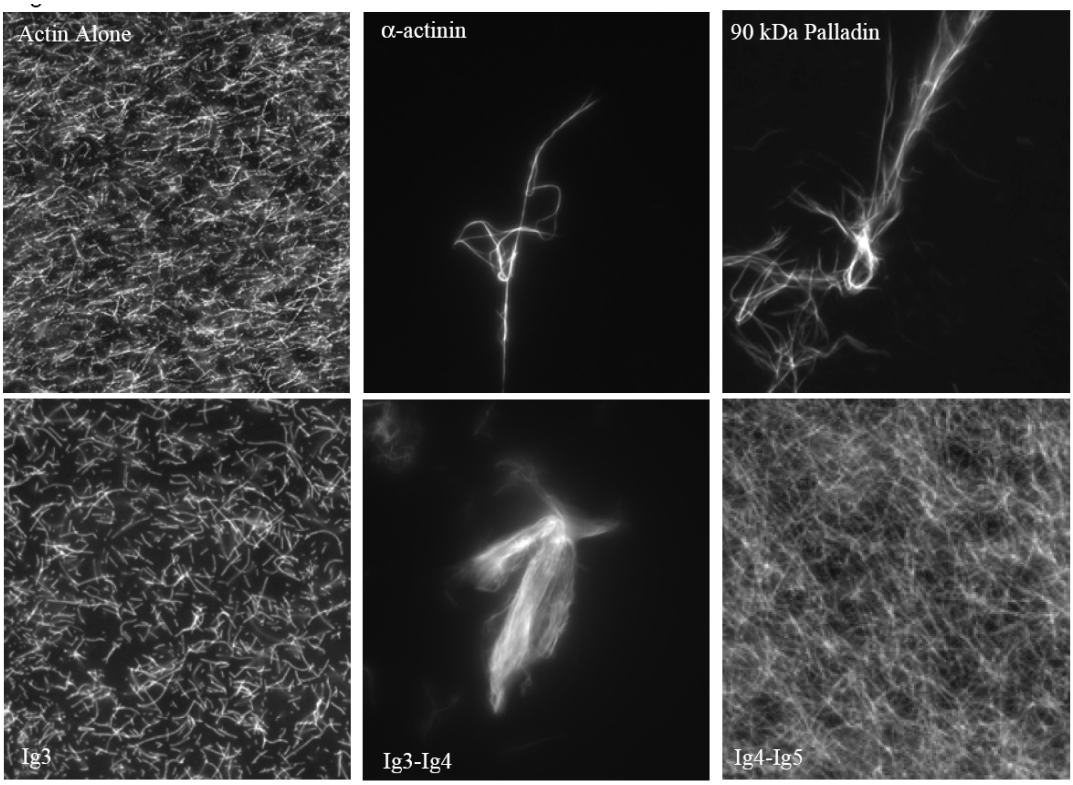

Figure 4.11. Bundling of F-actin by α-actinin, palladin and palladin fragments by fluorescence microscopy. Actin filaments were incubated either alone or with a-actinin, 90 kDa palladin, or Ig-domain containing fragments. Phalloidin-488 was added to visualize the F-actin by epifluorescence. Actin filaments in the absence of a cross-linking protein appear as thin fragments dispersed uniformly across the field. In the presence of α-actinin, the actin filaments are cross-linked, forming robust, stable bundles. Full length 90 kDa palladin is also able to generate similar F-actin bundles. Addition of a fragment containing Ig3 did not generate bundles, while a fragment representing Ig3-Ig4 (including the linker sequence between the Ig domains) did. The fragment containing Ig4-Ig5 did not generate bundles, suggesting that Ig3 plays an essential role in this function.

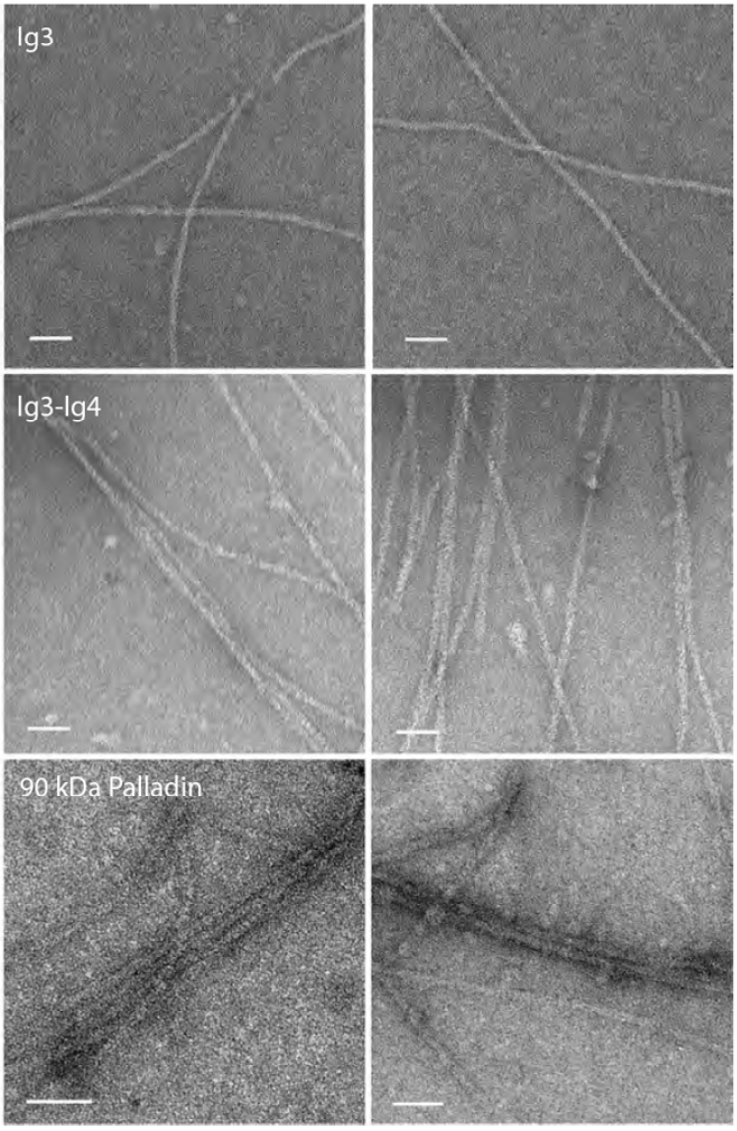

Figure 4.12. Full length palladin and palladin fragments containing Ig3-Ig4 bundle actin, as observed by electron microscopy (EM). F-actin was incubated with either 90 kDa palladin or Ig domain containing fragments. The addition of 90 kDa palladin consistently results in the close association of actin filaments while Ig3 samples contain only individual filaments. Bundles are also visible in Ig3-Ig4 containing samples.

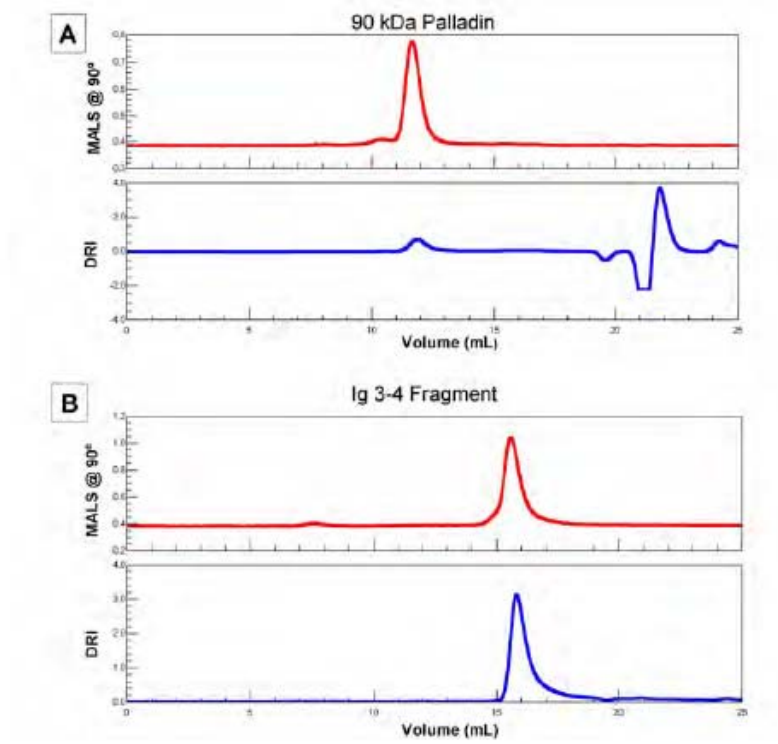

Figure 4.13. Size exclusion chromatography - multiple angle light scattering (SEC-MALS) analysis of the 90 kDa isoform of palladin and the Ig3-4 fragment. Light scattering at the 90º detector (top, red) and the differential refractive index (DRI) monitored by the forward detector (bottom, blue) were used to measure the molecular weights (MW) and hydrodynamic radius moments (Rh(w)) of the proteins and the polydispersities of the peaks. For the full-length 90 kDa palladin isoform, SEC-MALS analysis gave a molecular weight of 77.6 kDa (actual MW = 73.6 kDa), a Rh(w) of 4.7 nm, and a polydispersity for the peak of 1.007±0.003. These results indicate that the 90 kDa palladin isoform is monomeric and extended in solution. Likewise, SEC-MALS analysis of the Ig3-4 fragment determined a molecular weight of 31.5 kDa (actual MW = 26.6 kDa), a Rh(w) of 3.2 nm, and a polydispersity of the peak of 1.11±0.02, suggesting that the Ig3-4 fragment is also monomeric and not compact. Note: artifacts are commonly seen at elution volumes of ~7.5 mL and ~22 mL, associated with the V0 and Vmax of the Superdex 200 column; the antiphase peak in the 90 kDa palladin DRI trace at ~22 mL is due to the sample buffer.

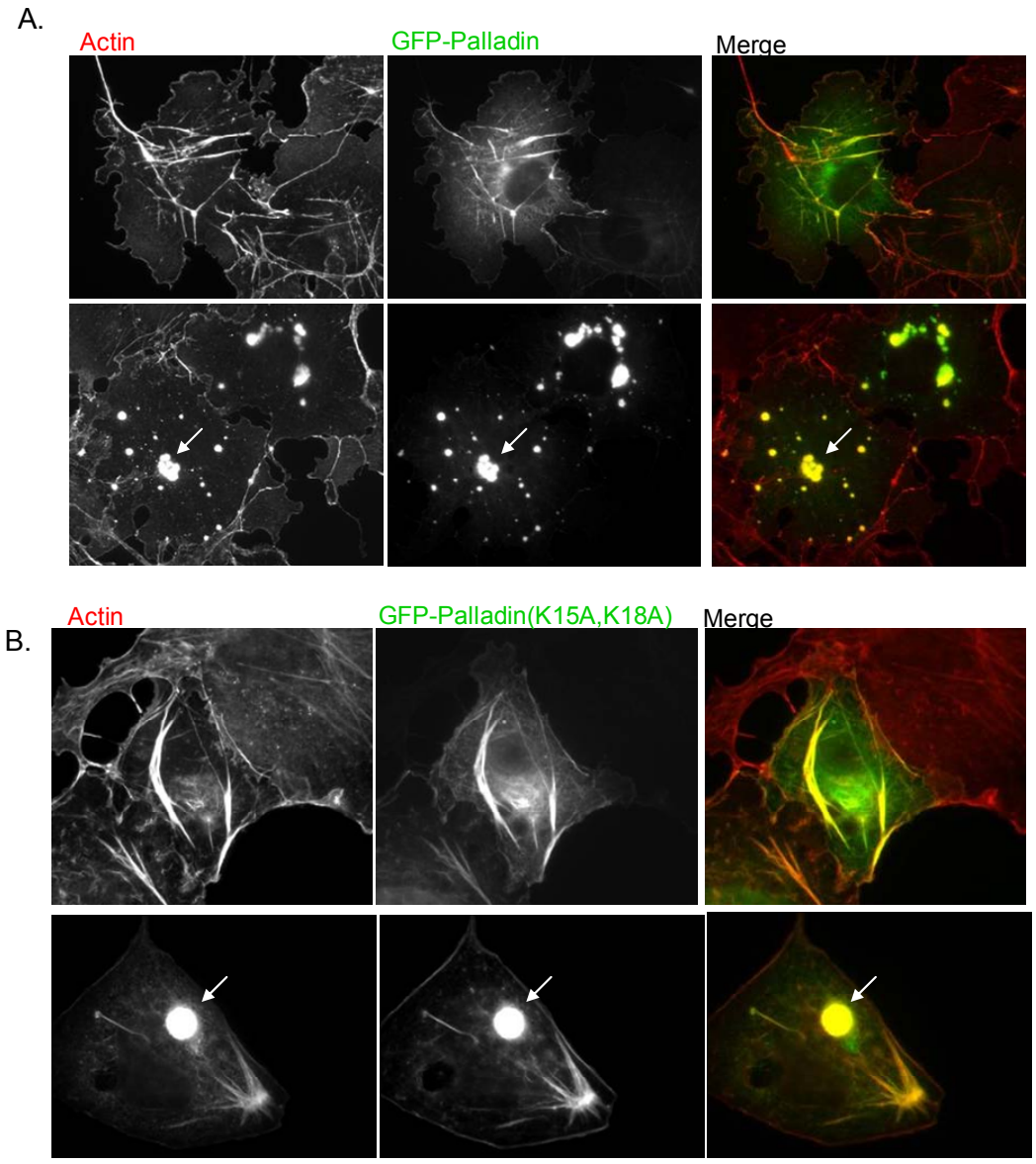

Figure 4.14. K15A,K18A palladin mutation does not alter actin bundling in Cos-7 cells. Cos-7 cells were transfected with either wild-type GFP-90 kDa palladin (A), or the K15A,K18A mutant form (B). In both cases, robust stress fibers are observed 24 hours after transfection, and stress fiber collapse leads to actin/palladin aggregates in the cell (Arrows)

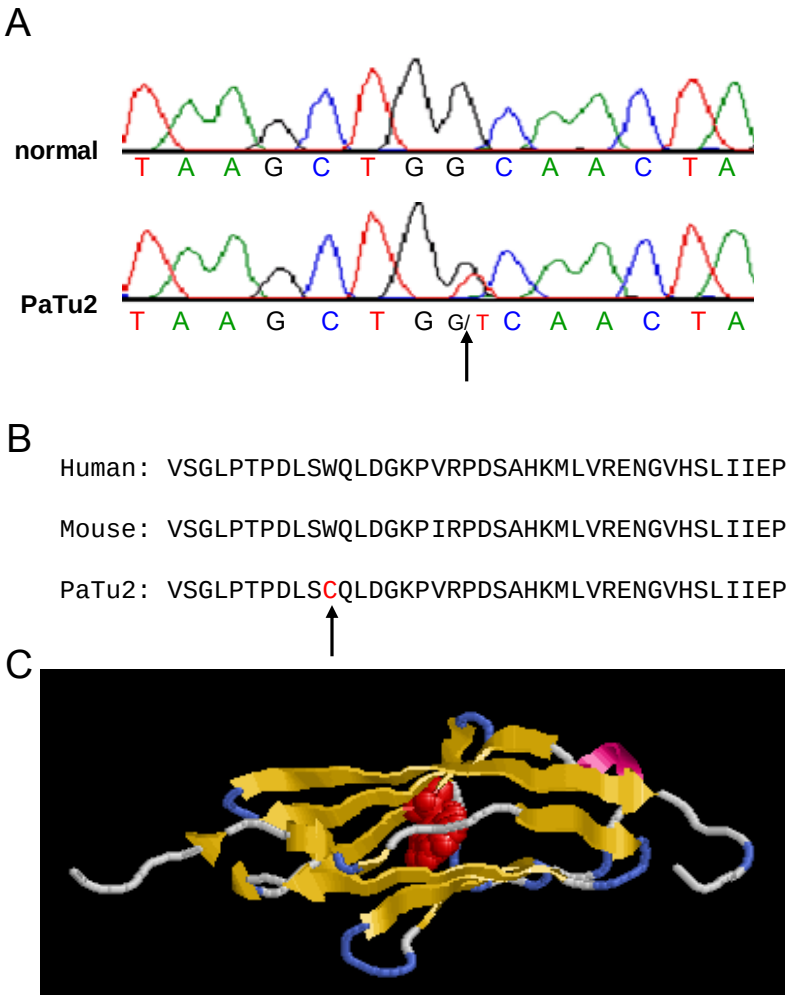

Figure 4.15. Patu2 mutation disrupts palladin's Ig4 domain. A single nucleotide mutation (A) identified in a highly migratory cancer cell line named "Patu2" leads to the substitution of a packed tryptophan in Ig4 for cysteine (B). (C) shows a homology model of Ig4 with the conserved tryptophan indicated in red.

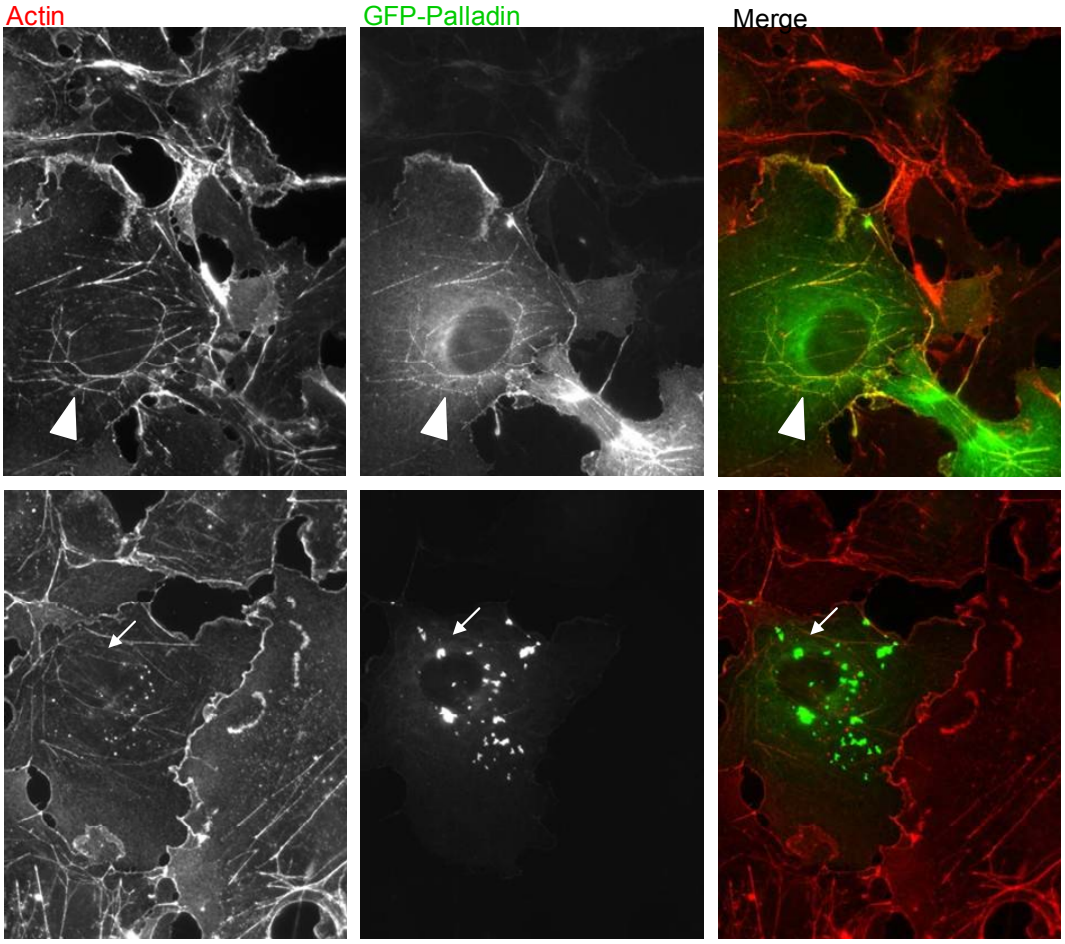

Figure 4.16. Patu2 palladin mutation prevents actin bundling in Cos-7 cells. Cos-7 cells were transfected with GFP-palladin containing a packed tryptophan to cysteine mutation in the Ig4 domain. This mutant fails to induce the formation of robust stress fibers, though it can still be seen decorating thin actin filaments (arrowheads). Interestingly, the mutant palladin aggregates do not appear to contain F-actin as observed in wild-type (arrows).

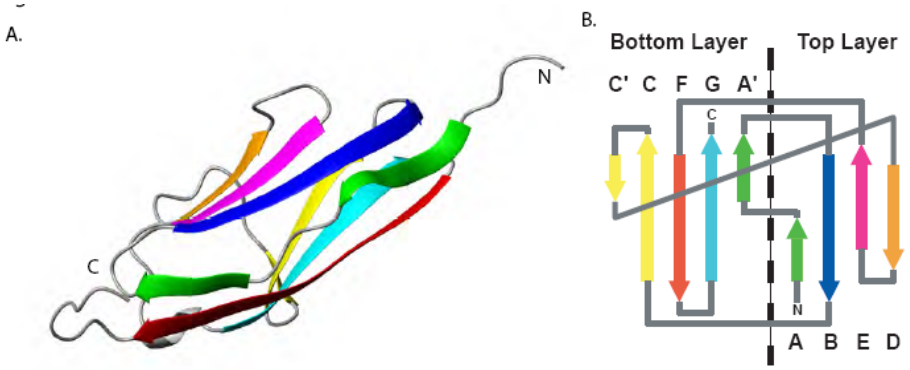

Figure 4.17 *A,* Homology model of palladin's Ig3 domain. The homology model of the Ig3 domain of palladin was constructed using the Homology module of Insight II (Accelrys) and the I1 domain of titin (1G1C) as a template. *B,* The I-set Ig frame. The Ig3 domain is a member of the I-set of immunoglobulin-like domains. The characteristic features of the I-frame are present: the domain contains eight beta strands (by convention labeled A, B, C, C', D, E, F, and G), the A strand is split and hydrogen bonds to both the B strand and the G strand, and the domain has both a C' and D strand.

CHAPTER 5

CONCLUSIONS AND DISCUSSION

5.1 SUMMARY

Reactive astrocytosis is the central nervous system's consistent response to injury. Activated astrocytes migrate to the wound periphery where they hypertrophy and deposit a dense extracellular matrix. Commonly, the glial scar that forms after physical trauma presents a barrier to neurite outgrowth and the functional recovery of severed axonal circuits. Previous reports from our lab demonstrated that palladin immunoreactivity rapidly increased in activated astrocytes both *in vitro* and *in vivo*, but further questions on the method of up-regulation and the functional significance of this change remained.

In this work, we have analyzed the expression patterns of palladin isoforms in a cell culture model of reactive gliosis and extended the biochemical and functional characterization of palladin's Ig domains, as described below:

1. Using a cell culture model of reactive astrocytosis, we have demonstrated that both 90 kDa and 140 kDa palladin are up-regulated on the mRNA level after endothelin treatment, and that this corresponds to an increase in protein levels.

2. The increases in 140 kDa isoform expression as detected by western blot were also observed by immunofluorescence in a scratch wound cell culture model and *in vivo* brain stab injury using a 140 kDa specific antibody.

3. In order to understand palladin's role in three-dimensional migration, we have described palladin's recruitment to a dynamic actin-based structure, the dorsal ruffle, after growth factor stimulation and shown that palladin is a necessary component for ruffle formation. We have also detected palladin in adhesive podosomes and shown that palladin is required for their formation or maintenance.

4. We have demonstrated that both 90 kDa and 140 kDa palladin bind to and bundle F-actin, which gives us new insight into palladin's molecular role in motility.

5. We have performed a molecular dissection of palladin's C-terminus and characterized the Ig3 domain as a novel F-actin binding domain, and the tandem Ig3-Ig4 as a fragment capable of bundling actin filaments *in vitro*. We have also shown that Ig4 and Ig5 are unable to bind F-actin, indicating that individual Ig domains can have unique functional properties.

6. We utilized mutational studies to identify the actin-binding residues of Ig3 and examined the effect on stress fiber bundling in cells.

5.2 DISCUSSION

Palladin's role in motility: expression patterns

The impetus for this study was the observation that palladin is up-regulated in reactive astrocytes after injury (Boukhelifa et al., 2003). Since those observations

were made, new results have shown that this response is not unique to astrocytes. Injured skin and aorta exhibit a similar wound healing response, with fibroblasts or smooth muscle cells near the injury displaying increased palladin expression (Ronty et al, 2006, Jin et al, 2007). This suggests that palladin may be a necessary and conserved feature in cases of wound healing or tissue remodeling.

Changes in palladin expression are not exclusive to pathological responses – the evidence for palladin's role in cell migration during development is also gaining strength. At the broadest level, palladin is required for normal mammalian embryogenesis, as demonstrated by the embryonic lethality of palladin knockout mice (Lou et al. 2005). Knockout embryos die at approximately day 15 and exhibit developmental abnormalities including exencephaly due to failure of neural tube closure and facial clefting. This phenotype may be partially explained by observations made in a microarray study showing that palladin is up-regulated in a subset of neural crest cells, and that palladin up-regulation correlates with subsequent cell migration (Gamill and Bronner-Fraser, 2002). Further, palladin has been identified as a key component for neurite outgrowth, as knocking down palladin in neurons inhibits growth cone extension (Boukhelifa et al., 2001).

Microarray studies done by the Condeelis lab demonstrate that palladin may also be important in cancer metastasis. Analysis of highly invasive breast cancer cells revealed that palladin is up-regulated ~3 fold compared to non-invasive tumor cells, suggesting that palladin plays a role in metastatic tumor progression (Wang et al., 2004). Recent work to identify the causitive mutation in a deadly form of familial pancreatic cancer found a point mutation in the palladin gene that was present in

tumors and pre-cancerous lesions, but not in healthy individuals (Pogue-Geile et al., 2006). Overexpression of this mutant in cultured cells increases their migration rate compared to the overexpression of wild-type palladin. Other reports from the Brentnall lab have identified a second mutation of the palladin gene in a highly migratory cancer cell line called "Patu2." This mutation also increases the migration rate of cultured cells when exogenously expressed (Terri Brentnall, personal communication).

In our own lab, studies of a group of breast cancer cell lines revealed that those exhibiting the greatest metastatic potential also express the highest levels of palladin (Silvia Goicoechea, personal communication.) These cells are also able to invade through an extracellular matrix, a hallmark of the invasive motility that gives rise to metastatic tumor progression. Knocking down palladin in these cells reduces the formation of podosomes, and correspondingly reduces their ability undergo invasive motility through an extracellular matrix. Because both cancer cells and reactive astrocytes are highly plastic and demonstrate an ability to migrate through complex tissue, they may share common cellular machinery, including palladin, to achieve this end.

Taken together, these studies indicate that palladin is an important component of the cellular machinery responsible for migration, and specifically for invasive motility or movement through a complex extracellular environment. While it is obvious that the cell requires a host of actin modifying proteins in order to perform the complicated cytoskeletal remodeling necessary for directed migration, palladin's function may be defined by its ability to activate, scaffold, or coordinate the activity of

these proteins in a tightly regulated manner. In this way, astrocytes and other cells may contain the necessary components for migration even at rest. Then, in the presence of an activating signal, they may up-regulate a small subset of scaffolding or signaling molecules, including palladin, to induce directed migration.

To date, only few "activating signals" that regulate palladin expression have been identified. In the injury models mentioned previously, palladin expression was regulated downstream of TGF-β1 stimulation in fibroblasts (Ronty et al., 2006) and angiotension II signaling in vascular smooth muscle cells (Jin et al, 2007). In this study, we have identified endothelin as a potent activator of palladin expression in cultured astrocytes, and we have demonstrated that two palladin isoforms, though they arise from nested exons within the same gene, are differentially regulated (Chapter 2). Another recent study examining the differentiation of human adipose-derived stem cells during osteogenesis showed that palladin is up-regulated in stem cells grown in osteogenic media, and when cells are subjected to cyclic tensile strain (Wall et al., 2007). This indicates that palladin expression is dependant not only to soluble growth factors and signaling molecules, but also on the physical properties of the extracellular environment.

It is not clear whether TGF-β1, angiotensin II, endothelin, and tensile forces modulate separate signaling pathways within the cell leading to palladin up-regulation, or whether these pathways converge into one common activator of gene transcription. Based on the observation that pharmacological stabilization or disassembly of the actin cytoskeleton regulates palladin expression (Jin et al, 2007), it may be possible that these growth factors and cytokines exert their effect on

palladin expression through a common cytoskeletal remodeling pathway. Because palladin isoforms appear to be differentially regulated in individual cells and tissues (Parast and Otey, 2000; this study, Chapter 2), it is likely that distinct transcriptional regulators exist.

Palladin's role in motility: the molecular basis of migration

While palladin up-regulation appears to correlate strongly with motility in a variety of cell types, palladin's molecular functions in promoting or allowing cell migration are more complex. First, palladin appears to play a critical role in cell-matrix interactions. Studies of cells cultured from knockout mice have shown that palladin null cells exhibit a reduced ability to bind to a deposited extracellular matrix, including fibronectin and collagen, *in vitro*. (Liu et al, 2006, current study, Chapter 2). This response alone may account for some of palladin's effects on cell motility, as proper translocation requires the formation of adhesive contacts that may later be disassembled as the cell moves forward. The ability to generate or stabilize adhesions may be particularly important in the cells surrounding skin and glial scar tissue, or for the ability of metastatic cells to migrate through the vascular basement membrane.

How does palladin achieve its effects on adhesion? Liu et al. (2006) demonstrated that palladin null fibroblasts are deficient in the adhesion molecule β1 integrin. Using protease inhibitors, they discovered that in the absence of palladin, β1 is targeted for degradation by the proteasome, suggesting that palladin plays

some role in integrin stabilization. The likely mechanism of action involves palladin's role in stress fiber formation and structure.

Focal adhesions depend on the tension generated by stress fibers for their maintenance, as blocking stress fiber contractility with myosin inhibitors leads to the dissolution of focal adhesions and the dispersal of integrins (Chrzanowska-Wodnika and Burridge, 1996). The opposite is also true – stimulation of contractility leads to integrin aggregation and the formation of focal adhesions.

In palladin knockdown cells and palladin null fibroblasts, focal adhesions near the center of the cell are dramatically reduced in number compared with control cells, while a few peripheral adhesions remain (Parast and Otey, 2000; Liu et al. 2006). This correlates with fewer and weaker stress fibers. Palladin's ability to modulate actin stress fibers has been investigated thoroughly, and the effects of palladin overexpression and knockdown have been examined in trophoblasts, astrocytes, fibroblasts, Cos-7 cells, and other cells (Parast and Otey, 2000; Boukhelifa et al., 2003; Liu et al. 2006; Ronty et al,, 2006; Rachlin and Otey 2006; Current study, Chapter 4). It was previously believed that palladin exerted this influence through its actin-associated binding partners, including α-actinin and VASP that also localize to stress fibers, but we have demonstrated that palladin is capable of forming actin bundles *in vitro* (Current study, Chapter 4). This may explain the observation that palladin is able to localize to stress fibers even when its N-terminus, including the α-actinin binding domain, is replaced in a differentially spliced isoform (Ronty et al. 2006). With this altered N-terminus, palladin was found to localize along the entire length of the stress fiber, not just in the dense bodies, suggesting

that it is capable of binding to actin by some mechanism independent of α-actinin. The punctate pattern of normal palladin localization may rely on an interaction with α-actinin, though it is unclear which protein is responsible for the definition of dense body boundaries.

Stress fibers are thought to have two related roles – contractility and cell-body translocation. Both rely on the interaction of bundled actin filaments with myosin II which generates the contractile force. When stress fibers are disassembled in the absence of palladin, we would expect contractility of the cells to decrease, though this has been difficult to quantify. We would also expect cell body translocation to be slower than in control cells. In fact, palladin null fibroblasts and knockdown cancer cells exhibit reduced migration rates (Luo et al., 2005, Silvia Goicoechea, personal communication), which is consistent with our hypothesis.

In this study, we have also discovered palladin in dorsal ruffles and podosomes – two dynamic, actin-based structures believed to play a role in invasion. Indeed, palladin seems to be a necessary component of these arrays, as palladin knockdown cells exhibit fewer ruffles and podosomes after stimulation with growth factors and phorbol esters, respectively (Chapter 3). Palladin's ability to bind and bundle filamentous actin (Chapter 4) suggests that it may play a structural role in stabilizing the actin arrays that give rise to dorsal ruffles and podosomes. Palladin also appears to participate in the signaling pathways leading to ruffle formation via its ability to modulate Rac activation (Goicoechea et al., 2006) and its ability to bind Src (Ronty et al. 2007) after growth factor stimulation. Knocking down palladin was shown to inhibit Src-induced ruffle formation, and it was determined that palladin is

tyrosine phosphorylated in cells expressing activated Src. These results place palladin in a unique molecular niche, as it appears to participate both as a structural component of ruffles and also as an activator and substrate for the signaling proteins that lead to ruffle formation.

Palladin's ability to modulate podosome formation may be critical during invasive motility. In addition to their role as adhesive structures, podosomes have also been found to contain matrix metalloproteases (MMPs) (Sato et al, 1997) that contribute to the cell's ability to modify and migrate through the extracellular matrix. This may be especially critical in the glial scar, as reactive astrocytes have been shown to increase their expression of MMP-1 and the membrane associated MT1-MMP in injury models and are hypothesized to be the main source of MMPs in among neural cells (Buss et al., 2007; Rathke-Hartlieb et al., 2000; Rivera and Khrestchatisky, 1999). MMP-2 was found to be critical for astrocyte migration in an agarose drop model of invasive motility (Ogier et al., 2006). It was found to co-localized with β1 integrin in peripheral membrane ruffles. Further, endothelin-1 treatment was shown to increase the activity of MMP-2 in human optic nerve head astrocytes (He et al, 2007). Because palladin expression also increases after endothelin treatment (Chapter 2) and palladin plays a role in β1 integrin stabilization and membrane ruffling (Liu et al., 2006; Chapter 3), palladin expression could directly or indirectly modulate the activity or localization of MMP-2 in migrating astrocytes. The interplay between palladin, podosomes, integrins, and MMPs in astrocytes is a subject worthy of further study.

In conclusion, palladin's roles in cytoskeletal remodeling and cell migration are multi-faceted, and exist in complex relationships requiring exquisite spatiotemporal regulation. While purified palladin is capable of bundling actin filaments on its own, multiple transient associations with its binding partners α-actinin, VASP, profilin, LPP, ArgBP2, Ezrin, Eps8, and others suggest that palladin's functional role extends well beyond actin bundling. Further study at all levels – biochemical, cellular, and physiological – will be required to understand palladin's myriad roles in cytoskeletal remodeling.

5.3 PRELIMINARY RESULTS AND FUTURE DIRECTIONS

Palladin's role in glial scar formation

To assess the importance of a particular gene product in glial scar formation, researchers have often relied on knockout animal models. Excellent methods exist for mimicking many forms of CNS injury, including stroke, concussive trauma, and spinal cord transection in lab animals. In our own lab, experiments were planned using a conditional palladin knockout mouse. Unfortunately, gene targeting in these mice led to unintentional interruption of the palladin gene, even in the absence of the conditional signal. Thus, the mice were not useful for experimental purposes.

In the future, it will be important to generate or obtain conditional palladin knockout mice for a variety of studies. As the number of tissue specific Cre lines grows, a Cre-Lox palladin mouse line would allow us to address the role of palladin in not only brain and spinal cord injury, but also neural tube closure, CNS development, and axon migration and regeneration. These experiments would

ultimately answer the question “Is palladin expression necessary for glial scar formation?”

A conditional knockout line would also allow us to develop a robust method for generating palladin null astrocytes. Though we were able to culture cells from the cortex of day 13 mouse embryos, it is likely that these cells are at a different developmental stage than the more mature astrocytes cultured from 1 day old pups used by others in the field. By using an astrocyte specific conditional line, palladin could be knocked out either *in vivo* at the timepoints of interest, or *in vitro* by the addition of a Cre expression vector. In this way, we could assess the cells’ ability to migrate, contract, or adhere with a uniform population of truly palladin null cells, rather than knockdowns.

Transcriptional regulation of palladin expression

As our understanding of palladin’s gene structure matures, new questions arise regarding the cell’s ability to regulate the expression of individual isoforms in a temporally controlled and tissue specific manner. Though we recognize three common isoforms in rodents (90 kDa, 140 kDa, and 200 kDa), there is evidence for additional isoforms that arise from splice variants or alternative promoters both in rodents and other mammals. Many of these variants have been discovered through the use of recently developed polyclonal antibodies.

By using the RT-PCR tools and methods developed in Chapter 2, we will be able to detect even small changes in gene expression of palladin isoforms both in cultured cells and in tissue preparations. By pharmacologically or physically

modulating the cellular environment and measuring palladin expression, we will be able to place palladin within well established transcriptional regulation pathways. Further work may be done by identifying conserved promoter regions in the palladin gene and using *in vitro* and *in silico* analysis to identify transcription factors.

Post-translational modification and regulation

Since its discovery, palladin was recognized as a phosphoprotein, and was found to be phosphorylated on serine and tyrosine residues (Parast and Otey, 2000; Ronty et al, 2007). Initial attempts to identify the phosphorylated residues using mass spectrometry were unsuccessful. One of the difficulties in identifying individual phosphorylation sites comes from the fact that the 90 kDa isoform contains almost 120 serines, threonines, and tyrosines, and subpopulations of palladin may exist in multiple phosphorylation states within a single cell. Separating and identifying these different pools which may have only miniscule differences in molecular weight has proved challenging. So far, tyrosine phosphorylation has been identified downstream of Src activation in fibroblasts (Ronty et al. 2007) and palladin's apparent molecular weight appears to shift as cells enter the mitosis, suggesting a shift in phosphorylation (Otey lab, unpublished results.) Based on these observations, we hypothesize that other intracellular signaling pathways are able to regulate palladin's phosphorylation state, and therefore its localization and binding interactions. It will be particularly interesting to examine whether phosphorylation plays a role in the rapid relocalization of palladin to dorsal ruffles after growth factor stimulation (Chapter 3).

Reports to date have demonstrated that VASP, profilin, Eps8, SPIN90, Src and other binding interactions are mediated by the same short proline-rich region at palladin's N-terminus (Boukhelifa et al., 2004; Boukhelifa et al., 2006; Goicoechea et al., 2006; Ronty et al., 2007). Due to steric hindrances, it is unlikely that these proteins bind palladin simultaneously, suggesting that post-translational modification of palladin or its binding partners can regulate intermolecular binding affinities. Immunoprecipitation and mass spectrometry of palladin from resting and growth factor stimulated cells may help to identify phosphorylation sites and the kinases responsible for regulating palladin's binding interactions.

Palladin/Actin interaction

In Chapter 4, we identified Ig3 as a novel F-actin binding domain and Ig3-Ig4 as an actin bundling region. While our mutagenesis results have identified the actin binding site on Ig3, future studies will be needed to describe the mechanism of actin bundling by Ig3-Ig4. Preliminary results using Size Exclusion Chromatography coupled with Multi-Angle Light Scattering (SEC-MALS) revealed that full length palladin and Ig3-Ig4 exist as monomers in solution at the salt concentrations we tested. If palladin is not dimerizing, then two actin binding domains must exist in order to crosslink filaments. As Ig3-Ig4 has only one confirmed actin binding domain, a more complicated bundling mechanism must be envisioned in which actin binding facilitates a conformational change that allows for either the binding of an additional filament, or domain dimerization.

Because our studies focused on palladin's C-terminus for actin binding, as suggested by studies of myotilin, there remains the possibility that palladin contains additional, non-canonical actin binding domains within its C-terminus. Using bacterial or insect cell expression systems, we will be able to determine whether these sites exist using the already developed co-sedimentation assays. Further study will be required to determine whether individual isoforms of palladin exhibit different binding affinities or bundling geometries that may contribute to their ability to organize actin within the cell.

Because palladin is an actin bundling protein that interacts with other actin bundling proteins (α-actinin, VASP, Eps8, etc.) it will be interesting to determine how their functions overlap or synergize. Other studies have demonstrated that a combination of bundling proteins generates actin arrays that are functionally distinct from those produced by the individual bundlers (Rivero et al., 1999; Tseng et al., 2005). Assessing the arrays generated by palladin alone and in tandem with its binding partners may help elucidate the physiological importance of their interactions *in vivo*.

Can palladin bind to myosin filaments?

The Ig domains of proteins such as Myosin Light Chain Kinase, Myosin Binding Protein C (MyBP-C) and MyBP-H have all been shown to bind to the thick filaments of myosin II in the sarcomere (Welikson and Fischman, 2002; Okagaki et al., 1993; Miyamoto et al., 1999). Because palladin overexpression results in the hyper-bundling of stress fibers, and ultimately stress fiber collapse in Cos-7 cells

(Supplemental movie 4.1), we decided to test whether palladin may also bind to myosin-II via its Ig domains.

Myosin-II forms dense filaments at physiological salt concentrations that can be treated much like filamentous actin in co-sedimentation assays. Neither Ig2 from 140 kDa palladin, Ig3, nor Ig4 sediments with myosin at 100 or 50 mM KCl (not shown). Full length 140 kDa palladin initially revealed a weak affinity for myosin filaments, but negative controls centrifuged without the presence of myosin also resulted in a small amount of palladin precipitation. Whether palladin or its Ig domains are capable of binding to myosin II filaments will be the subject of further study. In addition, palladin may be capable of binding other types of myosin, as a collaborator's recent pull-down assay detected an interaction between palladin and myosin-9 (personal communication.) Further experiments will be needed to confirm the preliminary results.

REFERENCES

Ababou A, Gautel M and Pfuhl M. Dissecting the N-terminal myosin binding site of human cardiac myosin-binding protein C. Structure and myosin binding of domain C2. J Biol Chem. 2007 Mar 23;282(12): 9204-9215.

Abbott NJ. Astrocyte-endothelial interactions and blood-brain barrier permeability. J Anat. 2002 Jun;200(6):629-38. Review.

Abd-El-Basset EM, Fedoroff S. Upregulation of F-actin and alpha-actinin in reactive astrocytes. J Neurosci Res. 1997 Sep 1;49(5):608-16.

Abe K, Misawa M. Astrocyte stellation induced by Rho kinase inhibitors in culture. Brain Res Dev Brain Res. 2003 Jun 12;143(1):99-104.

Adams JC. Roles of fascin in cell adhesion and motility. Curr Opin Cell Biol. 2004 Oct;16(5): 590-596.

Alonso G. 2005. NG2 proteoglycan-expressing cells of the adult rat brain: possible involvement in the formation of glial scar astrocytes following stab wound. Glia 49:318-338.

Altschul SF, Madden TL, Schaffer AA, Zhang J, Zhang Z, Miller W and Lipman DJ. Gapped BLAST and PSI-BLAST: a new generation of protein database search programs. Nucleic Acids Res. 1997 Sep 1;25(17): 3389-3402.

Amann KJ, Renley BA and Ervasti JM. A cluster of basic repeats in the dystrophin rod domain binds F-actin through an electrostatic interaction. J Biol Chem. 1998 Oct 23;273(43): 28419-28423.

Anton IM, Saville SP, Byrne MJ, Curcio C, Ramesh N, Hartwig JH, et al. WIP participates in actin reorganization and ruffle formation induced by PDGF. J Cell Sci 2003;116(Pt 12):2443-51.

Ard MD, Bunge RP. Changes in astrocyte extracellular matrix with differentiation and after contact with neurites. Ann N Y Acad Sci. 1988;540:420-2.

Bailly M, F Macaluso, M Cammer, A Chan, JE Segall, JS Condeelis. (1999) Relationship between Arp2/3 complex and the barbed ends of actin filaments at the leading edge of carcinoma cells after epidermal growth factor stimulation. J Cell Biol. 145:331-45

Baldwin SA, Scheff SW. 1996. Intermediate filament change in astrocytes following mild cortical contusion. Glia 16:266-275.

Banerjee S, Bhat MA. Neuron-glial interactions in blood-brain barrier formation. Annu Rev Neurosci. 2007;30:235-58. Review.

Bang ML, Mudry RE, McElhinny AS, Trombitas K, Geach AJ, Yamasaki R, Sorimachi H, Granzier H, Gregorio CC and Labeit S. Myopalladin, a novel 145-kilodalton sarcomeric protein with multiple roles in Z-disc and I-band protein assemblies. J Cell Biol. 2001 Apr 16;153(2): 413-427.

Barclay AN. Membrane proteins with immunoglobulin-like domains--a master superfamily of interaction molecules. Semin Immunol. 2003 Aug;15(4): 215-223.

Barone FC, Globus MY, Price WJ, White RF, Storer BL, Feuerstein GZ, Busto R, Ohlstein EH. Endothelin levels increase in rat focal and global ischemia. J Cereb Blood Flow Metab. 1994 Mar;14(2):337-42.

Bartles JR. Parallel actin bundles and their multiple actin-bundling proteins. Curr Opin Cell Biol. 2000 Feb;12(1): 72-78.

Barzik M, Kotova TI, Higgs HN, Hazelwood L, Hanein D, Gertler FB, Schafer DA. Ena/VASP Proteins Enhance Actin Polymerization in the Presence of Barbed End Capping Proteins. J Biol Chem. 2005 Aug 5;280(31):28653-62.

Bassell G and Singer RH. mRNA and cytoskeletal filaments. Curr Opin Cell Biol. 1997 Feb;9(1): 109-115.

Beach TG, Walker R, McGeer EG.Patterns of gliosis in Alzheimer's disease and aging cerebrum.Glia. 1989;2(6):420-36.

Bear JE, Svitkina TM, Krause M, Schafer DA, Loureiro JJ, Strasser GA, Maly IV, Chaga OY, Cooper JA, Borisy GG, Gertler FB. Antagonism between Ena/VASP proteins and actin filament capping regulates fibroblast motility. Cell. 2002 May 17;109(4):509-21.

Bennett PM, Furst DO and Gautel M. The C-protein (myosin binding protein C) family: regulators of contraction and sarcomere formation? Rev Physiol Biochem Pharmacol. 1999 138(203-234.

Bernstein, J.J., R. Getz, M. Jefferson and M. Kelemen, Astrocytes secrete basal lamina after hemisection of rat spinal cord. Brain Res 327 (1985), pp. 135–141.

Bezzi P, Volterra A. A neuron-glia signalling network in the active brain. Curr Opin Neurobiol. 2001 Jun;11(3):387-94. Review.

Bignami A and Dahl D The astroglial response to stabling. Immunofluorescence studies with antibodies to astrocyte-specific protein (GFA) in mammalian and submammalian vertebrates. Neuropath. Appl. Neurobiol. 1976 2, 99-100.

Blanchard A, Ohanian V and Critchley D. The structure and function of alpha-actinin. J Muscle Res Cell Motil. 1989 Aug;10(4): 280-289.

Bork P, Holm L and Sander C. The immunoglobulin fold. Structural classification, sequence patterns and common core. J Mol Biol. 1994 Sep 30;242(4): 309-320.

Boukhelifa M, Hwang SJ, Valtschanoff JG, Meeker RB, Rustioni A and Otey CA. A critical role for palladin in astrocyte morphology and response to injury. Mol Cell Neurosci. 2003 Aug;23(4): 661-668.

Boukhelifa M, Moza M, Johansson T, Rachlin A, Parast M, Huttelmaier S, Roy P, Jockusch BM, Carpen O, Karlsson R and Otey CA. The proline-rich protein palladin is a binding partner for profilin. Febs J. 2006 Jan;273(1): 26-33.

Boukhelifa M, Parast MM, Bear JE, Gertler FB and Otey CA. Palladin is a novel binding partner for Ena/VASP family members. Cell Motil Cytoskeleton. 2004 May;58(1): 17-29.

Boukhelifa M, Parast MM, Valtschanoff JG, LaMantia AS, Meeker RB and Otey CA. A role for the cytoskeleton-associated protein palladin in neurite outgrowth. Mol Biol Cell. 2001 Sep;12(9): 2721-2729.

Boukhelifa M, SJ Hwang, JG Valtschanoff, RB Meeker, A Rustioni, and CA Otey. (2003) A critical role for palladin in astrocyte morphology and response to injury. Mol Cell Neurosci. 23(4): 661-668.

Bowden ET, Barth M, Thomas D, Glazer RI, Mueller SC. An invasion-related complex of cortactin, paxillin and PKCmu associates with invadopodia at sites of extracellular matrix degradation. Oncogene 1999;18(31):4440-9.

Brandt D, Gimona M, Hillmann M, Haller H, Mischak H. Protein kinase C induces actin reorganization via a Src- and Rho-dependent pathway. J Biol Chem. 2002 Jun 7;277(23):20903-10. Epub 2002 Mar 29.

Brightman MW, Zis K, Anders J. Morphology of cerebral endothelium and astrocytes as determinants of the neuronal microenvironment. Acta Neuropathol Suppl. 1983;8:21-33.

Bryson K, McGuffin LJ, Marsden RL, Ward JJ, Sodhi JS and Jones DT. Protein structure prediction servers at University College London. Nucleic Acids Res. 2005 Jul 1;33(Web Server issue): W36-38.

Buccione R, Orth JD, McNiven MA. Foot and mouth: podosomes, invadopodia and circular dorsal ruffles. Nat Rev Mol Cell Biol 2004;5(8):647-57.

Bullard B, Burkart C, Labeit S and Leonard K. The function of elastic proteins in the oscillatory contraction of insect flight muscle. J Muscle Res Cell Motil. 2005 26(6-8): 479-485.

Bullard B, Garcia T, Benes V, Leake MC, Linke WA and Oberhauser AF. The molecular elasticity of the insect flight muscle proteins projectin and kettin. Proc Natl Acad Sci U S A. 2006 Mar 21;103(12): 4451-4456.

Bullard B, Linke WA and Leonard K. Varieties of elastic protein in invertebrate muscles. J Muscle Res Cell Motil. 2002 23(5-6): 435-447.

Calvo JL, Carbonell AL, Boya J. 1991. Co-expression of glial fibrillary acidic protein and vimentin in reactive astrocytes following brain injury in rats. Brain Res 566:333-336.

Carlsson L, Yu JG, Moza M, Carpen O and Thornell LE. Myotilin - a prominent marker of myofibrillar remodelling. Neuromuscul Disord. 2007 Jan;17(1): 61-68.

Castagnino P, Biesova Z, Wong WT, Fazioli F, Gill GN, Di Fiore PP. Direct binding of eps8 to the juxtamembrane domain of EGFR is phosphotyrosine- and SH2-independent. Oncogene 1995;10(4):723-9.

Choi, D.W. (1988) Glutamate neurotoxicity and diseases of the nervous system. Neuron, 1:623–634.

Chrzanowska-Wodnicka M, Burridge K. Rho-stimulated contractility drives the formation of stress fibers and focal adhesions. J Cell Biol. 1996 Jun;133(6):1403-15.

Chu J, Hatton JD, Su H. Effects of epidermal growth factor and dibutyryl cyclic adenosine monophosphate on the migration pattern of astrocytes grafted into adult rat brain. Neurosurgery. 1999 Oct;45(4):859-66.

Clemente CD (1955) Structural regeneration in the mammalian central nervous system and the role of neuroglia and connective tissue. In: Windle WF (ed) Regeneration in the nervous system. Charles C. Thomas, Springfield, Ill, pp 147-161.

Condeelis J, Vahey M. A calcium- and pH-regulated protein from Dictyostelium discoideum that cross-links actin filaments. J Cell Biol. 1982 Aug;94(2):466-71.

David S, Aguayo AJ. Axonal elongation into peripheral nervous system "bridges" after central nervous system injury in adult rats. Science. 1981 Nov 20;214(4523):931-3.

Davies SJ, Fitch MT, Memberg SP, Hall AK, Raisman G, Silver J. Regeneration of adult axons in white matter tracts of the central nervous system. Nature. 1997 Dec 18-25;390(6661):680-3.

Davies SJ, Goucher DR, Doller C, Silver J. Robust regeneration of adult sensory axons in degenerating white matter of the adult rat spinal cord. J Neurosci. 1999 Jul 15;19(14):5810-22.

Davoli R, Braglia S, Lama B, Fontanesi L, Buttazzoni L, Baiocco C and Russo V. Mapping, identification of polymorphisms and analysis of allele frequencies in the porcine skeletal muscle myopalladin and titin genes. Cytogenet Genome Res. 2003 102(1-4): 152-156.

de Arruda MV, Bazari H, Wallek M and Matsudaira P. An actin footprint on villin. Single site substitutions in a cluster of basic residues inhibit the actin severing but not capping activity of villin. J Biol Chem. 1992 Jun 25;267(18): 13079-13085.

Delaglio F, Grzesiek S, Vuister GW, Zhu G, Pfeifer J and Bax A. NMRPipe: a multidimensional spectral processing system based on UNIX pipes. J Biomol NMR. 1995 Nov;6(3): 277-293.

DeRosier DJ and Tilney LG. How actin filaments pack into bundles. Cold Spring Harb Symp Quant Biol. 1982 46 Pt 2(525-540.

DeRosier DJ, Tilney LG and Egelman E. Actin in the inner ear: the remarkable structure of the stereocilium. Nature. 1980 Sep 25;287(5780): 291-296.

Dharmawardhane S, Sanders LC, Martin SS, Daniels RH, Bokoch GM. Localization of p21-activated kinase 1 (PAK1) to pinocytic vesicles and cortical actin structures in stimulated cells. J Cell Biol 1997;138(6):1265-78.

Di Fiore PP, Scita G. Eps8 in the midst of GTPases. Int J Biochem Cell Biol 2002;34(10):1178-83.

Disanza A, Carlier MF, Stradal TE, Didry D, Frittoli E, Confalonieri S, et al. Eps8 controls actin-based motility by capping the barbed ends of actin filaments. Nat Cell Biol 2004;6(12):1180-8.

Disanza A, Mantoani S, Hertzog M, Gerboth S, Frittoli E, Steffen A, Berhoerster K, Kreienkamp HJ, Milanesi F, Di Fiore PP, Ciliberto A, Stradal TE and Scita G. Regulation of cell shape by Cdc42 is mediated by the synergic actin-bundling activity of the Eps8-IRSp53 complex. Nat Cell Biol. 2006 Dec;8(12): 1337-1347.

Dixon R, Arneman D, Rachlin A, Sundaresan N, Costello J, Campbell S and Otey C. Palladin is an Actin Crosslinking Protein that Uses Immunoglobulin-like Domains to Bind Filamentous Actin. Submitted. 2007

Doetsch F, Caillé I, Lim DA, García-Verdugo JM, Alvarez-Buylla A. Subventricular zone astrocytes are neural stem cells in the adult mammalian brain.Cell. 1999 Jun 1;97(6):703-16.

dos Remedios CG, Chhabra D, Kekic M, Dedova IV, Tsubakihara M, Berry DA and Nosworthy NJ. Actin binding proteins: regulation of cytoskeletal microfilaments. Physiol Rev. 2003 Apr;83(2): 433-473.

Douen AG, Dong L, Vanance S, Munger R, Hogan MJ, Thompson CS, Hakim AM. 2004. Regulation of nestin expression after cortical ablation in adult rat brain. Brain Res 1008:139-146.

Dowrick P, Kenworthy P, McCann B, Warn R. Circular ruffle formation and closure lead to macropinocytosis in hepatocyte growth factor/scatter factor-treated cells. Eur J Cell Biol 1993;61(1):44-53.

Drago J, Reid KL, Bartlett PF. 1989. Induction of the ganglioside marker A2B5 on cultured cerebellar neural cells by growth factors. Neurosci Lett 107:245-250.

Durieu-Trautmann O, Federici C, Creminon C, Foignant-Chaverot N, Roux F, Claire M, Strosberg AD, Couraud PO.

Edwards RA and Bryan J. Fascins, a family of actin bundling proteins. Cell Motil Cytoskeleton. 1995 32(1): 1-9.

Erecińska M, Silver IA.Metabolism and role of glutamate in mammalian brain. Prog Neurobiol. 1990;35(4):245-96. Review.

Eriksson A, Siegbahn A, Westermark B, Heldin CH, Claesson-Welsh L. PDGF alpha- and beta-receptors activate unique and common signal transduction pathways. Embo J 1992;11(2):543-50.

Faulkner JR, Herrmann JE, Woo MJ, Tansey KE, Doan NB, Sofroniew MV. Reactive astrocytes protect tissue and preserve function after spinal cord injury. J Neurosci. 2004 Mar 3;24(9):2143-55.

Fawcett JW, Asher RA. 1999. The glial scar and central nervous system repair. Brain Res Bull 49:377-391.

Fazioli F, Minichiello L, Matoska V, Castagnino P, Miki T, Wong WT, et al. Eps8, a substrate for the epidermal growth factor receptor kinase, enhances EGF-dependent mitogenic signals. Embo J 1993;12(10):3799-808.

Fedoroff S, White R, Neal J, Subrahmanyan L, Kalnins VI.Astrocyte cell lineage. II. Mouse fibrous astrocytes and reactive astrocytes in cultures have vimentin- and GFP-containing intermediate filaments.Brain Res. 1983 Apr;283(2-3):303-15.

Fields RD, Stevens-Graham B. New insights into neuron-glia communication.Science. 2002 Oct 18;298(5593):556-62.

Finkbeiner SM. Glial calcium. Glia. 1993 Oct;9(2):83-104. Review.

Fischer D. 3D-SHOTGUN: a novel, cooperative, fold-recognition meta-predictor. Proteins. 2003 May 15;51(3): 434-441.

Fitch MT, Silver J. Activated macrophages and the blood-brain barrier: inflammation after CNS injury leads to increases in putative inhibitory molecules. Exp Neurol. 1997 Dec;148(2):587-603.

Frisen J, Fried K, Sjogren AM, Risling M. Growth of ascending spinal axons in CNS scar tissue. Int J Dev Neurosci. 1993 Aug;11(4):461-75.

Fucini P, Renner C, Herberhold C, Noegel AA and Holak TA. The repeating segments of the F-actin cross-linking gelation factor (ABP-120) have an immunoglobulin-like fold. Nat Struct Biol. 1997 Mar;4(3): 223-230.

Fultz ME, Li C, Geng W, Wright GL. Remodeling of the actin cytoskeleton in the contracting A7r5 smooth muscle cell. J Muscle Res Cell Motil 2000;21(8):775-87.

Funato Y, Terabayashi T, Suenaga N, Seiki M, Takenawa T, Miki H. IRSp53/Eps8 complex is important for positive regulation of Rac and cancer cell motility/invasiveness. Cancer Res 2004;64(15):5237-44.

Furst, DO and M Gautel (1995) The anatomy of a molecular giant: how the sarcomere cytoskeleton is assembled from immunoglobulin superfamily molecules. J Mol Cardiol. 27:951-959.

Gammill LS, Bronner-Fraser M. Genomic analysis of neural crest induction. Development. 2002 Dec;129(24):5731-41.

Gavazzi I, Nermut MV, Marchisio PC. Ultrastructure and gold-immunolabelling of cell-substratum adhesions (podosomes) in RSV-transformed BHK cells. J Cell Sci 1989;94 (Pt 1):85-99.

Gertler FB, K Niebuhr, M Reinhard, J Wehland, and P Soriano. (1996) Mena, a relative of VASP and Drosophila Enabled, is implicated in the control of microfilament dynamics. Cell 87:227-239

Gerull B, Atherton J, Geupel A, Sasse-Klaassen S, Heuser A, Frenneaux M, McNabb M, Granzier H, Labeit S and Thierfelder L. Identification of a novel frameshift mutation in the giant muscle filament titin in a large Australian family with dilated cardiomyopathy. J Mol Med. 2006 Jun;84(6): 478-483.

Gerull B, Gramlich M, Atherton J, McNabb M, Trombitas K, Sasse-Klaassen S, Seidman JG, Seidman C, Granzier H, Labeit S, Frenneaux M and Thierfelder L. Mutations of TTN, encoding the giant muscle filament titin, cause familial dilated cardiomyopathy. Nat Genet. 2002 Feb;30(2): 201-204.

Gilbert R, Cohen JA, Pardo S, Basu A and Fischman DA. Identification of the A-band localization domain of myosin binding proteins C and H (MyBP-C, MyBP-H) in skeletal muscle. J Cell Sci. 1999 Jan;112 (Pt 1)(69-79.

Gimona M, Kaverina I, Resch GP, Vignal E, Burgstaller G. Calponin repeats regulate actin filament stability and formation of podosomes in smooth muscle cells. Mol Biol Cell 2003;14(6):2482-91.

Goicoechea S, Arneman D, Disanza A, Garcia-Mata R, Scita G and Otey CA. Palladin binds to Eps8 and enhances the formation of dorsal ruffles and podosomes in vascular smooth muscle cells. J Cell Sci. 2006 Aug 15;119(Pt 16): 3316-3324.

Gontier Y, Taivainen A, Fontao L, Sonnenberg A, van der Flier A, Carpen O, Faulkner G and Borradori L. The Z-disc proteins myotilin and FATZ-1 interact with each other and are connected to the sarcolemma via muscle-specific filamins. J Cell Sci. 2005 Aug 15;118(Pt 16): 3739-3749.

Granzier HL and Labeit S. Titin and its associated proteins: the third myofilament system of the sarcomere. Adv Protein Chem. 2005 71(89-119.

Grimpe B, Silver J. A novel DNA enzyme reduces glycosaminoglycan chains in the glial scar and allows microtransplanted dorsal root ganglia axons to regenerate beyond lesions in the spinal cord. J Neurosci. 2004 Feb 11;24(6):1393-7.

Grzesiek S, Anglister J, Ren H and Bax A. C-13 Line Narrowing by H-2 Decoupling in H-2/C-13/N-15-Enriched Proteins - Application to Triple-Resonance 4D J-Connectivity of Sequential Amides. Journal of the American Chemical Society. 1993 May 19;115(10): 4369-4370.

Gultice AD, Selesniemi KL and Brown TL. Hypoxia inhibits differentiation of lineage-specific Rcho-1 trophoblast giant cells. Biol Reprod. 2006 Jun;74(6): 1041-1050.

Guth L, Reier PJ, Barrett CP, Donati EJ (1983) Repair of the mammalian spinal cord. Trends Neurosci 6:120-124.

Hai CM, Hahne P, Harrington EO, Gimona M. Conventional protein kinase C mediates phorbol-dibutyrate-induced cytoskeletal remodeling in a7r5 smooth muscle cells. Exp Cell Res 2002;280(1):64-74.

Hakeda S, Endo S and Saigo K. Requirements of Kettin, a giant muscle protein highly conserved in overall structure in evolution, for normal muscle function, viability, and flight activity of Drosophila. J Cell Biol. 2000 Jan 10;148(1): 101-114.

Hall A. Rho GTPases and the actin cytoskeleton. Science 1998;279(5350):509-14.

Hardin, H., Bernard, A., Rajas, F., Fe`vre-Montange, M., Derrington,E., Belin, M.F., and Didier-Bazes, M. (1994) Modifications of glial metabolism of glutamate after serotonergic neuron degeneration inthe hippocampus of the rat. Mol. Brain. Res., 26:1–8.

Harpaz Y and Chothia C. Many of the immunoglobulin superfamily domains in cell adhesion molecules and surface receptors belong to a new structural set which is close to that containing variable domains. J Mol Biol. 1994 May 13;238(4): 528-539.

Harris AK, Wild P, Stopak D.

Hatton JD, Hoi SU. In vitro differentiation inhibits the migration of cultured neonatal rat cortical astrocytes transplanted to the neonatal rat cerebrum. Int J Dev Neurosci. 1993 Oct;11(5):583-94.

Hauser MA, Horrigan SK, Salmikangas P, Torian UM, Viles KD, Dancel R, Tim RW, Taivainen A, Bartoloni L, Gilchrist JM, Stajich JM, Gaskell PC, Gilbert JR, Vance JM, Pericak-Vance MA, Carpen O, Westbrook CA and Speer MC. Myotilin is mutated in limb girdle muscular dystrophy 1A. Hum Mol Genet. 2000 Sep 1;9(14): 2141-2147.

Haydon PG, Carmignoto G. Astrocyte control of synaptic transmission and neurovascular coupling. Physiol Rev. 2006 Jul;86(3):1009-31.

Hedberg KM, Bengtsson T, Safiejko-Mroczka B, Bell PB, Lindroth M. PDGF and neomycin induce similar changes in the actin cytoskeleton in human fibroblasts. Cell Motil Cytoskeleton. 1993;24(2):139-49.

Heidemann SR and Wirtz D. Towards a regional approach to cell mechanics. Trends Cell Biol. 2004 Apr;14(4): 160-166.

Heidemann SR, Kaech S, Buxbaum RE and Matus A. Direct observations of the mechanical behaviors of the cytoskeleton in living fibroblasts. J Cell Biol. 1999 Apr 5;145(1): 109-122.

Hermanns S, Reiprich P, Muller HW. A reliable method to reduce collagen scar formation in the lesioned rat spinal cord. J Neurosci Methods. 2001 Sep 30;110(1-2):141-6.

Hertz L, Schousboe A, Boechler N, Mukerji S, Fedoroff S. Kinetic characteristics of the glutamate uptake into normal astrocytes in cultures. Neurochem Res. 1978 Feb;3(1):1-14.

Hertz L, Schousboe I, Hertz L, Schousboe A.Receptor expression in primary cultures of neurons or astrocytes. Prog Neuropsychopharmacol Biol Psychiatry. 1984;8(4-6):521-7. Review.

Hertz L. An intense potassium uptake into astrocytes, its further enhancement by high concentrations of potassium, and its possible involvement in potassium homeostasis at the cellular level. Brain Res. 1978 Apr 21;145(1):202-8.

Herx LM, Rivest S, Yong VW. Central nervous system-initiated inflammation and neurotrophism in trauma: IL-1 beta is required for the production of ciliary neurotrophic factor.J Immunol. 2000 Aug 15;165(4):2232-9.

Herx LM, Yong VW.

Holden HM, Ito M, Hartshorne DJ and Rayment I. X-ray structure determination of telokin, the C-terminal domain of myosin light chain kinase, at 2.8 A resolution. J Mol Biol. 1992 Oct 5;227(3): 840-851.

Huttelmaier S, Harbeck B, Steffens O, Messerschmidt T, Illenberger S and Jockusch BM. Characterization of the actin binding properties of the vasodilator-stimulated phosphoprotein VASP. FEBS Lett. 1999 May 14;451(1): 68-74.

Hwang SJ, Pagliardini S, Boukhelifa M, Parast MM, Otey CA, Rustioni A, Valtschanoff JG.Palladin is expressed preferentially in excitatory terminals in the rat central nervous system.J Comp Neurol. 2001 Jul 23;436(2):211-24.

Improta S, Politou AS and Pastore A. Immunoglobulin-like modules from titin I-band: extensible components of muscle elasticity. Structure. 1996 Mar 15;4(3): 323-337.

Innocenti M, Frittoli E, Ponzanelli I, Falck JR, Brachmann SM, Di Fiore PP, et al. Phosphoinositide 3-kinase activates Rac by entering in a complex with Eps8, Abi1, and Sos-1. J Cell Biol 2003;160(1):17-23.

Inobe M, Katsube K, Miyagoe Y, Nabeshima Y, Takeda S. Identification of EPS8 as a Dvl1-associated molecule. Biochem Biophys Res Commun 1999;266(1):216-21.

Janssen ME, Kim E, Liu H, Fujimoto LM, Bobkov A, Volkmann N and Hanein D. Three-dimensional structure of vinculin bound to actin filaments. Mol Cell. 2006 Jan 20;21(2): 271-281.

Janzer R.C. and M.C. Raff, Astrocytes induce blood–brain barrier properties in endothelial cells (letter). Nature 325 (1987), pp. 353–355.

Jarvenpaa J, Vuoristo JT, Savolainen ER, Ukkola O, Vaskivuo T and Ryynanen M. Altered expression of angiogenesis-related placental genes in pre-eclampsia associated with intrauterine growth restriction. Gynecol Endocrinol. 2007 Jun;23(6): 351-355.

Jin L, Kern MJ, Otey CA, Wamhoff BR and Somlyo AV. Angiotensin II, focal adhesion kinase, and PRX1 enhance smooth muscle expression of lipoma preferred partner and its newly identified binding partner palladin to promote cell migration. Circ Res. 2007 Mar 30;100(6): 817-825.

John GR, Chen L, Rivieccio MA, Melendez-Vasquez CV, Hartley A, Brosnan CF. Interleukin-1beta induces a reactive astroglial phenotype via deactivation of the Rho GTPase-Rock axis. J Neurosci. 2004 Mar 17;24(11):2837-45.

Johnson BA. Using NMRView to visualize and analyze the NMR spectra of macromolecules. Methods Mol Biol. 2004 278(313-352.

Johnson RP and Craig SW. Actin activates a cryptic dimerization potential of the vinculin tail domain. J Biol Chem. 2000 Jan 7;275(1): 95-105.

Joosten EA, Dijkstra S, Brook GA, Veldman H, Bar PR. Collagen IV deposits do not prevent regrowing axons from penetrating the lesion site in spinal cord injury. J Neurosci Res. 2000 Dec 1;62(5):686-91.

Kalderon N, Fuks Z. Structural recovery in lesioned adult mammalian spinal cord by x-irradiation of the lesion site. Proc Natl Acad Sci U S A. 1996 Oct 1;93(20):11179-84.

Kalman M, Szabo A. Immunohistochemical investigation of actin-anchoring proteins vinculin, talin and paxillin in rat brain following lesion: a moderate reaction, confined to the astroglia of brain tracts. Exp Brain Res. 2001 Aug;139(4):426-34.

Kasper C, Rasmussen H, Kastrup JS, Ikemizu S, Jones EY, Berezin V, Bock E and Larsen IK. Structural basis of cell-cell adhesion by NCAM. Nat Struct Biol. 2000 May;7(5): 389-393.

Kato H, Takahashi A, Itoyama Y. Cell cycle protein expression in proliferating microglia and astrocytes following transient global cerebral ischemia in the rat. Brain Res Bull. 2003 May 15;60(3):215-21.

Kawa A, Stahlhut M, Berezin A, Bock E, Berezin V. A simple procedure for morphometric analysis of processes and growth cones of neurons in culture using parameters derived from the contour and convex hull of the object. J Neurosci Methods. 1998 Jan 31;79(1):53-64.

Kaye W and Mcdaniel JB. Low-Angle Laser Light Scattering-Rayleigh Factors and Depolarization Ratios. Applied Optics. 1974 13(8): 1934-1937.

Kelly T, Yan Y, Osborne RL, Athota AB, Rozypal TL, Colclasure JC, et al. Proteolysis of extracellular matrix by invadopodia facilitates human breast cancer cell invasion and is mediated by matrix metalloproteinases. Clin Exp Metastasis 1998;16(6):501-12.

Kim JH, Cho YS, Kim BC, Kim YS, Lee GS. Role of Rho GTPase in the endothelin-1-induced nuclear signaling. Biochem Biophys Res Commun. 1997 Mar 6;232(1):223-6.

Kimelberg HK. The problem of astrocyte identity. Neurochem Int. 2004 Jul-Aug;45(2-3):191-202. Review.

Kinouchi R, M Takeda, L Yang, U Wilhelmsson, A Lundkvist, M Pekny, and DF Chen. (2003) Robust neural integration from retinal transplants in mice deficient in GFAP and vimentin. Nature Neuro. 6(8): 863-868.

Koehler RC, Gebremedhin D, Harder DR. Role of astrocytes in cerebrovascular regulation. J Appl Physiol. 2006 Jan;100(1):307-17.

Koguchi K, Nakatsuji Y, Nakayama K, Sakoda S. Modulation of astrocyte proliferation by cyclin-dependent kinase inhibitor p27(Kip1). Glia. 2002 Feb;37(2):93-104.

Koprivica V, Cho KS, Park JB, Yiu G, Atwal J, Gore B, Kim JA, Lin E, Tessier-Lavigne M, Chen DF, He Z. EGFR activation mediates inhibition of axon regeneration by myelin and chondroitin sulfate proteoglycans. Science. 2005 Oct 7;310(5745):106-10.

Koradi R, Billeter M and Wuthrich K. MOLMOL: a program for display and analysis of macromolecular structures. J Mol Graph. 1996 Feb;14(1): 51-55, 29-32.

Kovar DR, Pollard TD. Insertional assembly of actin filament barbed ends in association with formins produces piconewton forces. Proc Natl Acad Sci U S A. 2004 Oct 12;101(41):14725-30.

Krueger EW, Orth JD, Cao H, McNiven MA. A dynamin-cortactin-Arp2/3 complex mediates actin reorganization in growth factor-stimulated cells. Mol Biol Cell 2003;14(3):1085-96.

Kruger S, Sievers J, Hansen C, Sadler M, Berry M.

Labeit S, Barlow DP, Gautel M, Gibson T, Holt J, Hsieh CL, Francke U, Leonard K, Wardale J, Whiting A and et al. A regular pattern of two types of 100-residue motif in the sequence of titin. Nature. 1990 May 17;345(6272): 273-276.

Langford GM. Actin- and microtubule-dependent organelle motors: interrelationships between the two motility systems. Curr Opin Cell Biol. 1995 Feb;7(1): 82-88.

Lanzetti L, Rybin V, Malabarba MG, Christoforidis S, Scita G, Zerial M, et al. The Eps8 protein coordinates EGF receptor signalling through Rac and trafficking through Rab5. Nature 2000;408(6810):374-7.

Laywell ED, Rakic P, Kukekov VG, Holland EC, Steindler DA.Identification of a multipotent astrocytic stem cell in the immature and adult mouse brain.Proc Natl Acad Sci U S A. 2000 Dec 5;97(25):13883-8.

Leake MC, Grutzner A, Kruger M and Linke WA. Mechanical properties of cardiac titin's N2B-region by single-molecule atomic force spectroscopy. J Struct Biol. 2006 Aug;155(2): 263-272.

Lee HS, Bellin RM, Walker DL, Patel B, Powers P, Liu H, Garcia-Alvarez B, de Pereda JM, Liddington RC, Volkmann N, Hanein D, Critchley DR and Robson RM. Characterization of an actin-binding site within the talin FERM domain. J Mol Biol. 2004 Oct 22;343(3): 771-784.

Lee J, Leonard M, Oliver T, Ishihara A, Jacobson K. Traction forces generated by locomoting keratocytes. J Cell Biol. 1994 Dec;127(6 Pt 2):1957-64.

Lepekhin EA, Eliasson C, Berthold CH, Berezin V, Bock E, Pekny M. Intermediate filaments regulate astrocyte motility. J Neurochem. 2001 Nov;79(3):617-25.

Levitt P, Rakic P. Immunoperoxidase localization of glial fibrillary acidic protein in radial glial cells and astrocytes of the developing rhesus monkey brain. J Comp Neurol. 1980 Oct 1;193(3):815-40.

Li H and Fernandez JM. Mechanical design of the first proximal Ig domain of human cardiac titin revealed by single molecule force spectroscopy. J Mol Biol. 2003 Nov 14;334(1): 75-86.

Li X, Matsuoka Y and Bennett V. Adducin preferentially recruits spectrin to the fast growing ends of actin filaments in a complex requiring the MARCKS-related domain and a newly defined oligomerization domain. J Biol Chem. 1998 Jul 24;273(30): 19329-19338.

Li Y, Raisman G. Sprouts from cut corticospinal axons persist in the presence of astrocytic scarring in long-term lesions of the adult rat spinal cord. Exp Neurol. 1995 Jul;134(1):102-11.

Liang W, Yang H, Xue X, Huang Q, Bartlam M and Chen S. Expression, crystallization and preliminary X-ray studies of the immunoglobulin-like domain 3 of human palladin. Acta Crystallograph Sect F Struct Biol Cryst Commun. 2006 Jun 1;62(Pt 6): 556-558.

Liberto CM, Albrecht PJ, Herx LM, Yong VW, Levison SW. Pro-regenerative properties of cytokine-activated astrocytes. J Neurochem. 2004 Jun;89(5):1092-100. Review.

Liesi P, Dahl D, Vaheri A. Laminin is produced by early rat astrocytes in primary culture. J Cell Biol. 1983 Mar;96(3):920-4.

Linder S, Aepfelbacher M. Podosomes: adhesion hot-spots of invasive cells. Trends Cell Biol 2003;13(7):376-85.

Linke WA. Stretching molecular springs: elasticity of titin filaments in vertebrate striated muscle. Histol Histopathol. 2000 Jul;15(3): 799-811.

Lipsitz RS and Tjandra N. Residual dipolar couplings in NMR structure analysis. Annu Rev Biophys Biomol Struct. 2004 33(387-413.

Liu XS, Luo HJ, Yang H, Wang L, Kong H, Jin YE, Wang F, Gu MM, Chen Z, Lu ZY and Wang ZG. Palladin regulates cell and extracellular matrix interaction through maintaining normal actin cytoskeleton architecture and stabilizing Beta1-integrin. J Cell Biochem. 2006 Nov 17;

Luo H, Liu X, Wang F, Huang Q, Shen S, Wang L, Xu G, Sun X, Kong H, Gu M, Chen S, Chen Z and Wang Z. Disruption of palladin results in neural tube closure defects in mice. Mol Cell Neurosci. 2005 Aug;29(4): 507-515.

Ma K and Wang K. Interaction of nebulin SH3 domain with titin PEVK and myopalladin: implications for the signaling and assembly role of titin and nebulin. FEBS Lett. 2002 Dec 18;532(3): 273-278.

Mahoney NM, Janmey PA and Almo SC. Structure of the profilin-poly-L-proline complex involved in morphogenesis and cytoskeletal regulation. Nat Struct Biol. 1997 Nov;4(11): 953-960.

Matoskova B, Wong WT, Nomura N, Robbins KC, Di Fiore PP. RN-tre specifically binds to the SH3 domain of eps8 with high affinity and confers growth advantage to NIH3T3 upon carboxy-terminal truncation. Oncogene 1996;12(12):2679-88.

Matsudaira P, Mandelkow E, Renner W, Hesterberg LK and Weber K. Role of fimbrin and villin in determining the interfilament distances of actin bundles. Nature. 1983 Jan 20;301(5897): 209-214.

McCarthy KD, de Vellis J.Preparation of separate astroglial and oligodendroglial cell cultures from rat cerebral tissue.J Cell Biol. 1980 Jun;85(3):890-902.

McCoy AJ, Fucini P, Noegel AA and Stewart M. Structural basis for dimerization of the Dictyostelium gelation factor (ABP120) rod. Nat Struct Biol. 1999 Sep;6(9): 836-841.

McGuffin LJ, Bryson K and Jones DT. The PSIPRED protein structure prediction server. Bioinformatics. 2000 Apr;16(4): 404-405.

McKeon RJ, Schreiber RC, Rudge JS, Silver J. Reduction of neurite outgrowth in a model of glial scarring following CNS injury is correlated with the expression of inhibitory molecules on reactive astrocytes. J Neurosci. 1991 Nov;11(11):3398-411.

Menet V, M Prieto, A Privat, and M Gimenez y Ribotta. (2003) Axonal plasticity and functional recovery after spinal cord injury in mice deficient in both glial fibrillary acidic protein and vimentin genes. PNAS 100(15): 8999-9004.

Mockrin S.C. and E.D. Korn, Acanthamoeba profilin interacts with G-actin to increase the rate of exchange of actin-bound adenosine 5′-triphosphate, Biochemistry 19 (1980), pp. 5359–5362.

Mologni L, Moza M, Lalowski MM and Carpen O. Characterization of mouse myotilin and its promoter. Biochem Biophys Res Commun. 2005 Apr 15;329(3): 1001-1009.

Mologni L, Salmikangas P, Fougerousse F, Beckmann JS and Carpen O. Developmental expression of myotilin, a gene mutated in limb-girdle muscular dystrophy type 1A. Mech Dev. 2001 May;103(1-2): 121-125.

Monsky WL, Lin CY, Aoyama A, Kelly T, Akiyama SK, Mueller SC, et al. A potential marker protease of invasiveness, seprase, is localized on invadopodia of human malignant melanoma cells. Cancer Res 1994;54(21):5702-10.

Moolman-Smook J, Flashman E, de Lange W, Li Z, Corfield V, Redwood C and Watkins H. Identification of novel interactions between domains of Myosin binding

protein-C that are modulated by hypertrophic cardiomyopathy missense mutations. Circ Res. 2002 Oct 18;91(8): 704-711.

Moon C, Ahn M, Kim S, Jin JK, Sim KB, Kim HM, Lee MY, Shin T. 2004. Temporal patterns of the embryonic intermediate filaments nestin and vimentin expression in the cerebral cortex of adult rats after cryoinjury. Brain Res 1028:238-242.

Moreau V, Tatin F, Varon C, Genot E. Actin can reorganize into podosomes in aortic endothelial cells, a process controlled by Cdc42 and RhoA. Mol Cell Biol 2003;23(19):6809-22.

Mothe AJ, Tator CH. 2005. Proliferation, migration, and differentiation of endogenous ependymal region stem/progenitor cells following minimal spinal cord injury in the adult rat. Neuroscience 131:177-187.

Moza M, Mologni L, Trokovic R, Faulkner G, Partanen J and Carpen O. Targeted deletion of the muscular dystrophy gene myotilin does not perturb muscle structure or function in mice. Mol Cell Biol. 2007 Jan;27(1): 244-252.

Murphy S, Pearce B.Functional receptors for neurotransmitters on astroglial cells. Neuroscience. 1987 Aug;22(2):381-94. Review.

Myer DJ, Gurkoff GG, Lee SM, Hovda DA, Sofroniew MV. Essential protective roles of reactive astrocytes in traumatic brain injury. Brain. 2006 Oct;129(Pt 10):2761-72.

Mykkanen OM, Gronholm M, Ronty M, Lalowski M, Salmikangas P, Suila H and Carpen O. Characterization of human palladin, a microfilament-associated protein. Mol Biol Cell. 2001 Oct;12(10): 3060-3073.

Newman EA. New roles for astrocytes: regulation of synaptic transmission. Trends Neurosci. 2003 Oct;26(10):536-42.

Nguyen QT, Sanes JR, Lichtman JW. Pre-existing pathways promote precise projection patterns. Nat Neurosci. 2002 Sep;5(9):861-7.

Nishida E, Maekawa S, Sakai H.Cofilin, a protein in porcine brain that binds to actin filaments and inhibits their interactions with myosin and tropomyosin. Biochemistry. 1984 Oct 23;23(22):5307-13.

Nishio T, Kawaguchi S, Yamamoto M, Iseda T, Kawasaki T, Hase T. Tenascin-C regulates proliferation and migration of cultured astrocytes in a scratch wound assay. Neuroscience. 2005;132(1):87-102.

Norton WT, Aquino DA, Hozumi I, Chiu FC, Brosnan CF.Quantitative aspects of reactive gliosis: a review.Neurochem Res. 1992 Sep;17(9):877-85. Review.

Oakley CE, Hambly BD, Curmi PM and Brown LJ. Myosin binding protein C: structural abnormalities in familial hypertrophic cardiomyopathy. Cell Res. 2004 Apr;14(2): 95-110.

O'Callaghan JP.Quantitative features of reactive gliosis following toxicant-induced damage of the CNS.Ann N Y Acad Sci. 1993 May 28;679:195-210. Review.

Offenhauser N, Borgonovo A, Disanza A, Romano P, Ponzanelli I, Iannolo G, et al. The eps8 family of proteins links growth factor stimulation to actin reorganization generating functional redundancy in the Ras/Rac pathway. Mol Biol Cell 2004;15(1):91-8.

Okagaki T, Weber FE, Fischman DA, Vaughan KT, Mikawa T and Reinach FC. The major myosin-binding domain of skeletal muscle MyBP-C (C protein) resides in the COOH-terminal, immunoglobulin C2 motif. J Cell Biol. 1993 Nov;123(3): 619-626.

Ono K, Yu R, Mohri K and Ono S. Caenorhabditis elegans kettin, a large immunoglobulin-like repeat protein, binds to filamentous actin and provides mechanical stability to the contractile apparatuses in body wall muscle. Mol Biol Cell. 2006 Jun;17(6): 2722-2734.

Ono S, Mohri K and Ono K. Molecular and biochemical characterization of kettin in Caenorhabditis elegans. J Muscle Res Cell Motil. 2005 26(6-8): 449-454.

Orth JD, McNiven MA. Dynamin at the actin-membrane interface. Curr Opin Cell Biol 2003;15(1):31-9.

Osiak AE, Zenner G, Linder S. Subconfluent endothelial cells form podosomes downstream of cytokine and RhoGTPase signaling. Exp Cell Res 2005;307(2):342-53.

Otey CA and Carpen O. Alpha-actinin revisited: a fresh look at an old player. Cell Motil Cytoskeleton. 2004 Jun;58(2): 104-111.

Otey CA, Rachlin A, Moza M, Arneman D and Carpen O. The palladin/myotilin/myopalladin family of actin-associated scaffolds. Int Rev Cytol. 2005 246(31-58.

Otto JJ. Actin-bundling proteins. Curr Opin Cell Biol. 1994 Feb;6(1): 105-109.

Parast MM and Otey CA. Characterization of palladin, a novel protein localized to stress fibers and cell adhesions. J Cell Biol. 2000 Aug 7;150(3): 643-656.

Pelham RJ Jr, Wang Y. High resolution detection of mechanical forces exerted by locomoting fibroblasts on the substrate. Mol Biol Cell. 1999 Apr;10(4):935-45.

Perez V, Bouschet T, Fernandez C, Bockaert J, Journot L. Dynamic reorganization of the astrocyte actin cytoskeleton elicited by cAMP and PACAP: a role for phosphatidylInositol 3-kinase inhibition. Eur J Neurosci. 2005 Jan;21(1):26-32.

Pervushin K, Riek R, Wider G and Wuthrich K. Attenuated T2 relaxation by mutual cancellation of dipole-dipole coupling and chemical shift anisotropy indicates an avenue to NMR structures of very large biological macromolecules in solution. Proc Natl Acad Sci U S A. 1997 Nov 11;94(23): 12366-12371.

Pogue-Geile KL, Chen R, Bronner MP, Crnogorac-Jurcevic T, Moyes KW, Dowen S, Otey CA, Crispin DA, George RD, Whitcomb DC and Brentnall TA. Palladin mutation causes familial pancreatic cancer and suggests a new cancer mechanism. PLoS Med. 2006 Dec;3(12): e516.

Politou AS, Gautel M, Improta S, Vangelista L and Pastore A. The elastic I-band region of titin is assembled in a "modular" fashion by weakly interacting Ig-like domains. J Mol Biol. 1996 Feb 2;255(4): 604-616.

Popowicz GM, Schleicher M, Noegel AA and Holak TA. Filamins: promiscuous organizers of the cytoskeleton. Trends Biochem Sci. 2006 Jul;31(7): 411-419.

Porter JT, McCarthy KD. Astrocytic neurotransmitter receptors in situ and in vivo. Prog Neurobiol. 1997 Mar;51(4):439-55. Review.

Prinjha R, Moore SE, Vinson M, Blake S, Morrow R, Christie G, Michalovich D, Simmons DL, Walsh FS. Inhibitor of neurite outgrowth in humans. Nature. 2000 Jan 27;403(6768):383-4.

Provenzano C, Gallo R, Carbone R, Di Fiore PP, Falcone G, Castellani L, et al. Eps8, a tyrosine kinase substrate, is recruited to the cell cortex and dynamic F-actin upon cytoskeleton remodeling. Exp Cell Res 1998;242(1):186-200.

Puchala E, Windle WF. The possibility of structural and functional restitution after spinal cord injury. A review. Exp Neurol. 1977 Apr;55(1):1-42.

Puius YA, Mahoney NM and Almo SC. The modular structure of actin-regulatory proteins. Curr Opin Cell Biol. 1998 Feb;10(1): 23-34.

Rachlin AS and Otey CA. Identification of palladin isoforms and characterization of an isoform-specific interaction between Lasp-1 and palladin. J Cell Sci. 2006 Mar 15;119(Pt 6): 995-1004.

Ramakers GJ, Moolenaar WH. Regulation of astrocyte morphology by RhoA and lysophosphatidic acid. Exp Cell Res. 1998 Dec 15;245(2):252-62.

Ramon y Cajal S. Degeneration and regeneration of the nervous system. 1928 London: Oxford UP.

Rao MS, Noble M, Mayer-Proschel M. 1998. A tripotential glial precursor cell is present in the developing spinal cord. Proc Natl Acad Sci U S A 95:3996-4001.

Rathke-Hartlieb S, Budde P, Ewert S, Schlomann U, Staege MS, Jockusch H, Bartsch JW, Frey J. Elevated expression of membrane type 1 metalloproteinase (MT1-MMP) in reactive astrocytes following neurodegeneration in mouse central nervous system. FEBS Lett. 2000 Sep 22;481(3):227-34.

Razumova MV, Shaffer JF, Tu AY, Flint GV, Regnier M and Harris SP. Effects of the N-terminal domains of myosin binding protein-C in an in vitro motility assay: Evidence for long-lived cross-bridges. J Biol Chem. 2006 Nov 24;281(47): 35846-35854.

Ren XD, Kiosses WB, Schwartz MA. Regulation of the small GTP-binding protein Rho by cell adhesion and the cytoskeleton. Embo J 1999;18(3):578-85.

Reynolds BA, Weiss S.Generation of neurons and astrocytes from isolated cells of the adult mammalian central nervous system.Science. 1992 Mar 27;255(5052):1707-10.

Richards LJ, Kilpatrick TJ, Bartlett PF.De novo generation of neuronal cells from the adult mouse brain.Proc Natl Acad Sci U S A. 1992 Sep 15;89(18):8591-5.

Ridet JL, Malhotra SK, Privat A, Gage FH. Reactive astrocytes: cellular and molecular cues to biological function. Trends Neurosci. 1997 Dec;20(12):570-7. Review. Erratum in: Trends Neurosci 1998 Feb;21(2):80.

Ridley AJ, Hall A. The small GTP-binding protein rho regulates the assembly of focal adhesions and actin stress fibers in response to growth factors. Cell. 1992 Aug 7;70(3):389-99.

Rivera S, Khrestchatisky M. 1999. Matrix metalloproteinases and tissue inhibitors of metalloproteinases in neuronal plasticity and pathology. In: Baudry M, Thomsom RF, Davis JL, editors. Advances in synaptic plasticity. Cambridge, Massachusetts: The MIT Press. pp 53-86.

Rogers SD, Demaster E, Catton M, Ghilardi JR, Levin LA, Maggio JE, Mantyh PW. Expression of endothelin-B receptors by glia in vivo is increased after CNS injury in rats, rabbits, and humans. Exp Neurol. 1997 May;145(1):180-95.

Ronty M, Taivainen A, Heiska L, Otey CA, Ehler E, Song WK and Carpen O. Exp Cell Res. 2007 in press

Ronty M, Taivainen A, Moza M, Kruh GD, Ehler E and Carpen O. Involvement of palladin and alpha-actinin in targeting of the Abl/Arg kinase adaptor ArgBP2 to the actin cytoskeleton. Exp Cell Res. 2005 Oct 15;310(1): 88-98.

Ronty M, Taivainen A, Moza M, Otey CA and Carpen O. Molecular analysis of the interaction between palladin and alpha-actinin. FEBS Lett. 2004 May 21;566(1-3): 30-34.

Ronty MJ, Leivonen SK, Hinz B, Rachlin A, Otey CA, Kahari VM and Carpen OM. Isoform-Specific Regulation of the Actin-Organizing Protein Palladin during TGF-beta1-Induced Myofibroblast Differentiation. J Invest Dermatol. 2006 Nov;126(11): 2387-2396.

Rosen MK, Gardner KH, Willis RC, Parris WE, Pawson T and Kay LE. Selective methyl group protonation of perdeuterated proteins. Journal of Molecular Biology. 1996 Nov 15;263(5): 627-636.

Rottner K, B Behrendt, JV Small and J Wehland (1999) VASP dynamics during lamellipodia protrusion. Nature Cell Biol. 1:321-322

Safavi-Abbasi S, Wolff JR, Missler M. Rapid morphological changes in astrocytes are accompanied by redistribution but not by quantitative changes of cytoskeletal proteins. Glia. 2001 Oct;36(1):102-15.

Sahin Kaya S, Mahmood A, Li Y, Yavuz E, Chopp M. 1999. Expression of nestin after traumatic brain injury in rat brain. Brain Res 840:153-157.

Salmikangas P, Mykkanen OM, Gronholm M, Heiska L, Kere J and Carpen O. Myotilin, a novel sarcomeric protein with two Ig-like domains, is encoded by a candidate gene for limb-girdle muscular dystrophy. Hum Mol Genet. 1999 Jul;8(7): 1329-1336.

Salmikangas P, van der Ven PF, Lalowski M, Taivainen A, Zhao F, Suila H, Schroder R, Lappalainen P, Furst DO and Carpen O. Myotilin, the limb-girdle muscular dystrophy 1A (LGMD1A) protein, cross-links actin filaments and controls sarcomere assembly. Hum Mol Genet. 2003 Jan 15;12(2): 189-203.

Santoro MM and Bolen DW. Unfolding free energy changes determined by the linear extrapolation method. 1. Unfolding of phenylmethanesulfonyl alpha-chymotrypsin using different denaturants. Biochemistry. 1988 Oct 18;27(21): 8063-8068.

Sato T, del Carmen Ovejero M, Hou P, Heegaard AM, Kumegawa M, Foged NT, et al. Identification of the membrane-type matrix metalloproteinase MT1-MMP in osteoclasts. J Cell Sci 1997;110 (Pt 5):589-96.

Schikorski T, Stevens CF.Quantitative fine-structural analysis of olfactory cortical synapses.Proc Natl Acad Sci U S A. 1999 Mar 30;96(7):4107-12.

Schnitzer J, Franke WW, Schachner M.Immunocytochemical demonstration of vimentin in astrocytes and ependymal cells of developing and adult mouse nervous system. J Cell Biol. 1981 Aug;90(2):435-47.

Schousboe A, Hertz L. Role of astroglial cells in glutamate homeostasis. Adv Biochem Psychopharmacol. 1981;27:103-13.

Schousboe A, Westergaard N, Sonnewald U, Petersen SB, Yu AC, Hertz L. Regulatory role of astrocytes for neuronal biosynthesis and homeostasis of glutamate and GABA. Prog Brain Res. 1992;94:199-211. Review.

Schroder R, Reimann J, Salmikangas P, Clemen CS, Hayashi YK, Nonaka I, Arahata K and Carpen O. Beyond LGMD1A: myotilin is a component of central core lesions and nemaline rods. Neuromuscul Disord. 2003 Aug;13(6): 451-455.

Schwab JM, Brechtel K, Mueller CA, Failli V, Kaps HP, Tuli SK, Schluesener HJ. Experimental strategies to promote spinal cord regeneration--an integrative perspective. Prog Neurobiol. 2006 Feb;78(2):91-116. Epub 2006 Feb 17. Review.

Scita G, Nordstrom J, Carbone R, Tenca P, Giardina G, Gutkind S, et al. EPS8 and E3B1 transduce signals from Ras to Rac. Nature 1999;401(6750):290-3.

Scita G, Tenca P, Areces LB, Tocchetti A, Frittoli E, Giardina G, et al. An effector region in Eps8 is responsible for the activation of the Rac-specific GEF activity of Sos-1 and for the proper localization of the Rac-based actin-polymerizing machine. J Cell Biol 2001;154(5):1031-44.

Scolding NJ, Rayner PJ, Compston DA. 1999. Identification of A2B5-positive putative oligodendrocyte progenitor cells and A2B5-positive astrocytes in adult human white matter. Neuroscience 89:1-4.

Selmaj KW, Farooq M, Norton WT, Raine CS, Brosnan CF. Proliferation of astrocytes in vitro in response to cytokines. A primary role for tumor necrosis factor. J Immunol. 1990 Jan 1;144(1):129-35.

Seri B, García-Verdugo JM, McEwen BS, Alvarez-Buylla A.Astrocytes give rise to new neurons in the adult mammalian hippocampus.J Neurosci. 2001 Sep 15;21(18):7153-60.

Shiffman D, Ellis SG, Rowland CM, Malloy MJ, Luke MM, Iakoubova OA, Pullinger CR, Cassano J, Aouizerat BE, Fenwick RG, Reitz RE, Catanese JJ, Leong DU, Zellner C, Sninsky JJ, Topol EJ, Devlin JJ and Kane JP. Identification of four gene

variants associated with myocardial infarction. Am J Hum Genet. 2005 Oct;77(4): 596-605.

Simard M, Nedergaard M. The neurobiology of glia in the context of water and ion homeostasis. Neuroscience. 2004;129(4):877-96. Review.

Slupsky CM, Boyko RF, Booth VK and Sykes BD. Smartnotebook: a semi-automated approach to protein sequential NMR resonance assignments. J Biomol NMR. 2003 Dec;27(4): 313-321.

Soll DR, Voss E, Varnum-Finney B, Wessels D. "Dynamic Morphology System": a method for quantitating changes in shape, pseudopod formation, and motion in normal and mutant amoebae of Dictyostelium discoideum. J Cell Biochem. 1988 Jun;37(2):177-92.

Sorimachi H, Freiburg A, Kolmerer B, Ishiura S, Stier G, Gregorio CC, Labeit D, Linke WA, Suzuki K, Labeit S. Tissue-specific expression and alpha-actinin binding properties of the Z-disc titin: implications for the nature of vertebrate Z-discs. J Mol Biol. 1997 Aug 1;270(5):688-95.

Steindler DA, Laywell ED. Astrocytes as stem cells: nomenclature, phenotype, and translation. Glia. 2003 Jul;43(1):62-9.

Stichel CC, Hermanns S, Luhmann HJ, Lausberg F, Niermann H, D'Urso D, Servos G, Hartwig HG, Muller HW. Inhibition of collagen IV deposition promotes regeneration of injured CNS axons. Eur J Neurosci. 1999 Feb;11(2):632-46.

Stichel CC, Muller HW. The CNS lesion scar: new vistas on an old regeneration barrier. Cell Tissue Res. 1998 Oct;294(1):1-9. Review.

Svitkina TM, Borisy GG. Arp2/3 complex and actin depolymerizing factor/cofilin in dendritic organization and treadmilling of actin filament array in lamellipodia. J Cell Biol. 1999 May 31;145(5):1009-26.

Swanson JA, Watts C. Macropinocytosis. Trends Cell Biol 1995;5(11):424-8.

Syková E, Svoboda J, Simonová Z, Jendelová P. Role of astrocytes in ionic and volume homeostasis in spinal cord during development and injury. Prog Brain Res. 1992;94:47-56. Review.

Tang JX, Szymanski PT, Janmey PA and Tao T. Electrostatic effects of smooth muscle calponin on actin assembly. Eur J Biochem. 1997 Jul 1;247(1): 432-440.

Tang S, Qiu J, Nikulina E, Filbin MT. Soluble myelin-associated glycoprotein released from damaged white matter inhibits axonal regeneration. Mol Cell Neurosci. 2001 Sep;18(3):259-69.

Thompson JD, Gibson TJ, Plewniak F, Jeanmougin F and Higgins DG. The CLUSTAL_X windows interface: flexible strategies for multiple sequence alignment aided by quality analysis tools. Nucleic Acids Res. 1997 Dec 15;25(24): 4876-4882.

Tilney LG, Connelly PS, Vranich KA, Shaw MK and Guild GM. Why are two different cross-linkers necessary for actin bundle formation in vivo and what does each cross-link contribute? J Cell Biol. 1998 Oct 5;143(1): 121-133.

Tom VJ, Steinmetz MP, Miller JH, Doller CM, Silver J. Studies on the development and behavior of the dystrophic growth cone, the hallmark of regeneration failure, in an in vitro model of the glial scar and after spinal cord injury. J Neurosci. 2004 Jul 21;24(29):6531-9.

Tseng Y, Fedorov E, McCaffery JM, Almo SC and Wirtz D. Micromechanics and ultrastructure of actin filament networks crosslinked by human fascin: a comparison with alpha-actinin. J Mol Biol. 2001 Jul 6;310(2): 351-366.

Tseng Y, Kole TP, Lee JS, Fedorov E, Almo SC, Schafer BW, Wirtz D. How actin crosslinking and bundling proteins cooperate to generate an enhanced cell mechanical response. Biochem Biophys Res Commun. 2005 Aug 19;334(1):183-92.

van der Flier A and Sonnenberg A. Structural and functional aspects of filamins. Biochim Biophys Acta. 2001 Apr 23;1538(2-3): 99-117.

van der Ven PF, Wiesner S, Salmikangas P, Auerbach D, Himmel M, Kempa S, Hayess K, Pacholsky D, Taivainen A, Schroder R, Carpen O and Furst DO. Indications for a novel muscular dystrophy pathway. gamma-filamin, the muscle-specific filamin isoform, interacts with myotilin. J Cell Biol. 2000 Oct 16;151(2): 235-248.

Vaughan KT, Weber FE, Einheber S and Fischman DA. Molecular cloning of chicken myosin-binding protein (MyBP) H (86-kDa protein) reveals extensive homology with MyBP-C (C-protein) with conserved immunoglobulin C2 and fibronectin type III motifs. J Biol Chem. 1993 Feb 15;268(5): 3670-3676.

Ventura R, Harris KM.Three-dimensional relationships between hippocampal synapses and astrocytes.J Neurosci. 1999 Aug 15;19(16):6897-906.

Vise WM, Liss L, Yashon D, Hunt WE. Astrocytic processes: A route between vessels and neurons followingblood-brain barrier injurt.J Neuropathol Exp Neurol. 1975 Jul;34(4):324-34.

von Nandelstadh P, Gronholm M, Moza M, Lamberg A, Savilahti H and Carpen O. Actin-organising properties of the muscular dystrophy protein myotilin. Exp Cell Res. 2005 Oct 15;310(1): 131-139.

Wang K, Bekar LK, Furber K, Walz W. 2004. Vimentin-expressing proximal reactive astrocytes correlate with migration rather than proliferation following focal brain injury. Brain Res 1024:193-202.

Wang W, Goswami S, Lapidus K, Wells AL, Wyckoff JB, Sahai E, Singer RH, Segall JE and Condeelis JS. Identification and testing of a gene expression signature of invasive carcinoma cells within primary mammary tumors. Cancer Res. 2004 Dec 1;64(23): 8585-8594.

Warn R, Brown D, Dowrick P, Prescott A, Warn A. Cytoskeletal changes associated with cell motility. Symp Soc Exp Biol 1993;47:325-38.

Watkins H, Conner D, Thierfelder L, Jarcho JA, MacRae C, McKenna WJ, Maron BJ, Seidman JG and Seidman CE. Mutations in the cardiac myosin binding protein-C gene on chromosome 11 cause familial hypertrophic cardiomyopathy. Nat Genet. 1995 Dec;11(4): 434-437.

Welch MD, A Iwamatsu, and TJ MItchison. (1997) Actin polymerization is induced by the Arp2/3 complex at the surface of Listeria monocytogenes. Nature 385:265-269.

Welch MD, Mallavarapu A, Rosenblatt J and Mitchison TJ. Actin dynamics in vivo. Curr Opin Cell Biol. 1997 Feb;9(1): 54-61.

Welikson RE and Fischman DA. The C-terminal IgI domains of myosin-binding proteins C and H (MyBP-C and MyBP-H) are both necessary and sufficient for the intracellular crosslinking of sarcomeric myosin in transfected non-muscle cells. J Cell Sci. 2002 Sep 1;115(Pt 17): 3517-3526.

Wender R, Brown AM, Fern R, Swanson RA, Farrell K, Ransom BR. 2000. Astrocytic glycogen influences axon function and survival during glucose deprivation in central white matter. J Neurosci 20: 6804-6810.

Williams AF and Barclay AN. The immunoglobulin superfamily--domains for cell surface recognition. Annu Rev Immunol. 1988 6(381-405.

Wishart DS, Bigam CG, Yao J, Abildgaard F, Dyson HJ, Oldfield E, Markley JL and Sykes BD. 1H, 13C and 15N chemical shift referencing in biomolecular NMR. J Biomol NMR. 1995 Sep;6(2): 135-140.

Wislet-Gendebien S, Wautier F, Leprince P, Rogister B. Astrocytic and neuronal fate of mesenchymal stem cells expressing nestin. Brain Res Bull. 2005 Dec 15;68(1-2):95-102. Epub 2005 Sep 21. Review.

Woiciechowsky C, Schoning B, Stoltenburg-Didinger G, Stockhammer F, Volk HD. Brain-IL-1 beta triggers astrogliosis through induction of IL-6: inhibition by propranolol and IL-10. Med Sci Monit. 2004 Sep;10(9):BR325-30.

Wu VW and JP Schwartz (1998) Cell Culture Models for Reactive Gliosis: New Perspectives. J. Neuro. Res. 51:675-81

Wujek JR, Akeson RA. Extracellular matrix derived from astrocytes stimulates neuritic outgrowth from PC12 cells in vitro. Brain Res. 1987 Jul;431(1):87-97.

Wymann M, Arcaro A. Platelet-derived growth factor-induced phosphatidylinositol 3-kinase activation mediates actin rearrangements in fibroblasts. Biochem J. 1994 Mar 15;298 Pt 3:517-20.

Yarmola EG, Edison AS, Lenox RH and Bubb MR. Actin filament cross-linking by MARCKS: characterization of two actin-binding sites within the phosphorylation site domain. J Biol Chem. 2001 Jun 22;276(25): 22351-22358.

Yin HL, Stossel TP. Control of cytoplasmic actin gel-sol transformation by gelsolin, a calcium-dependent regulatory protein. Nature. 1979 Oct 18;281(5732):583-6.

Yu AC, Lee YL, Eng LF. Astrogliosis in culture: I. The model and the effect of antisense oligonucleotides on glial fibrillary acidic protein synthesis. J Neurosci Res. 1993 Feb 15;34(3):295-303.

Zhou S, Webb BA, Eves R, Mak AS.

Zlotnik I. The reaction of astrocytes to acute virus infections of the central nervous system. Br. J. exp. Pathol 1968 49, 555-564.